

Archive ouverte UNIGE

https://archive-ouverte.unige.ch

Thèse 2010

Open Access

This version of the publication is provided by the author(s) and made available in accordance with the copyright holder(s).

Multiconfigurational perturbation theory : Recent developments and applications

Moughal Shahi, Abdul Rehaman

How to cite

MOUGHAL SHAHI, Abdul Rehaman. Multiconfigurational perturbation theory: Recent developments and applications. Doctoral Thesis, 2010. doi: 10.13097/archive-ouverte/unige:5158

This publication URL: https://archive-ouverte.unige.ch/unige:5158

Publication DOI: <u>10.13097/archive-ouverte/unige:5158</u>

© This document is protected by copyright. Please refer to copyright holder(s) for terms of use.

UNIVERSITÉ DE GENÈVE Section de chimie et biochimie Département de chimie physique FACULTÉ DES SCIENCES Professeur L. Gagliardi Dr. T. A. Wesolowski

Multiconfigurational Perturbation Theory:

Recent Developments and Applications

THÈSE

présentée à la Faculté des sciences de l'Université de Genève

pour obtenir le grade de Docteur ès sciences, mention chimie

par

Abdul Rehaman Moughal Shahi

de l'

Inde

Thèse N° 4172

GENÈVE

Atelier d'impression ReproMail

2010



Doctorat ès sciences mention chimie

Thèse de Monsieur Abdul Rehaman MOUGHAL SHAHI

intitulée :

" Multiconfigurational Perturbation Theory : Recent Developments and Applications "

La Faculté des sciences, sur le préavis de Monsieur T.A. WESOLOWSKI, docteur et directeur de thèse (Département de chimie), de Madame L. GAGLIARDI, professeure et codirectrice de thèse (Department of Chemistry, University of Minnesota, Minneapolis, United States of America) de Messieurs L. SERRANO ANDRES, docteur (Departamento de Química Física, Instituto de Ciencia Molecular, Universitat de Valencia, España) et V. VERYAZOV, docteur (Theoretical chemistry, Chemical Center, Lund, Sweden), autorise l'impression de la présente thèse, sans exprimer d'opinion sur les propositions qui y sont énoncées.

Genève, le 12 janvier 2010

Thèse - 4172 -

Le Doyen, Jean-Marc TRISCONE

N.B.- La thèse doit porter la déclaration précédente et remplir les conditions énumérées dans les "Informations relatives aux thèses de doctorat à l'Université de Genève".

Nombre d'exemplaires à livrer par colis séparé à la Faculté : - 4 -

Remerciements

Completing a Ph.D, is not possible without the support of many people. It is therefore a pleasant task to express my sincere gratitude to all who contributed in many ways to the outcome of the present work. There are many people who have contributed, in different ways, to make these four years of life and research in Geneva four successful, beautiful years.

The first in the list is my supervisor and mentor Prof. Laura Gagliardi, to whom I would like to express my gratitude for the opportunities she has created for me and for her care and patience. I have profited enormously from her encouragement, guidance and support, from the freedom she provided to find own pathways, and I have enjoyed our many discussions on chemistry and unrelated matters. It has been a great privilege to work with her over the past years.

It is a great pleasure to thank Dr. Luis Serrano, Dr. Valera veryazov and Dr. Tomasz A. Wesolowski for accepting to be the members of the thesis committee and for taking the time to read the thesis. I would like to thank Prof. Per-Ake Malmqvist and Prof. C. J. Cramer for their continuous support and the fruitful collaborations during the past years.

There are many people whom I worked with and to whom I am indebted. Juraj Raab and Eugeniusz Bednarz, two guys who helped me a lot in the initial stages of my Ph.D. It has been fun to work side by side with many young scientists: to spend my working and non-working hours in the company of Ivan Infante, Tanya Todorova, Daniel Hagberg, Stefan Huber and Helena Masso. I also want to express my deep appreciation to Francesco Aquilante who spent his valuable time making me understand several theoretical concepts pertaining to perturbation theory and also for proofreading the thesis. I am grateful to Giovanni La Macchia who from day one has helped me with all kinds of bureaucratic issues and everyday needs. I also thank him for the french translation of the synopsis and summary of this thesis. I wish to thank all other group members, Jakub Kaminski, Giovanni Li Manni, Cesar

Bouchet, for the stimulating atmosphere.

I wish to express my sincere thanks to the MOLCAS team. Without their expertise and support much of this work couldn't have been accomplished. I am especially thankful to Prof. Bjorn. O. Roos, who initiated the RASPT2 project and whose passion for research has been an inspiration for me. My deepest gratitude goes to my parents and sister for their love, support, encouragement and understanding. Without them, none of this would have been possible.

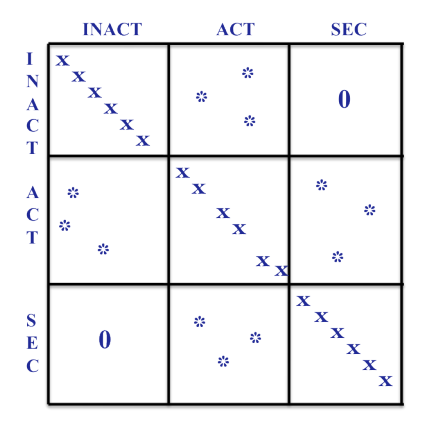
Résumé en français

Cette thèse va traiter de la méthodologie impliquée dans le développement de la théorie de la perturbation de l'espace actif restreint (RASPT2), qui se base sur une fonction d'onde de type RASSCF (champ auto-cohérent dans l'espace actif restreint). Cette théorie est une extension de CASPT2, qui se base sur une fonction d'onde de type CASSCF (champ auto-cohérent dans l'espace actif complet). Le modèle RASSCF/RASPT2 permet d'utiliser un espace actif plus étendu et par conséquent, est capable de traiter une plus grande variété de problèmes rencontrés en chimie. Contrairement à CASSCF, l'espace active dans la méthode RASSCF est divisé en trois sous-espaces, imposant un certain nombre de restrictions par rapport au nombre d'excitations autorisé. Par conséquent, il y a une réduction du nombre de configurations. Par la suite, l'utilisation de la théorie de la perturbation permet une meilleure description de la corrélation dynamique.

La différence principale entre la méthode CASSCF et RASSCF réside dans la manière de traiter les orbitales de l'espace actifs, réduisant dans le dernier cas le nombre d'excitations possible. L'imposition de contraintes dans le cas de RASSCF permet de traiter des problèmes plus complexes. Ainsi, si CASSCF peut traiter jusqu'à 15-16 électrons dans 15-16 orbitales, RASSCF permet de gérer un espace actif constitué de 30 électrons distribués dans 30 orbitales actives. RASSCF a donc un grand potentiel et le développement de RASPT2 est la continuation logique du processus visant à étudier des systèmes compliqués qui ne pouvaient pas jusqu'alors être traités par des méthodes multiconfigurationnelles classiques.

RASPT2 se différencie de CASPT2 de par la fonction d'onde qui est utilisée dans le traitement perturbatif, RASSCF et CASSCF. L'opérateur de Fock est défini par la fonction d'onde. Il ne dépend pas des coefficents CI et des orbitales, pour autant que ces derniers représentent la même fonction d'onde. Cependant, les orbitales sont ensuites modifiées de tel sorte à ce qu'elles diagonalisent la matrice de Fock. Ce processus s'accompagne par des modifications des coefficents CI. Ce processus ne peut pas aboutir complètement étant donné que la rotation des orbitales ne peut se faire qu'au sein d'un même groupe d'orbitales, c'est-à-dire inactives-inactives, ... et par conséquent à la fin du processus de diagonalisation, il

y aura des élements matriciels non nuls, correspondant par exemple au bloc inactif/actif de la matrice. Dans le cas de CASPT2, ce genre de situation est géré par l'intermédiaire d'un processus itératif (PCG), qui permet de résoudre les équations pour la fonction d'ordre perturbée même quand ce genre d'élements matriciels se trouve dans l'Hamiltonien d'ordre zero. La différence entre CASPT2 et RASPT2 est que ce dernier ne permet pas des rotations qui couplent des orbitales appartenant par exemple à RAS1 et RAS2, ou RAS1 et RAS3. La diagonalisation de la matrice de Fock est donc incomplète.



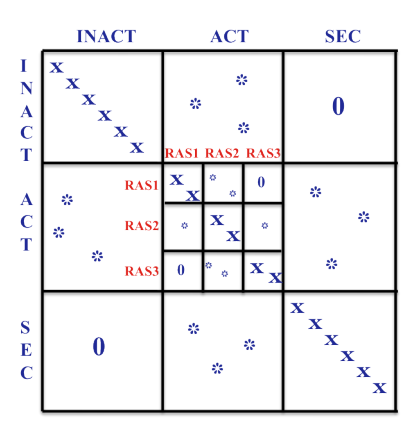


Figure 1: Une représentation schématique de la matrice de Fock après un calcul CASSCF (gauche) et RASSCF (droite).

Cette thèse se propose de tester en détail la méthode RASPT2 à travers l'étude de problèmes concernant différents domaines en chimie. En premier lieu, nous avons examiné la performance du modèle RASPT2 dans la résolution de deux problèmes liés à l'activation de la molécule de O_2 par le cuivre. L'activation de la molécule d'oxygene au moyen d' un ou deux ions Cu(I) est un processus répandu dans de nombreux processus en biologie et en catalyse. Dans le cas de $LCuO_2$, où L correspond à un nombre indéterminé de ligands, un état d'oxydation possible est $LCu(II)O_2(-)$; Ainsi, l'atome de cuivre a été oxidé et l'espèce O_2 est donc l'anion radicalaire superoxide. De la meme manière, dans le cas de composés contenant un dimère de cuivre, $(LCu)_2O_2$, un état d'oxydation possible est $[LCu(II)]_2[(O_2)(2-)]$; Dans ce dernier cas, chaque atome de cuivre a été oxidé et donc l'espèce O_2 est donc le di-anion peroxide. Dans les deux cas, les différents composés peuvent être, dans leur état fondamental,

les diradicaux dans un état singulet. Ce dernier peut correspondre soit à deux ions d⁹ Cu(II), soit à un seul ion de cuivre et un superoxide radical anion. Les théories se basant sur une fonction d'onde constituée d'un seul déterminant ne sont pas capable de decrire de tels systèmes, étant donné que des singulets diradicaux nécessitent au minimum deux déterminants pour être décrit correctement. De plus, même si certains composés sont caractérisés par une couche de valence complète, comme par exemple dans le cas de ., [LCu(III)]₂[O(2-)]₂, des études de chimie computationnelles ont montré que la contribution du à la corrélation dynamique a une influence sur l'énergie relative de différents isomères. Cette étude montre que dans le cas impliquant un seul atome de cuivre, RASPT2 et CASPT2 donnent des résultats très similaires. Dans le cas où deux Cu sont impliqués, RASPT2 est beaucoup plus avantageux car il peut gérer un espace actif plus étendu, nécessaire dans le cas de l'étude du système à deux atomes.

Ensuite, nous avons comparé les méthodes CASPT2 et RASPT2 afin de déterminer la variation de la différence en énergie entre les états singulets-triplets de 5 intermédiaires impliqués dans la formation et la réaction d'espèces cuivre-oxo dérivées de l'oxygénation de complexes de type Cu(I)-α-ketocarboxylate. A travers l'étude de différents espaces actifs, nous avons déterminé que CASPT2 convergeait correctement pour un espace actif (12,12). En incluant toutes les excitations allant jusqu'aux doubles excitations de RAS1 à RAS3, il y a une diminution de deux ordres de magnitude du nombre de fonctions d'état de configuration par rapport aux calculs CASPT2(12,12), sans pour autant diminuer la qualité des résultats. En augmentant le nombre d'excitation de RAS1 à RAS3 permet d'amméliorer les résultats obtenus.

Nous avons également utilisé la méthode RASSCF/RASPT2 pour calculer les potentiels d'ionization et les différences d'énergie électronique d'oligomères de longueur n formés à partir de l'éthylèlne (n = 1–10), acetylene (n = 1–5), and phenylene (n = 1–3). L'approche RASSCF/RASPT2 offre une précision similaire à CASSCF/CASPT2 mais permet de réduire les coûts du point de vue computationnel (les deux méthodes sont en accord avec les données expérimentales disponibles). Une des particularités de RASPT2 est que cette méthode permet d'utiliser des espaces actifs plus grand.

Dans tous les cas, les résultats RASPT2 et CASPT2 concordent entre eux et avec les données expérimentales. La différence entre les deux méthodes est d'environ 0.1 eV mais correspond à une variation du nombre de fonctions d'état de configuration de l'ordre de 3 ordre de magnitude. La méthode RASSCF/RASPT2 permet l'investigation de systèmes plus compliqués, qui ne pourraient pas être étudiés par CASPT2.

Néanmoins, la méthode RASSCF n'est pas autant solide que la méthode CASSCF. En effet la convergence dans le premier cas n'est pas aussi aisée que dans le second. De plus, elle est étroitement associée à la qualité des orbitales de départ. Par conséquent, en plus de choisir correctement l'espace actif, il est important d'obtenir de bonnes orbitales de départs avant de lancer un calcul. Cette remarque est également valable dans le cas de calculs CASPT2. Etant donné que la description de la corrélation dynamique n'était pas possible, l'utilisation de RASSCF se limitait à faire des optimisations de géométrie ou était utilisé afin de sélectionner les orbitales à inclure dans l'espace actif pour des calculs CASSCF restreints. L'association de la méthode RASSCF avec la théorie de la perturbation de second ordre (RASPT2) a permis d'étendre son champs d'utilisation à la résolution de problèmes plus compliqués. A cause des contraintes associées aux orbitales inclues dans les différents sousgroupes de l'espace actif, seulement RAS1 et RAS3 seraient capables de décrire la corrélation dynamique, RAS2 décrivant la corrélation non-dynamique. Malheureusement ce type de fractionnement n'est pas clairement défini. Par conséquent, pour décrire la corrélation dynamique dans le cadre de la méthode RASPT2, un traitement perturbatif des excitations internes doit être inclus. Ceci implique dans la formulation actuelle de H₀, de construire des matrices de densité d'ordre quatre, ce qui est impossible si l'espace actif est trop grand. De nouvelles approximations de H₀ sont nécessaires pour résoudre ce problème. Dans le cadre de calculs CASPT2 et RASPT2

De la même manière que dans le cadre de calculs CASPT2 se basant sur un seul état, les calculs RASPT2 basés également sur un seul état à partir d'une fonction d'onde de référence CASSCF ne sont pas orthogonaux aux autres états de même espace et de même symétrie de spin. Par conséquent, les solutions obtenues ne tiennent pas compte du couplage entre les états. La méthode MS-CASPT2, qui permet de tenir compte de plusieurs états, constitue

une extension de la méthode CASPT2 pour le traitement de la perturbation dans le cadre de problèmes chimiques qui ont besoin de deux ou plusieurs états de référence. Par exemple, la description d'intersections coniques et de situations ou les états de Rydberg et de valence sont proches en énergie ne peut pas être pleinement prise en compte en utilisant simplement un seul état lors du traitement de la perturbation.

Afin de tester les performances de MS-RASPT2, nous avons choisis un groupe de 11 molécules de taille moyenne (composés aromatiques et bases azotées). Les énergies d'excitation verticale sont calculées pour les états excités de valence en utilisant MS-CASPT2 et MS-RASPT2, se basant sur des géométries identiques obtenues par des calculs DFT(B3LYP) utilisant les mêmes bases (TZVP). Une évaluation des effets du choix de l'espace active et des excitations vers l'espace RAS supérieur est entreprise de manière systématique. Les résultats RASPT2 sont accord avec ceux obtenus avec CASPT2 (à 0.2 eV près). L'application générale de la méthode RASPT2 afin d'étudier les états excités est analysée.

Les conclusions générales de ces différentes études sont:

- 1. Les calculs RASSCF/RASPT2 aboutissent à la même que les calculs CASSCF/CASPT2 lorsque les quadruple excitations sont inclues. La différence entre les deux résultats est de l'ordre d'environ 0.1 eV.
- 2. La méthode RASSCF n'est pas aussi solide que la méthode CASSCF. Elle ne converge pas aussi bien et est plus sensible à la qualité des orbitales de départ. Il a été noté qu'une faible convergence de la fonction RASSCF, quand les excitations triples et quadruples sont incluses, peut être corrigée en utilisant des orbitales de départ optimisées par un calcul RASSCF incluant jusqu'aux doubles excitations. Ainsi, des énergies d'excitation précises sont obtenues.

Néanmoins, nous sommes loin de pouvoir décrire à l'heure actuelle de manière précise tous les processus biologiques caractéristiques des êtres vivants. Il y a encore des défis à relever et la synergie entre les expériences menées en laboratoire et la théorie va permettre d'améliorer les différents modèles utilisés en chimie computationnelle. La chimie quantique a de beaux jours devant elle et de nombreux défis l'attendent.

Contents

1	Introduction							
	1.1	Descri	iption and motivation	13				
	1.2	Thesis	s Outline	15				
2	Quantum Chemistry							
	2.1	Time-	independent Schrödinger Equation	17				
		2.1.1	Born-Oppenheimer Approximation	18				
		2.1.2	Electronic Schrödinger Equation	19				
	2.2	Solution to the Electronic Schrödinger Equation						
		2.2.1	Hartree-Fock	20				
		2.2.2	Configuration Interaction (CI)	26				
		2.2.3	Multi-configurational Self-consistent Field	32				
3	The Restricted Active Space followed by Second Order Perturbation The-							
_	ory Method: Theory and Application to the study Cu ₂ O and Cu ₂ O ₂ Sys-							
	tems							
	3.1	Introd	duction	44				
		Metho	Method					
		3.2.1	The CASSCF/CASPT2 Model	45				
		3.2.2	The RASSCF/RASPT2 Method	52				
	3.3	Applie	cation to supported CuO_2 and Cu_2O_2 systems	54				
		3.3.1	Computational Details	55				
		332	Singlet-triplet splitting in the (C ₂ N ₂ H ₂)CuO ₂ system	58				

12 CONTENTS

		3.3.3 Relative energy of peroxo and bis- μ -oxo isomers of $\{[Cu(NH_3)_n]_2O_2\}^{2+}$					
		(n=0,1,2,3)	59				
	3.4	Discussion and Conclusions	62				
4	What Active Space Adequately Describes Oxygen Activation by a Late Transition Metal? CASPT2 and RASPT2 Applied to Intermediates from						
	the	Reaction of O_2 with a $Cu(I)$ - α -Ketocarboxylate	7 3				
	4.1	Introduction	74				
	4.2	Computational Details	79				
	4.3	Results and Discussion	83				
	4.4	Significance	93				
5	Second-Order pertubation theory with complete and restricted active space						
	\mathbf{refe}	reference functions applied to oligimeric hydrocarbons					
	5.1	Introduction	102				
	5.2	Computational Details	105				
	5.3	Results and Discussion	109				
	5.4	Conclusions	119				
6	Multistate CASPT2 vs Multistate RASPT2						
	6.1	Introduction					
	6.2	Computational details	131				
	6.3	Results and Discussion	133				
		6.3.1 Benzene (Table 6.1, Fig 6.2 and 6.3)	133				
		6.3.2 Furan (Table 6.2, Fig. 6.4)	135				
		6.3.3 Naphthalene (Table 6.4, Fig. 6.6 & 6.7)	136				
		6.3.4 Pyrrole, Pyridine, Pyrazine, Pyrimidine (Table 6.5 - 6.8, Fig. 6.7					
		-6.15):	137				
		6.3.5 Adenine, Thymine, Uracil, Cytosine (Table 6.9 - 6.16, Fig. 6.16 -6.31):	147				
	6.4	Conclusions	159				
7	Con	cluding Remarks	167				

Chapter 1

Introduction

1.1 Description and motivation

Quantum chemistry is a science that has sprung from a more general physical discipline, quantum mechanics, and is traditionally occupied with the explanation of electronic structure of molecules by means of quantum-mechanical models. Such models, aimed at the description of molecules and their interactions, are usually characterized as quantum-chemical. Computational chemistry, a field of study closely related to quantum chemistry, deals with the efficient computer implementation of existent quantum-chemical models and their application for the interpretation of specific chemical phenomena. The distinction between the quantum and the computational directions in chemical research is often helpful when it comes to the choice of methodology and interpretation of the results. Quantum chemistry adopts a physical approach, striving for the understanding of a phenomenon and its qualitative explanation in terms of a physically sound mathematical model.

Ab initio quantum chemistry has become an important tool to study atoms and molecules and increasingly in modeling complex systems such as those arising in biology and materials science. The goal of all the problems is to solve the electronic Schrödinger equation, given the positions of a collection of atomic nuclei, and the total number of electrons in a system. Thereby, to calculate the electronic energy, electron density, and other properties by means

of a well defined, automated approximation. Many models and approximations have been developed to compute wave functions and energies from which properties like optimal geometries, electronic, vibrational and rotational energy levels, reaction barriers, etc., can be deduced. The ability to obtain "good enough" solutions to the electronic Schrödinger equation for systems containing tens, or even hundreds, of atoms has revolutionized the ability of theoretical chemistry to address important problems in a wide range of disciplines; the Nobel Prize awarded to John Pople and Walter Kohn in 1998 is a reflection of this observation.

The electronic Schrödinger equation is a many-body problem, whose computational complexity grows factorially with the number of electrons, and hence, an exact solution is intractable. Hartree–Fock (HF) theory, a mean field approach, produces reasonable results for many properties but is incapable of providing a robust description of reactive chemical events in which the description of electron motion has a major role. Thus, a key problem has been the development of treatments of electron correlation that exhibit a tractable scaling in computational effort with the size of the system. Most of the quantum chemical models available today are good for ground states of stable products and reactants, but have limitations in studies involving radical states produced by bond breaking and studies in photochemistry, transition metal chemistry, and spectroscopic properties. These kind of chemical problems usually require more complicated methods.

Such problems in chemistry demand a more advanced computational methods called multiconfigurational ab initio methods. To use them properly one requires some specialized knowledge and they are therefore not the standard tools that any mainstream chemist would choose to apply, but there are now some software packages available. The Complete active space multiconfigurational method followed by second-order perturbation theory (CASSCF/CASPT2), within the MOLCAS suite of programs from University of Lund, is currently one of the most successful methods for treating chemical bonds, excited states, dissociated states, transition states for chemical reactions, etc. The CASSCF wave function fulfills, in principle, this requirement because it is full CI, albeit in a limited space of active orbitals. CASSCF can therefore be regarded as a method to describe chemical situations which are not predominantly single configurational. Therefore CASSCF/CASPT2 theory

1.2. THESIS OUTLINE

in principle allows applications to a wide variety of systems and many electrons. However, the CASSCF/CASPT2 method has the limitation of size and selection of the active space associated with memory and disk storage limit. This bottleneck has stunted the applicability of the CASSCF/CASPT2 method.

My Ph.D work has been focussed on learning the basic theory behind such methods, learning how to apply them to specific quantum chemistry problems, how to use MOLCAS on a computer cluster in order to do the calculations, and how to understand the results. In particular, this thesis describes the multireference second order perturbation theory using a restricted active space self-consistent field wave function as reference (RASSCF/RASPT2) which is an extension of the CASSCF/CASPT2 method. After which most of my work is directed towards it's applications and benchmarking of this newly developed method against the CASPT2 method. Thereby also show how this RASPT2 model permits larger active spaces to be employed for the reference wave function and thus extends the range of multiconfigurational wave function methods to a wider variety of chemical problems.

1.2 Thesis Outline

Chapter 2 gives the key points on basic quantum chemistry and serves as a general introduction in going from the fundamental Hartree-Fock theory to CASPT2 theory. Although this material is available in many introductory texts its appearance here is justified even if it were only to specify our notation and terms used in the rest of the thesis. Each subsequent chapter presents a separate project preceded by a brief introduction. Every such project was either published as an original scientific paper or (at the moment of writing this thesis) submitted for publication. Therefore the material presented in chapters 3-6 is the work done during my thesis and can be found in the corresponding publications. Chapter 3 deals with the work which gives the title to the thesis: the development of a second order perturbation theory over the restricted active space wave function (RASPT2) which is an extension of the well known CASPT2 method, which would be described in detail in the chapter and further its application to study the electronic structure of CuO₂ and Cu₂O₂ systems will

be presented. This theory has been applied to study the electronic structure of complexes involved in the activation of molecular oxygen. We show here that for the mono-copper complex both CASPT2 and RASPT2 provide similar results and for the binuclear copper complex, RASPT2 proves quantitatively useful owing to the very large size of the active space. In Chapter 4 the work concerning the application of the newly developed theory in the determination of singlet-triplet state energy splitting of three supported copper-dioxygen and two supported copper-oxo complexes will be discussed. The effects of different active active spaces has been examined and the general applicability of the RASPT2 protocol has been studied. Chapter 5 consists of our work on the oligomeric unsaturated hydrocarbons with the new method compared to the existing methods. Within this work, we show that RASPT2 approach yields similar accuracy to that of CASPT2 at significantly reduced computational expense. Finally in Chapter 6, we benchmark the multi-state formulation with in this method against multi-state CASPT2 method while studying electronically excited states of a benchmark set of organic molecules and conclude this thesis with some remarks in chapter 7.

Chapter 2

Quantum Chemistry

It is the goal of this chapter to describe the pertinent theory of quantum chemistry in order to obtain accurate physical information on the electronic character of a molecular system: the equilibrium geometry, the electronic spectrum, excited electronic states, permanent and transition dipole moments, potential energy surfaces, as well as the vibrational eigenfunctions and eigenvalues. At the center of solving the non-relativistic time-independent Schrödinger equation (TISE) lies the Born-Oppenheimer approximation. Its application to the TISE validates a separation of the electrons from the nuclei, leading to two eigenvalue equations: the electronic and the nuclear Schrödinger equations. In the following it will also be shown how one is able to (accurately) solve these equations for the two unknowns, i.e. the energies and wave functions.

2.1 Time-independent Schrödinger Equation

The nonrelativistic time-independent Schrödinger equation [1] is given as

$$\hat{H} |\Psi\rangle = E |\Psi\rangle \tag{2.1}$$

where the total energy, E, is obtainable by operation of the time-independent molecular Hamiltonian, \hat{H} , onto the complete wave function, $|\Psi\rangle$. The molecular Hamiltonian is given

below,

$$\hat{H} = \underbrace{-\sum_{a} \hbar/2m_{e} \nabla_{a}^{2}}_{\hat{T}_{el}} \underbrace{-\sum_{A} \hbar/2m_{A} \nabla_{A}^{2}}_{\hat{T}_{nu}} \underbrace{-\sum_{a} \sum_{A} \frac{Z_{A}e^{2}}{4\pi\epsilon_{0}r_{aA}}}_{\hat{V}_{el,nu}} \underbrace{+\sum_{a} \sum_{b>a} \frac{e^{2}}{4\pi\epsilon_{0}r_{ab}}}_{\hat{V}_{el,el}} \underbrace{+\sum_{A} \sum_{B>A} \frac{Z_{A}Z_{B}e^{2}}{4\pi\epsilon_{0}R_{AB}}}_{\hat{V}_{nu,nu}}$$
(2.2)

where ∇^2 is the Laplacian operator, m_e and m_A are the mass of the electron and the nucleus, respectively, which are used to define the two kinetic energy terms, \hat{T}_{el} and \hat{T}_{nu} . The third term $\hat{V}_{el,nu}$ represents the Coulomb attraction between an electron and a nucleus while the remaining two terms, $\hat{V}_{el,el}$ and $\hat{V}_{nu,nu}$, represent the repulsion between two electrons and two nuclei, respectively. The variable Z_A represents the atomic number of nucleus A, r_{ab} the distance between electron a and b, r_{aA} the distance between electron a and nucleus A, R_{AB} the distance between two nuclei, and ϵ_0 a constant: the permittivity of vacuum. The last three terms define the potential energy operator \hat{V} , which contains the interaction between the electrons and the nuclei, between the electrons, and between the nuclei. Relativistic effects including, spin-orbital couplings have not been considered in this work.

2.1.1 Born-Oppenheimer Approximation

The time-independent Schrödinger equation, eq. 2.1, is not solvable for a many-electron molecule. As a first step to circumvent this inability, the nuclear terms are separated from the electronic terms [2]. This is done by invoking the Born-Oppenheimer approximation [3]. The approximation takes into account the mass difference between the electron and the nucleus. Considering the lightest of all atoms, the hydrogen atom, the mass ratio of the nucleus to the electron is 1836, exemplifying this approximation. Furthermore, the lagging nuclei, due to this mass difference, are so slow in adapting to the change in the electronic configuration that the geometry of the nuclei can be considered fixed, when describing the electronic problem.

2.1.2 Electronic Schrödinger Equation

The consequence of the Born-Oppenheimer approximation is the ability to separate the motion of the electrons from that of the nuclei. Accordingly, the electronic Hamiltonian

$$\hat{H}_{el} = -\sum_{a} \frac{\hbar}{2m_e} \nabla^2 - \frac{1}{4\pi\epsilon_0} \left(\sum_{a} \sum_{b>a} \frac{e^2}{r_{ab}} \right)$$
 (2.3)

is the part of the molecular Hamiltonian given in eq. 2.2, which describes the electrons. The kinetic energy term for the nuclei as well as the nuclear repulsion, now a constant, are neglected. The electronic Schrödinger equation is then given as the following,

$$\hat{H}_{el} \left| \Psi_{el}(r_a; R_A) \right\rangle = E_{el}(R_A) \left| \Psi_{el}(r_a; R_A) \right\rangle, \tag{2.4}$$

where the electronic wave function, $|\Psi_{el}(r_a; R_A)\rangle$, depends directly on the electron coordinates, \mathbf{r}_a , and parametrically on the nuclear coordinates, \mathbf{R}_A , as do the electronic energies, $\mathbf{E}_{el}(\mathbf{R}_A)$.

It is the intendment of quantum chemical programs to solve the stationary Schrödinger equation, eq. 2.4. In doing so, the sum of the electronic energy, E_{el} (R_A) and the nuclear repulsion, $\hat{V}_{nu,nu}(R_A)$ at a specific nuclear configuration R_A provides a potential energy. The potential energy for a given electronic state - a point in the potential energy surface - is defined as

$$\hat{V}_{el}(R_A) = E_{el}(R_A) + \hat{V}_{nu,nu}(R_A)$$
(2.5)

A series of stationary points for different nuclear configurations will produce potential energy surfaces.

2.2 Solution to the Electronic Schrödinger Equation

Solving the electronic Schrödinger equation, eq. 2.4, for different nuclear coordinates produces a series of single point energies that can be connected to form potential energy surfaces.

It is essential to represent the electronic wave functions appropriately, such that the electronic energy approaches the exact value or in the case of multiple electronic states, that the relative energy between states is representative of the molecule. Of course solving this equation exactly is possible only for the simplest of molecules. So in order to solve these equations for larger molecules more approximations have to be made. The most fundamental of these approximations is the Hartree-Fock approximation.

2.2.1 Hartree-Fock

The Hartree-Fock (HF) method [4-6] is an approximation which determines the ground state energy and wave function for an N-electron system. It approximates the exact wave function as a single antisymmetrized determinant that is optimized by solving the Hartree-Fock equation iteratively, in a process known as the self-consistent field (SCF) method. The antisymmetrized determinant is termed a Slater determinant and from this point the theory will be expanded.

Slater Determinant

A Slater determinant is the simplest antisymmetrized wave function that can be used to describe the ground state of an N -electron system. The Slater determinant in its complete normalized form,

$$\Psi_0(X) = \frac{1}{\sqrt{N!}} \begin{vmatrix} \chi_1(X_1) & \chi_2(X_1) & \cdots & \chi_N(X_1) \\ \chi_1(X_2) & \chi_2(X_2) & \cdots & \chi_N(X_2) \\ \vdots & \vdots & \ddots & \vdots \\ \chi_1(X_N) & \chi_2(X_N) & \cdots & \chi_N(X_2) \end{vmatrix}$$
(2.6)

is described by single particle functions, $\chi(X)$, also known as spin orbitals, and the index from eq. 2.4 is dropped for clarity. A spin orbital is formed from the product of a spatial orbital, $\psi(r)$, which depends on the position of the electron, with a spin function, either an $\alpha(\omega)$ or a $\beta(\omega)$ spin

$$\chi_a(X_a) = \chi_a(r, \omega) = \psi(r). \begin{cases} \alpha(\omega) \\ \beta(\omega) \end{cases}$$
(2.7)

and is assumed to be orthonormal

$$\langle \chi_a | \chi_b \rangle = \delta_{ab} \tag{2.8}$$

According to the variational principle, the best wave function $\Psi_0(X)$ is the one that gives the lowest energy

$$E_0 = \left\langle \Psi_0(X) \left| \hat{H}_{el} \right| \Psi_0(X) \right\rangle. \tag{2.9}$$

The minimization of the energy when $\Psi_0(X)$ is a single determinantal wave function (eq. 2.6) leads to the Hartree-Fock equations.

Hartree-Fock equations

The minimization of the energy in eq. 2.9 is attainable by varying the spin orbitals. The Hartree-Fock equation

$$\hat{f}(X_a)|\chi(X_a)\rangle = \varepsilon_a |\chi(X_a)\rangle \tag{2.10}$$

is an eigenvalue equation whose solution provides the minimum energy, E_0 and consequently the optimal spin orbitals, $\chi(X_a)$. The Fock operator

$$\hat{f}(X_a) = \underbrace{\frac{\hbar}{2m_e} \nabla_a^2 - \sum_A \frac{Ze^2}{4\pi\epsilon_0 r_a A}}_{\hat{h}(X_a)} + \underbrace{\sum_b^N [\hat{J}_b(X_a) - \hat{K}_b(X_a)]}_{\hat{V}^{HF}(X_a)}$$
(2.11)

is defined by the single electron Hamiltonian or core Hamiltonian, denoted as $\hat{h}(X_a)$, and the effective Hartree-Fock potential operator $\hat{V}^{HF}(X_a)$. The effective Hartree-Fock potential is defined by two terms that result from the electron-electron repulsion term of eq. 2.2. The first term is the coulomb operator

$$\hat{J}_b(X_1) |\chi_a(X_1)\rangle = \left[\int dX_2 \chi_a^*(X_2) \frac{e^2}{4\pi\epsilon_0 \hat{r}_{12}} \chi_b(X_2) \right] |\chi_a(X_1)\rangle$$
 (2.12)

and is described classically as the interaction of one electron, in this case electron a, with the remaining N-1 electrons. The exchange operator

$$\hat{K}_b(X_1) |\chi_a(X_1)\rangle = \left[\int dX_2 \chi_b^*(X_2) \frac{e^2}{4\pi\epsilon_0 \hat{r}_{12}} \chi_a(X_2) \right] |\chi_b(X_1)\rangle$$
 (2.13)

is of purely quantum mechanical nature, i.e. it does not have a classical counterpart. The two-electron potential operator $1/r_{12}$ describes the interaction of electron 1 with electron 2. It is termed the exchange operator, as can be seen from eq. 2.13, where upon its application, the position and spin of electron a has been exchanged with that of electron b. The exchange of position and spin between two electrons can also be induced by the permutation operator, ρ_{12} , and a succinct form of the Fock operator can be written as

$$\hat{f}(X_1) = h(X_1) + \sum_{b \neq a}^{N/2} \int \hat{K}_b(X_1) |\chi_a(X_1)\rangle = \int dX_2 \chi_b^*(X_2) \frac{e^2}{4\pi\epsilon_0 \hat{r}_{12}} (1 - \rho_{12}) \chi_b(X_2)$$
 (2.14)

Restricted Closed-shell Hartree-Fock

To solve the Hartree-Fock equation, eq. 2.10, it is necessary to evaluate the form of the spin orbitals. For α and β spin orbitals, one can restrict the spatial part. Such spin orbitals are referred to as restricted spin orbitals and unrestricted when the spatial part is not restricted to be the same. The restricted case is given below,

$$\chi_{2i}(X) = \begin{cases} \psi_i(r)\alpha(\omega) \\ \psi_i(r)\beta(\omega) \end{cases} i = 1, 2, ..., K$$
 (2.15)

where the index runs from 1 to the maximum number of spatial orbitals K. Inserting this equation into the Hartree-Fock eq. 2.10 results in two separate Hartree-Fock equations,

$$\hat{f}(X_1) |\psi_i(r_1)\alpha(\omega_1)\rangle = \varepsilon_i |\psi_i(r_1)\alpha(\omega_1)\rangle \tag{2.16}$$

$$\hat{f}(X_1) |\psi_i(r_1)\beta(\omega_1)\rangle = \varepsilon_i |\psi_i(r_1)\beta(\omega_1)\rangle \tag{2.17}$$

defined in terms of their spin functions, $\alpha(\omega_a)$ and $\beta(\omega_a)$, and results in the orbital energy, ε_i . In order to obtain an expression exclusively in terms of the spatial orbitals, it is necessary to purge the Fock operator of the spin function. This is done by first replacing the spin orbital by its spatial orbital and spin functions.

Recognizing that in a closed-shell scenario, the results from the α terms are identical to those for β , it is sufficient to multiply eq. 2.16 from the left by $\alpha^*(\omega_a)$ and integrate over its spin

$$\int d\omega_1 \alpha^*(\omega_1) \hat{f}(X_1) |\psi_i(r_1)\alpha(\omega_1)\rangle = \varepsilon_i |\psi_i(r_1)\rangle$$
(2.18)

The closed-shell Fock operator has the following form

$$\hat{f}(r_1) = \hat{h}(r_1) + \sum_{a=1}^{N/2} (2\hat{J}_a(r_1) - \hat{K}_a(r_1), \tag{2.19}$$

where the sum over N is replaced by N/2, i.e. the number of α or β electrons. The Fock operator can be written in terms of the permutation operator and the spatial orbitals as

$$\hat{f}(r_1) = \hat{h}(r_1) + \sum_{a=1}^{N/2} \int dr_2 \psi_a^*(r_2) \frac{e^2}{4\pi\epsilon_0 \hat{r}_{12}} (2 - \rho_{12}) \psi_a(r_2)$$
(2.20)

The Coulomb and exchange operators are now defined with respect to the spatial orbitals and are analogous to equations 2.12 and 2.13, specifically

$$\hat{J}_a(r_1) |\psi_i(r_1)\rangle = \left[\int dr_2 \psi_a^*(r_2) \frac{e^2}{4\pi\epsilon_0 r_{12}^2} \psi_a(r_2) \right] |\psi_i(r_1)\rangle$$
 (2.21)

$$\hat{K}_a(r_1) |\psi_i(r_1)\rangle = \left[\int dr_2 \psi_b^*(r_2) \frac{e^2}{4\pi\epsilon_0 \hat{r}_{12}} \psi_i(r_2) \right] |\psi_b(r_1)\rangle$$
 (2.22)

Now that the Fock operator has been defined in terms of the spatial orbitals, the Roothaan-

Hall equations, which provide an algebraic method that aids in solving the Hartree-Fock equations, will be discussed.

Roothaan-Hall Equations

As seen from the previous section, the spatial orbitals were obtained by integrating out the spin functions. The Hartree-Fock eq. 2.10 can be rewritten in terms of these spatial orbitals,

$$\hat{f}(r_1) |\psi_i(r_1)\rangle = \varepsilon_i |\psi_i(r_1)\rangle. \tag{2.23}$$

where the wave function $|\psi_i(r_1)\rangle$ is a molecular orbital, and ε_i is the corresponding energy. For molecular systems, eq. 2.23 can not be solved analytically, but instead is converted into a set of algebraic equations by first introducing a set of known spatial functions, as introduced by Roothaan and Hall [7, 8].

The premise for the Roothaan-Hall equations is that the molecular orbitals can be expanded as a linear combination of known K one-electron functions,

$$|\psi_i\rangle = \sum_{\mu=1}^K C_{\mu i} |\phi_{\mu}\rangle \tag{2.24}$$

where the basis functions are denoted by the Greek indices and the molecular orbitals with Latin indices. Equation 2.24 can be inserted into eq. 2.23 and by multiplying from the left with ϕ_{ν}^{*} and integrating results in the following matrix equation

$$\sum_{\mu}^{K} C_{\mu i} \underbrace{\int dr_{1} \phi_{\nu}^{*}(r_{1}) \hat{f}(r_{1}) \phi_{\mu}(r_{1})}_{F_{\mu\nu}} = \varepsilon_{i} \sum_{\mu}^{K} C_{\mu i} \underbrace{\int dr_{1} \phi_{\nu}^{*}(r_{1}) \phi(r_{1})}_{S_{\mu\nu}}$$
(2.25)

The one-electron basis functions ϕ_{μ} are not necessarily orthogonal and therefore the matrix elements $S_{\nu\mu}$ describe the overlap between two functions, ν and μ , and form the $K \otimes K$ overlap matrix S. The Fock matrix F, also $K \otimes K$, is formed from the matrix elements $F_{\mu\nu}$.

Both matrices are Hermitian, for real orbitals, they are real and symmetric. This allows for the diagonalization of $S_{\nu\mu}$ via a unitary transformation. Equation 2.25 can be compactly written as

$$FC = SC\varepsilon \tag{2.26}$$

where the matrix C contains the coefficients for the molecular orbitals ψ_i in a column wise fashion, i.e. the first column gives the coefficients for ψ_1 , the second column those for ψ_2 , and the K^{th} column those for ψ_k . The energies of each molecular orbital are found in the diagonalized matrix ε .

Analyzing the one-electron Fock operator in eq. 2.20 by applying the expansion from eq. 2.24, it becomes apparent that the Fock matrix F depends on the coefficients, C. This deems the Roothaan-Hall equations nonlinear and in order to solve a nonlinear system an iterative approach is used: the self-consistent field procedure.

Self-consistent Field

The Self-consistent Field method was introduced by Hartree in 1928. It is used to solve the nonlinear Hartree-Fock equations iteratively [4] and has been applied to the nonlinear equations of Roothaan-Hall. This method begins by solving the non-linear equations with a guessed set of molecular orbital coefficients. Because the Fock operator also depends on these coefficients a new set of coefficients will be produced along with new energies. After each iteration the density matrix is compared to the previous one obtained and if it has not changed within a specified criterion then the procedure has reached self-consistency, and the iterative process is stopped. The Hartree-Fock energy for the ground electronic state is then given as

$$E_{HF} = \left\langle \Psi_0(X) \left| \hat{H}_{el} \right| \Psi_0(X) \right\rangle, \tag{2.27}$$

The accuracy of the Hartree-Fock energy lies in the size and quality of the basis set expansion of eqs. 2.24. The larger the basis set, of a particular quality, the more accurate are the

energies. If the basis set is consistently increased until the energy values do not change it is said that the Hartree-Fock limit has been reached.

Basis Sets and Natural Orbitals

The basis set used to expand the Hartree-Fock spatial orbitals (ψ_i see eq. 2.7) are typically a set of atomic functions, in a linear combination of atomic orbitals (LCAO), recall eq. 2.24

$$|\psi_i\rangle = \sum_{\mu=1}^K C_{\mu i} |\phi_{\mu}\rangle, \qquad (2.28)$$

The coefficients $C_{\mu i}$ are varied in order to minimize the energy and are known as molecular orbital expansion coefficients. The atomic orbitals ϕ_{μ} were initially introduced as a set of Slater-type orbitals (STO) which are proportional to $e^{-\xi r}$. When evaluating the two electron integrals, see eqs. 2.12 and 2.13, STO orbitals are very cumbersome. Gaussian-type orbitals (GTO) are proportional to $e^{-\xi r^2}$, and due to the property that the multiplication of two 1s Gaussian orbitals produces another 1s Gaussian orbital their use as a basis simplifies the evaluation of the two electron integrals. Boys proposed to use a linear combination of Gaussian-type functions to represent the STO [10]. Since that time, there has been a wide development of different types of basis sets, and for a comprehensive overview the reader is referred to [11, 12]. The calculations presented in this work were performed using the MOL-CAS [13] package. The basis sets employed are the atomic natural orbitals (ANOs) [14, 15], chosen for their accuracy and compactness which tends to reduce the computational time [16, 17]. They are compact as they are near-optimum correlating functions for the atomic problem and therefore are good functions to describe molecular electron motion as well.

2.2.2 Configuration Interaction (CI)

Although HF theory captures more than \sim 99% of the total energy of a system, the remaining \sim 1% is frequently very critical for chemical problems. This correlation energy, E_{corr}

$$E_{corr} = E_{exact} - E_{HF} \tag{2.29}$$

is defined as the energy difference between the exact energy E_{exact} ($\equiv E_{el}$ from eq. 2.4), within the bounds of the Born-Oppenheimer approximation, and the Hartree-Fock energy EHF. This "missing" energy is negative due to the Hartree-Fock energy defining an upper bound to the energy. The most common classes of electron correlation methods are derived from configuration interaction (CI) theory, many-body perturbation theory (MBPT) and coupled cluster (CC) theory.

The correlation energy is often separated into two parts, a short range effect arising due to the reduction in probability of two electrons coming together, and a long range effect which among other things is responsible for electrons proceeding correctly to their atoms as the molecule dissociates.

The first part is referred to as dynamic correlation. This is associated with the necessity of including the inter-electronic distance r_{ij}^{-1} in accurate wave function. In 1957, Kato explained that many-electron wave functions must exhibit cusps in regions where the coordinates of two electrons coalesce [18]. However, for determinantal wave functions this condition is never fully achieved, and with finite basis sets, such wave functions exhibit minima at $r_{ij} = 0$. Nevertheless, as the basis set approaches completeness, the curvature of the correlated wave function around the coalescence point increases and thereby it approximates better and better the true nature of the "cusp"

The second part is called static correlation. Many times also referred to as non-dynamic correlation or near-degeneracy correlation. When non-dynamical correlation is weak, Hartree-Fock theory already provides a qualitatively correct description of the wave function. Under such circumstances, which, fortunately, apply for the majority of molecules in their ground state near equilibrium geometry, one may use single-reference methods for representing the dynamical correlation effect. These methods build on the SCF reference determinant, typically using perturbative ansatz to define classes of configurations or excitations deemed to

be of most importance in constructing an approximate correlated wave function. For most excited states, for molecules that are close to dissociation, and for situations in which there is near electronic degeneracy, Hartree-Fock is a poor approximation.

Static correlation effects often mean that there is no single Slater determinant that dominates the wave function, and perturbative or other approaches that assume a good single-reference starting point are doomed to failure. Under such circumstances, a viable way forward is to first deal with the static correlation problem using a CI expansion that covers all the important effects.

The lack of accounting for instantaneous dynamical correlation between electrons and the inadequacies of a single Slater determinant reference are significant enough to warrant the development of other more sophisticated approaches that go beyond single determinantal wave functional approaches.

HF theory provides the best single Slater determinant wave function for a given oneparticle basis set. The other component of this problem is the n-particle problem, which deals with the correlation of electrons. One way to account for the correlation energy is to expand the exact electronic wave function in terms of a linear combination of Slater Determinants as just mentioned above.

From the Hartree-Fock description, a set of 2K spin orbitals can be produced that describe a single determinant ground-state wave function for the N electrons.

$$|\Psi_0\rangle = |\chi_1\chi_2\chi_3...\chi_a\chi_b...\chi_N\rangle \tag{2.30}$$

The configuration of the N electrons is such that the lower energy spin orbitals are occupied and the higher energized 2K - N virtual orbitals are not, following a basic Aufbau principle. It is clear however, that many other determinants can be formed from the many different possible excitations of the electrons.

Excited determinants can be described with respect to the HF determinant. Didactically, a singly excited determinant

$$|\Psi_a^r\rangle = |\chi_1\chi_2\chi_3....\chi_r\chi_b....\chi_N\rangle \tag{2.31}$$

is one in which a single electron is relocated from its occupied spin orbital a to one of the virtual spin orbitals r. And in the same manner a doubly excited determinant can be formed

$$|\Psi_{ab}^{rs}\rangle = |\chi_1\chi_2\chi_3....\chi_r\chi_s....\chi_N\rangle \tag{2.32}$$

where two electrons have been relocated from their original positions, a and b, to two virtual spin orbitals, r or s. This procedure continues until all N electrons have been promoted to various virtual states. The number of possible determinants is defined by the binomial coefficient and are termed accordingly to the number of electrons that have been promoted to virtual orbitals: Hartree-Fock ground state, singly, doubly, triply, ... N-tuply excited states. The full-CI expansion of the ground-state wave function

$$|\Phi_0\rangle = |\Psi_0\rangle + \sum_{ar} |\Psi_a^r\rangle + \sum_{a>b}^{r>s} |\Psi_{ab}^{rs}\rangle + \sum_{a>b>c}^{r>s>t} |\Psi_{abc}^{rst}\rangle + \dots$$
 (2.33)

is a sum of the unique possible configurations, organized above in terms of the N-electron determinants, and is exact for a given basis. Most electron correlation methods differ in the way that they determine the weights or coefficients of these excited states in the expansion.

The full CI wave function can be reduced in size based on symmetry properties. If the state that is being calculated is a singlet state of gerade symmetry, then only the configurations that share those same properties are used. In order for the configurations to be eigenfunctions of the spin and angular momentum operators, a new configuration can be generated from a linear combination of the original configurations. These configurations are termed configuration state functions (CSF). A CI calculation that is based on these considerations is still termed a full-CI, and is the best calculation one can do to recover the correlation energy.

Therefore, the molecular problem would have two dimensions - one on each of the one - and n-particle basis. As shown below, one would have to increase both the one- and n-particle basis to get to the exact answer within the non-relativistic Born-Oppenheimer approximation as shown below in the figure 2.1.

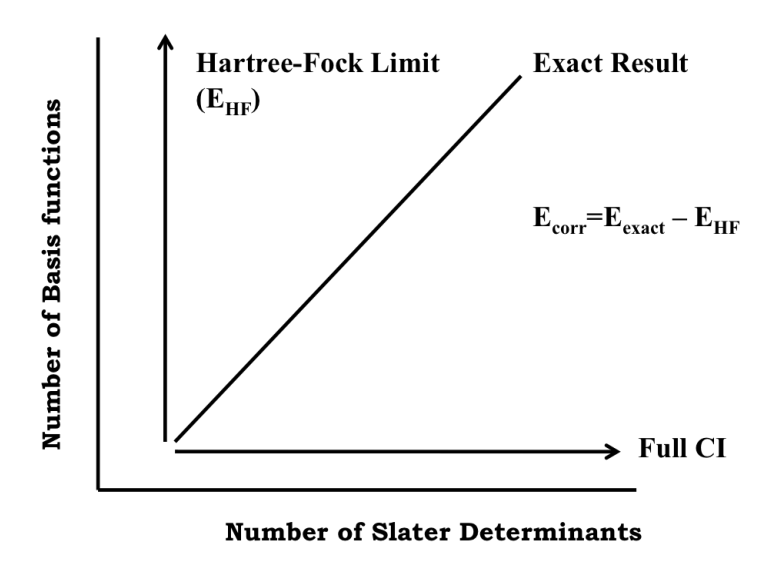


Figure 2.1: A graphical representation of the two-dimensional problem of electron correlation.

Even if the CI wave function is represented by symmetry adapted CSFs, for larger molecules a full CI calculation is computationally impossible. It is for this reason that the CI calculation is truncated. The most common truncation is one of singles and doubles, a CISD calculation. The single configurations play an insignificant role in the determination of the correlation energy [19] but are significant in the determination of the dipole moments [20] and the double configurations tend to account for the major part of the correlation energy but are highly dependent on the basis size [1]. For larger molecules a CISD calculation is not sufficient in describing the correlation energy and the calculations can incorporate further triplet and quadruplet excitations, again at the cost of computational effort. Another shortcoming of this method is that once the CI expansion has been truncated the method is no longer size consistent nor size extensive. These two terms become important while

understanding and discussing the importance of multiconfigurational methods.

Size consistency and Size extensivity:

Size consistency and size extensivity are two important concepts in electronic structure theory. Often in literature these two terms are used interchangeably. But there are very important distinctions between them. There are two primary definitions of size consistency in use. The first was employed by Pople [21] as one criterion for a well-constructed quantum chemical method. If we imagine two molecules H_2 , separated by a large distance (large enough that we may consider them to be non-interacting) then the energy calculated for both molecules simultaneously should be exactly twice that calculated for only one, isolated molecule of H_2 , just like the exact energy. This "non-interacting limit" description is the original concept of size consistency. From this perspective, size consistency describes what has been referred to as the "additive separability" of the wave function. However, a more recently imposed definition [22] requires that the method not only correctly describe the fragmentation limit, but the entire process (in a qualitative sense). That is, the entire potential energy curve mapped out when we bring our two non-interacting H_2 molecules close together must be correctly described as well. For example, both spin-unrestricted Hartree-Fock (UHF) and spin-restricted Hartree-Fock (RHF) wave functions are size-consistent for the separated H_2 dimer system described above. However, for a closed-shell molecule dissociating into open-shell fragments, a RHF wave function does not conform to the second definition of size consistency, as we will discuss further below.

Size extensivity is a mathematically formal characteristic, which refers to the correct (linear) scaling of a method with the number of electrons. The term was introduced to electronic structure theory by Bartlett [23] and is based on analogous "extensive" thermodynamic properties. Hartree-Fock method qualifies as size-extensive, as well as many-body perturbation theory and coupled-cluster theories. Truncated configuration interaction methods, however, are not size-extensive. An important advantage of a size-extensive method is that it allows straightforward comparisons between calculations involving variable numbers of electrons, e.g. ionization processes or calculations using different numbers of active electrons. Lack of

size extensivity implies that errors from the exact energy increase as more electrons enter the calculation.

Size extensivity and size consistency are not mutually exclusive properties, by any means. At the non-interacting limit, size extensivity of a method is a necessary and sufficient condition to ensure size consistency, implying that the former is more general than the latter. However, size extensivity does not ensure correct fragmentation. For example, we may consider two different fragmentation processes for N_2 :

$$N_2(^7\sum_u^+) \to 2N(^4S)$$

and
 $N_2(^1\sum_u^+) \to 2N(^4S)$

The first process is correctly described by both RHF and UHF wave functions, and hence, both methods are size-consistent. However, the second process is not correctly described by a RHF wave function (and, therefore, perturbation theory and coupled-cluster theory methods which use this as a reference will not be size-consistent.) Both RHF and UHF are always size-extensive, though. This implies, then, that size consistency is more general than size extensivity, but this is also incorrect. At non-interacting limits, size extensivity is a more general property, and its existence implies that of size consistency. However, size consistency has the additional requirement of correct fragmentation that is not necessarily dependent on the mathematical scaling of the energy. Chapter 1 of the review by Taylor [22] deals explicitly with these concepts.

2.2.3 Multi-configurational Self-consistent Field

The truncated CI formalism gives rise to both these problems of size extensivity and size consistency. A truncated CI calculation optimizes the CI expansion coefficients c, see eq. 2.35. An extra flexibility in the quest to retrieve the correlation energy is obtained by allowing for the optimization of the molecular orbital coefficients, eq. 2.24, and accounts for what is termed static correlation. This is the essence of the multi-configurational self-consistent field (MCSCF) method.

The MCSCF method is also based on the variational principle, in which the minimization of the energy,

$$\frac{\left\langle \Psi^{MCSCF} \left| \hat{H} \right| \Psi^{MCSCF} \right\rangle}{\left\langle \Psi^{MCSCF} \middle| \Psi^{MCSCF} \right\rangle} \tag{2.34}$$

is found by varying the orbital coefficients - an optimization of the MCSCF wave function.

The MCSCF wave function is a truncated CI expansion and is given equationally as

$$\left|\Psi^{MCSCF}\right\rangle = \sum_{A} c_A \left|\Phi_A\right\rangle \tag{2.35}$$

where the index A runs over the configuration state functions $\Phi_A = |\psi_a \bar{\psi}_a \psi_b \bar{\psi}_b \dots \rangle$. Each state function is composed of a set of molecular orbitals that are occupied by an α spin electron ψ_i or by a β spin electron $\bar{\psi}_i$. These MOs can also be expanded in a basis of atomic orbitals as

$$|\psi_i\rangle = \sum_{\lambda=1}^K C_{\lambda i} |\phi_{\mu}\rangle \tag{2.36}$$

giving rise to another set of coefficients $C_{\mu i}$. It is the task of MCSCF to optimize all the CI expansion coefficients c_A , as well as the molecular orbital coefficients $C_{\mu i}$ for the atomic orbitals simultaneously.

Aside from the optimization of two sets of coefficients, another difficulty that remains in the MCSCF method is the choice of the CSFs that should be used to describe the wave function. It is imperative to include the CSFs that are most important to the wanted molecular properties. The daunting task of choosing the appropriate CSFs to be included in the MCSCF wave function has been alleviated to some extent by employing the complete active space self-consistent field approach.

Complete Active Space Self-consistent Field (CASSCF)

The complete active space self-consistent field method is a descendant of MCSCF and has been developed by Roos et al. [24]. The method prevents the manual picking of every configuration state function which should be included in the optimization of the wave function. Instead, the molecular orbitals are partitioned into two groups: the primary and secondary orbitals, as can been seen in fig. 2.2. The primary orbitals are further partitioned into two subgroups; the inactive and the active orbitals. The inactive orbitals are constrained to be doubly occupied throughout the calculation and the secondary or virtual orbitals remain unoccupied. The active orbitals consist of a combination of occupied and unoccupied orbitals whose occupation number is allowed to smoothly vary from 0 to 2. This in principle, would accommodate every possible configuration, with consideration of symmetry and spatial constraints. CASSCF therefore constitutes a full-CI calculation within the restricted complete active space.

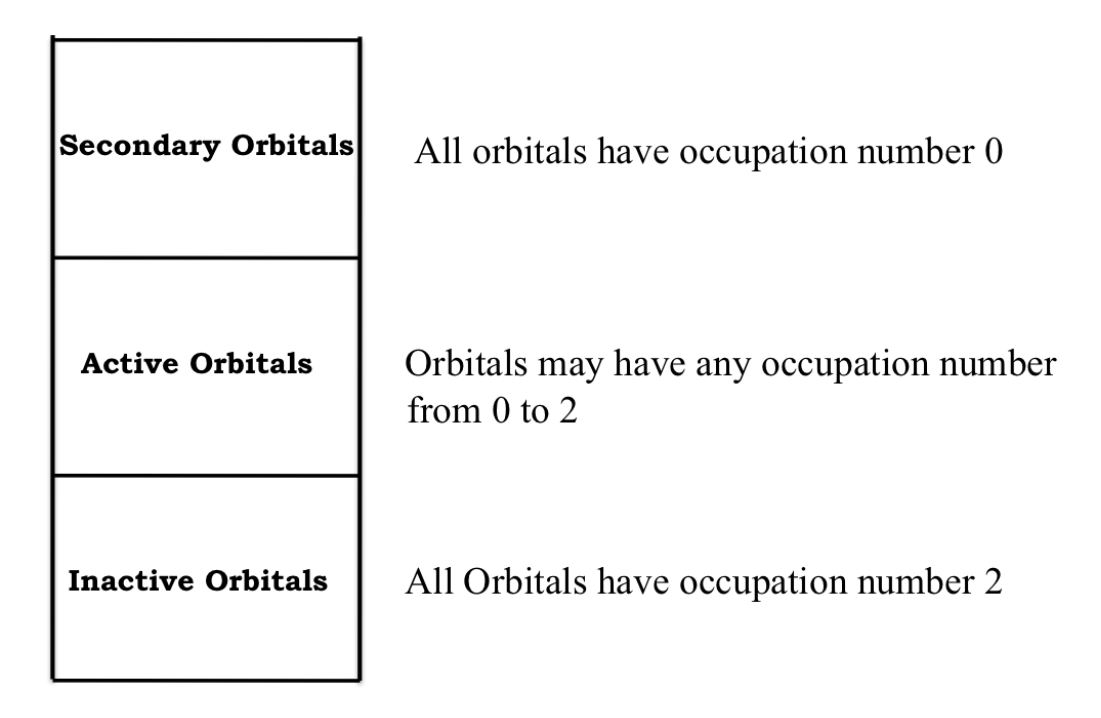


Figure 2.2: A schematic representation of the orbital classification in the CASSCF method.

In this way, an active space defines the realm in which the electrons can form all configurations. Although this method reduces the difficulty of picking the CSFs, it is still not a black box. The proper orbitals that represent the molecular system and its properties must be selected by hand. A state average CASSCF (SA-CASSCF) formulation is used to calculate electronic excited states for a given symmetry and spin, by minimizing the weighted sum of their energies. The result of the minimization is the procurement of the CASSCF wave function Ψ^{CASSCF} as well as the energy E^{CASSCF} for each electronic state i. The method is good at obtaining the static correlation by allowing for partially occupied orbitals and describes well values at dissociation but it has difficulties in recovering the dynamic correlation, i.e. the correlation of electron motion. The dynamic correlation can be accounted for either perturbationally via a CASPT2 calculation or variationally via a multireference configuration interaction (MRCI), where the former is used in this work.

Complete Active Space and the 2nd Order Perturbation Theory (CASPT2)

A standard approach used to recover at least part of the dynamical correlation energy is the Møller and Plesset [25] method, which is size extensive and size consistent [26].

This aspect, together with the fact that it is very efficient at low orders has made the method very popular over limited CI approaches. These properties have become strong motivations for the development of more advanced approaches in perturbation theory. The method is based on perturbation theory where the Hamiltonian operator \hat{H} is split into two parts: a part that is solvable \hat{H}_0 , the zeroth-order Hamiltonian and a part which is not $\lambda \hat{V}$, the perturbation.

$$\hat{H} |\Psi_i\rangle = (\hat{H_0} + \lambda \hat{V}) |\Psi_i\rangle = E_i |\Psi_i\rangle \tag{2.37}$$

The eigen energies and eigenfunctions can be expanded as a Taylor series for small perturbations to the system $\lambda \ll 1$,

$$|\Psi_i\rangle = \left|\Psi_i^{(0)}\right\rangle + \lambda \left|\Psi_i^{(1)}\right\rangle + \lambda^2 \left|\Psi_i^{(2)}\right\rangle + \dots$$
 (2.38)

$$E_i = E_i^{(0)} + \lambda E_i^{(1)} + \lambda^2 E_i^{(2)} + \dots$$
 (2.39)

where λ is an ordering parameter. Once the eqs. 2.38, 2.39 are inserted into the eigenvalue equation, eq. 2.37, the terms can be ordered according to λ and the following energy corrections up to II order are retrieved.

$$E_i^{(0)} = \left\langle \Psi_i^{(0)} \middle| \hat{H}_0 \middle| \Psi_i^{(0)} \right\rangle \tag{2.40}$$

$$E_i^{(1)} = \left\langle \Psi_i^{(0)} \middle| \hat{V} \middle| \Psi_i^{(0)} \right\rangle \tag{2.41}$$

$$E_i^{(2)} = \left\langle \Psi_i^{(0)} \middle| \hat{V} \middle| \Psi_i^{(1)} \right\rangle \tag{2.42}$$

If the unperturbed Hamiltonian is replaced by a sum of one-electron Fock operators, as suggested by Møller and Plesset [25], it can be shown that the first energy correction term is already included in the Hartree-Fock energy. Therefore, it is the second order energy term in eq. 2.38 that accounts for the dynamical correlation that is missing from the Hartree-Fock; this formalism is named as second order perturbation theory (PT2).

Analogously, the dynamical correlation energy that is missing from a CASSCF calculation can be retrieved in part by applying perturbation theory [27]. The reference wave function is taken as the SA-CASSCF wave function $|\Psi_i^{CASSCF}\rangle$ for a particular electronic state i. The CASPT2 wave function, $|\Psi_i^{CASPT2}\rangle$, is a sum of the reference wave function, $|\Psi_i^{CASSCF}\rangle$, with the first order perturbative wave function, $|\Psi_i^{Pert}\rangle$

$$\left|\Psi_{i}^{CASPT2}\right\rangle = \left|\Psi_{i}^{CASSCF}\right\rangle + \left|\Psi_{i}^{pert}\right\rangle \tag{2.43}$$

As was seen in eq. 2.42, the second order energy correction depends on the first order wave function. For this purpose, the second order perturbation to the effective energy matrix elements, ε_{ii} , can be defined as

$$\varepsilon_{ii} = \left\langle \Psi_i^{CASSCF} \middle| \hat{V} \middle| \Psi_i^{pert} \right\rangle \tag{2.44}$$

and the complete CASPT2 energy for the electronic state i

$$E_i^{SS-CASPT2} = E_i^{CASSCF} + \varepsilon_{ii} \tag{2.45}$$

is then given as a sum of the reference energy, E_i^{CASSCF} with the second order energy correction, ε_{ii} . This single state (SS) CASPT2 energy, $E_i^{SS-CASPT2}$, refers to each electronic state i. The SS-CASPT2 calculation also has its limitations. The CASSCF wave function is inadequate in describing the states around avoided crossings and where erroneous valence-Rydberg mixing occur, and therefore the multi-state CASPT2 (MS-CASPT2) was developed [28].

The MS-CASPT2 method [28] is able to describe well the near degenerate electronic states and is also able to differentiate the valence from the Rydberg states, see e.g. refs. [28, 29, 30]. Instead of using a CASSCF wave function, the method uses a "Perturbation Modified CASSCF" wave function Ψ_i^{PMCAS} as the reference function: a linear combination of the CASSCF reference wave functions. Within this formulation, the Hamiltonian is reformulated with the addition of reference states and is termed the effective Hamiltonian

$$H_{ij}^{eff} = E_i^{CASSCF} \delta_{ij} + \frac{1}{2} (\varepsilon_{ij} + \varepsilon_{ji})$$
 (2.46)

where the diagonal elements are the SS-CASPT2 energies and the off-diagonal elements are the couplings between CASSCF electronic states i and j. This allows for the simultaneous treatment of all the electronic states being calculated and can account for a substantial amount of dynamic correlation energy. The final energies are obtained by diagonalizing the effective Hamiltonian H_{ij}^{eff} .

The MS-CASPT2 wave function is then

$$\left|\Psi_{i}^{MS-CASPT2}\right\rangle = \underbrace{\sum_{t} C_{ia} \left|\Psi_{a}^{CASSCF}\right\rangle}_{\Psi_{i}^{PMCAS}} + \left|\Psi_{i}^{pert}\right\rangle \tag{2.47}$$

where C_{ia} are determined by diagonalizing the effective Hamiltonian (eq. 2.46).

An alternative to the CASSCF method called Restricted Active Space (RAS) SCF method exists which will be discussed in detail and the second order perturbation theory using the RASSCF wave function as a reference function will be described in Chapter 3.

Bibliography

- [1] A. Szabo and N. S. Ostlund. Modern Quantum Chemistry: Introduction to Advanced Electronic Structure Theory. McGray-Hill, New York (1989).
- [2] I. N. Levine. Quantum Chemistry. Prentice Hall, New Jersey (2000).
- [3] M. Born and R. Oppenheimer. Zur Quantentheorie der Molekeln. Ann. Phys., 84, 457 (1927).
- [4] D. R. Hartree. The Wave Mechanics of an Atom with a Non-coulomb Central Field. Part I Theory and Methods. Proc. Cambridge Phil. Soc., 24, 89 (1928).
- [5] D. R. Hartree. The Wave Mechanics of an Atom with a Non-coulomb Central Field. Part II Some Results and Discussion. Proc. Cambridge Phil. Soc., 24, 111 (1928).
- [6] V. A. Fock. Zur SchrÖdingerschen Wellenmechanik. Zeitschrift fur Physik, 38, 242 (1926).
- [7] C. C. J. Roothaan. New Developments in Molecular Orbital Theory. Rev. Mod. Phys., 23, 69 (1951).
- [8] G. G. Hall. The Molecular Orbital Theory of Chemical Valency. VIII A Method of Calculating Ionization Potentials. Proc. Roy. Soc. (London), A205, 541 (1951).
- [9] J. A. Pople and R. K. Nesbet. Self-consistent Orbitals for Radicals. J. Chem. Phys., 22, 571 (1954).

[10] S. F. Boys. Electronic Wave Functions I. A General Method of Calculation for the Stationary States of any Molecular System. Proc. Roy. Soc., A200, 542 (1950).

- [11] E. R. Davidson and D. Feller. Basis Set Selection for Molecular Calculations. Chem. Rev., 4, 681 (1986).
- [12] F. Jensen. Computational Chemistry. Wiley, Chichester (1999).
- [13] Karlström, G.; Lindh, R.; Malmqvist, P.-Å.; Roos, B. O.; Ryde, U.; Veryazov, V.; Widmark, P. O.; Cossi, M.; Schimmelpfennig, B.; Neogrady, P.; Seijo, L., Comput. Matl. Sci. 2003, 28 (2), 222-239.
- [14] J. Almlof and P. R. Taylor. General Contraction of Gaussian Basis Sets. I. Atomic Natural Orbitals for First- and Second-row Atoms. J. Chem. Phys., 86, 4070 (1987).
- [15] C. W. Bauschlicher, and P. R. Taylor. Atomic Natural Orbital Basis Sets for Transition Metals. Theoret. Chimica Acta, 86, 13 (1993).
- [16] A.C.Hurley. Electron Correlation in Small Molecules. Academic, London (1976).
- [17] I. Shavitt. Methods of Molecular Electronic Structure Theory. Plenum, New York (1977).
- [18] T. Kato, Commun. Pure Appl. Math. 10, 151 (1957).
- [19] B. J. Rosenberg and I. Shavitt. Ab Initio SCF and CI Studies on the Ground State of the Water Molecule. I. Comparison of CGTO and STO Basis Sets Near the Hartree-Fock Limit. J. Chem. Phys., 63, 2162 (1975).
- [20] F. Grimaldi, A. Lecourt and C. Moser. The Calculation of the Electric Dipole Moment of CO. Int. J. Quantum Chem., S1, 153 (1967).
- [21] J. A. Pople, J. S. Binkley, and R. Seeger, Int. J. Quantum Chem., Symp. 10, 1 (1976).
- [22] P. R. Taylor, Lecture Notes in Quantum Chemistry: European Summer School (Springer-Verlag, Berlin, 2007), pp. 317.
- [23] R. J. Bartlett, Ann. Rev. Phys. Chem. 32, 359 (1981).

[24] B. O. Roos and P. R. Taylor. A Complete Active Space SCF Method (CASSCF) Using a Density Matrix Formulated Super-CI Approach. Chem. Phys., 48, 157 (1980).

- [25] C. Møller and M.S.Plesset. Note on an Approximate Treatment for Many-electron Systems. Phys. Rev., 46, 618 (1934).
- [26] D. M. Hirst. A Computational Approach to Chemistry. Blackwell Scientific Publications, Oxford (1990).
- [27] K. Andersson, P. A. Malmqvist and B. O. Roos. Second-order Perturbation Theory with a Complete Active Space Self-consistent Field Reference Function. J. Chem. Phys., 96, 1218 (1992).
- [28] J.Finley, P.Malmqvist, B.O.Roos and L.Serrano-Andres. TheMulti-state CASPT2 Method. Chem. Phys. Lett., 288, 299 (1998).
- [29] L. Serrano-Andres, M. Merchan, I. Nebot-Gil, R. Lindh and B. O. Roos. Towards an Accurate Molecular Orbital Theory for Excited States: Ethene, Butadiene, and Hexatriene. J. Chem. Phys., 98, 3151 (1993).
- [30] R. Crespo, M. Merchan and J. Michl. Electronic Excitation in Saturated Chains: An MS-CASPT2 Treatment of the Anti Conformer of n-tetrasilane. J. Phys. Chem., 104, 8593 (2000).

Chapter 3

The Restricted Active Space followed by Second Order Perturbation Theory Method: Theory and Application to the study Cu₂O and Cu₂O₂ Systems

Per Åke Malmqvist¹, Kristine Pierloot ², Abdul Rehaman Moughal Shahi ³, Christopher J. Cramer⁴ and Laura Gagliardi³

Published in Journal of Chemical Physics, 128 (20), 2008, p204109

¹Department of Theoretical Chemistry, University of Lund P.O.B 124 S-221 00 Lund, Sweden

²Department of Chemistry, University of Leuven, Celestijnenlaan 200 F, bus 2404, B-3001 Leuven, Belgium

³Department of Chemistry, University of Geneva, 30 quai E. Ansermet, Geneva 1211, Switzerland

⁴Department of Chemistry and Supercomputing Institute, University of Minnesota, 207 Pleasant, St. SE. Minneapolis, Minnesota 55455-0431, USA

The Restricted Active Space followed by Second Order Perturbation Theory Method: Theory and Application to the study Cu₂O and Cu₂O₂ Systems

A multireference second-order perturbation theory using a restricted active Space self-consistent field wave function as reference (RASPT2/RASSCF) is described. This model is particularly effective for cases where a chemical system requires a balanced orbital active space that is too large to be addressed by the complete active space self-consistent field (CASSCF) model with or without second-order perturbation theory (CASPT2). Rather than permitting all possible electronic configurations of the electrons in the active space to appear in the reference wave function, certain orbitals are sequestered into two subspaces that permit a maximum number of occupations or holes, respectively, in any given configuration, thereby reducing the total number of possible configurations. Subsequent second-order perturbation theory captures additional dynamical correlation effects. Applications of the theory to the electronic structure of complexes involved in the activation of molecular oxygen by mono- and binuclear copper complexes are presented. In the mononuclear case, RASPT2 and CASPT2 provide very similar results. In the binuclear cases, however, only RASPT2 proves quantitatively useful owing to the very large size of the necessary active space.

3.1 Introduction

Accurate treatment of electron correlation is of paramount importance when *ab initio* quantum mechanical methods are applied to realistic chemical problems. Many chemical systems, especially those containing transition metals and heavier elements, cannot be well described using methods that depend upon a single determinantal Hartree-Fock (HF) reference wave function (a problem which can also diminish the utility of the Kohn-Sham formulation of density functional theory (DFT)). Instead, a multideterminantal approach is needed, where the wave function is described as a combination of different electronic configurations. One of the most successful multideterminantal approaches is to determine a reference wave function with the Complete Active Space Self Consistent Field (CASSCF) method, and then account

3.2. METHOD 45

for additional electron correlation effects using multiconfigurational second order perturbation theory (CASPT2). The CASSCF/CASPT2 method has been demonstrated to provide accurate results for ground and electronically excited states of molecules containing atoms throughout the entire periodic table [1, 2, 3, 4, 5, 6, 7]. While in principle it can be applied to every type of electronic problem, there is a practical limitation associated with the size of the active space employed in the CASSCF model (see Method, 3.2 section).

We here describe an extension of the CASSCF/CASPT2 method, namely, the Restricted Active Space (RAS)SCF/RASPT2 method. The RASSCF/RASPT2 model permits larger active spaces to be employed for the reference wave function and thus extends the range of multiconfigurational wave function methods to a wider variety of chemical problems. We note that Celani et al. [8] have previously described a model (CIPT2) having a similar motivation in which excitations solely from the active space are treated by multireference configuration interaction (MRCI) while all other excitations are treated by second-order multi-reference perturbation theory. We anticipate that both models will serve as useful foundations for future development. Other MR perturbation theory models have been developed by Dyall [9], Schmidt et al. [10], Witek et al. [11], and Angeli et al. [12].

The remainder of the paper is organized as follows: In Section 3.2 the new methodology is described. In Section 3.3 we present applications of the new model to supported CuO_2 and CuO_2 systems, where it is challenging or impossible to apply conventional CASSCF/CASPT2. Some final discussion of future possible improvements in the theory is provided in Section 3.4.

3.2 Method

3.2.1 The CASSCF/CASPT2 Model

The CASSCF/CASPT2 model has been described previously in detail [13, 14] (and references therein). We shall review here only those aspects of the method most relevant to its extension to the RAS implementation.

In a CASSCF wave function, the initial molecular orbital space (which may be taken from a HF calculation, for example) is divided into three subspaces: inactive, active, and external (see Figure 3.1). The inactive orbitals are assumed to be doubly occupied in all configuration state functions (CSFs) that are used to build the multiconfigurational wave function. The external orbitals are assumed to be unoccupied in all such CSFs. The remaining active orbitals include both occupied and virtual orbitals from the original MO space, and the number of electrons included in the active space is dictated by the number present in the occupied orbitals that are assigned to it. All CSFs having a given spatial and spin symmetry that can be formed from assignment of the active electrons to orbitals within the active space are included in the multiconfigurational wave function. The inactive orbitals then constitute a Hartree-Fock "sea" in which the active orbitals and CSF expansion coefficients variationally relax. This is the concept of the Complete Active Space (CAS) introduced by Roos in the 80's [15, 16].

	1
VIRTUAL	All orbitals have occupation number 0
RAS3	Orbitals may have any occupation number from 0 to 2, but the maximum number of electrons in the space is limited to <i>n</i>
RAS2	Orbitals may have any occupation number from 0 to 2
RAS1	Orbitals may have any occupation number from 0 to 2, but the maximum number of holes in the space is limited to <i>n</i>
INACTIVE	All orbitals have occupation number 2

Figure 3.1: A schematic representation of the orbital classification in the CASSCF method.

Choosing the "correct" active space for a specific application is by no means trivial; often the practitioner must "experiment" with different choices in order to assess adequacy and convergence behavior. While every chemical system poses its own challenges, certain rules of thumb apply. For example, in a chemical reaction where a bond is formed/broken, all of the 3.2. METHOD 47

orbitals involved in the bond must be included in the active space, as well as antibonding orbitals that typically contribute significantly to correlating the bonding electrons. Similarly, when several electronic states are under consideration, all those molecular orbitals involved in electronic excitations that connect the states must be included in the active space. More detailed considerations on the construction of multiconfigurational (MC)SCF wave functions in general [10] and for the special case of transition metal compounds [17, 18] may be found in the literature. Practical issues associated with memory and disk storage limit the size of the active space in modern software packages to about 15 electrons in 15 orbitals, which is on the order of 1 to about 16 million CSFs depending on spin and spatial symmetry. This restriction on active space size is the most severe limitation of the CASSCF (and subsequent CASPT2) model and renders it inapplicable to systems where a larger active space is chemically necessary.

When the active space has been adequately chosen, the CASSCF wave function will include the most important CSFs in the full CI wave function. In particular, it includes all near-degenerate configurations, which describe static, non-dynamical, correlation effects, as found for example in bond-breaking processes. The CASSCF wave function can thus exhibit qualitatively correct behavior over an entire chemical process, e.g., mapping the potential energy surface for a chemical reaction or studying a multi-state photochemical conversion. Nevertheless, computed CASSCF energies are typically not very accurate, as smaller active spaces fail to include those CSFs that are important for capturing remaining dynamical correlation effects. Thus, including non-dynamical correlation is as important for quantitative accuracy in the multiconfigurational approach as it is in cases where the HF single-determinantal approximation is applicable.

How can dynamical electron correlation be included? One method that has been used with some success is multireference configuration interaction (MRCI), where the most important CSFs of the CAS wave function are used as a multiconfigurational reference in a CI expansion that includes additional CSFs generated by single, double, or higher excitations from occupied orbitals of the reference to inactive orbitals [19]. This method, however, quickly demands enormous computational resources for systems with many electrons and also fails to be size-extensive, although this latter problem can be corrected for in an approximate fashion [20].

In a single configuration approach, the preferred choices for including dynamical correla-

tion derive from size-extensive many body theory and include coupled cluster (CC) methods or, if the system is too large, less demanding approximations like second order perturbation theory. Møller-Plesset second-order perturbation theory (MP2) has long been used to estimate electron correlation for single determinantal ground states, and is known to give reasonably accurate results for structural, energetic, and other properties of molecular ground states when a single determinantal reference is appropriate. The idea of using second order perturbation theory with a multiconfigurational wave function was first suggested soon after the introduction of the CASSCF method [21] and a full implementation was accomplished in the late 1980's [22, 23]. The resulting CASPT2 model is computationally more efficient than MRCI and is now the most widely used method to compute dynamical electron correlation effects for multiconfigurational (CASSCF) wave functions.

The principle is simple: one computes the second order energy with a CASSCF wave function as the zeroth order approximation. That said, there are some issues in the multiconfigurational case that do not arise for single determinantal MP2. In particular, one needs to define a zeroth order Hamiltonian for which the CASSCF wave function is an eigenfunction, just as in MP2 the single-determinantal HF wave function is an eigenfunction of the Hamiltonian defined as the sum of one-electron Fock operators. The multiconfigurational zeroth-order Hamiltonian should preferably also be a one-electron operator in order to avoid too complicated a formalism. We next address those technical features of CASPT2 that are relevant to the current implementation of RASPT2.

We seek an approximate Hamiltonian $\widehat{H}^{(0)}$, such that the root function $\Psi^{(0)}$ is an unperturbed eigenfunction satisfying

$$\hat{H}^{(0)}\Psi^{(0)} = E_0\Psi^{(0)} \tag{3.1}$$

with eigenvalue E_0 . The conventional single-reference Rayleigh-Schrödinger perturbation theory then gives for the first-order wave function

$$\left(\widehat{H}^{(0)} - E_0\right)\Psi^{(1)} = -\left(\widehat{H} - E_0\right)\Psi^{(0)} \tag{3.2}$$

$$\Psi^{(1)} = -\left(\widehat{H}^{(0)} - E_0\right)^{-1} \left(\widehat{H} - E_0\right) \Psi^{(0)} \tag{3.3}$$

3.2. METHOD 49

where \widehat{H} is the Full CI Hamiltonian, i.e., the exact Hamiltonian in the relevant Fock space restricted only by the use of a finite set of one-electron basis functions, and the inverse is taken in the space of functions normal to $\Psi^{(0)}$.

The most simple and convenient form for the operator $\widehat{H}^{(0)}$ is a non-interacting Hamiltonian, which in second quantized form is associated with orbitals that diagonalize a one-electron Hamiltonian. With a single-determinantal root function, this defines Møller-Plesset perturbation theory. With a multiconfigurational root function, a simple one-electron $\widehat{H}^{(0)}$ cannot be used, as a multiconfigurational $\Psi^{(0)}$ is generally not an eigenfunction of such a non-interacting Hamiltonian. In the CASPT2 model, this is addressed by the introduction of projection operators. Thus, $\widehat{H}^{(0)}$ is defined as

$$\widehat{H}^{(0)} = \widehat{P}_{CAS}\widehat{H}\widehat{P}_{CAS} + \widehat{P}_{SD}\widehat{F}\widehat{P}_{SD} + \widehat{P}_{TQ}\widehat{F}\widehat{P}_{TQ} + \dots$$
(3.4)

where \widehat{P}_{CAS} projects onto the root function, \widehat{P}_{SD} onto the space spanned by single and double replacement states, and \widehat{P}_{TQ} ... onto the space spanned by higher order excitations. This form ensures that the first-order wave function $\Psi^{(1)}$ can be found in the finite-dimensional space S_{SD} .

The generalized Fock matrix \hat{F} is, as usual, of the form

$$\widehat{F} = \sum_{pq} F_{pq} \widehat{E}_{pq} \tag{3.5}$$

where \widehat{E}_{pq} is the conventional spin-summed excitation operator in second quantization, and F_{pq} is the matrix element for molecular orbitals ψ_p, ψ_q (we use the convention that orbital indices are denoted i, j, k, l for inactive orbitals, t, u, v, x for active ones, a, b, c, d for virtual orbitals, and p, q, r, s in the absence of any particular specification).

The molecular orbitals are to some extent arbitrary, in the sense that the root function is equally well described if any arbitrary unitary transformation is applied that does not mix the inactive, active and external orbitals of the CASSCF calculation. This introduces another difference compared to single-determinantal MP2: while the orbitals can be chosen to make the Fock matrix consist of diagonal submatrices with orbital energies on the diagonal, there may remain non-zero elements that couple inactive/active, inactive/external, or active/external

orbitals. When using the CASPT2 subdivision of the spaces as shown by Eq. (3.4), multiconfigurational cases can show size inextensivity, but this deficiency is usually small in magnitude. A final distinction between single-determinantal and multi-determinantal root functions $\Psi^{(0)}$ is that, in the former, the wave function expansion can either be regarded to be in terms of single determinants having one or more replacements of orbitals, or in terms of contributions generated by the action of excitation operators on the root function; in either case these determinants are eigenfunctions of $\hat{H}^{(0)}$. For multi-determinantal root functions, however, these two ansätze are very different, in that the first can require extremely large expansions, while the second gives a dimension of the expansion space that is not much larger than that for a similar MP2 calculation. An advantage with the first approach is that the $\hat{H}^{(0)}$ operator can be defined to be diagonal in the expansion space. In CASPT2, however, we have chosen the latter ansatz. The $\Psi^{(1)}$ wave function is then defined in terms of two-electron excitations from the root function,

$$\Psi^{(1)} = \sum_{pqrs} t_{pqrs} \, \widehat{E}_{pqrs} \Psi^{(0)} \tag{3.6}$$

Equation (3.6) can then be satisfied by the solution of a system of linear equations in the variables t_{pqrs} appearing in Eq.(3.6).

Not all possible excitations covered by Eq. (3.6) are necessary. If the CI expansion in the CASSCF root function is converged, (not necessarily with optimized orbitals) terms with four active orbital indices are not needed. Of the remaining possibilities, only combinations with p, r active or virtual and with q, s active or inactive are needed. The excitations are then classified into eight types:

Internal:	Semi-internal:	External:
\widehat{E}_{tiuv}	\widehat{E}_{atuv}	\widehat{E}_{atbu}
\widehat{E}_{tiuj}	\widehat{E}_{aitu} or \widehat{E}_{tiau}	\widehat{E}_{aibt}
·	\widehat{E}_{tiaj}	\widehat{E}_{aibj}

The resulting Fock matrix cannot in general be fully diagonalized. However, the part consisting of the inactive/inactive submatrix, the active/active submatrix, and the external/external submatrix can be diagonalized, while changing at the same time the CI ex-

3.2. METHOD 51

pansion coefficients, such that the root function is unchanged while the above-mentioned block-diagonal parts are represented by orbital energies in the usual way:

$$\widehat{F} = \sum_{p} \varepsilon_{p} \widehat{E}_{pp} + \sum_{ti} F_{ti}(\widehat{E}_{ti} + \widehat{E}_{it}) + \sum_{ai} F_{ai}(\widehat{E}_{ai} + \widehat{E}_{ia}) + \sum_{au} F_{au}(\widehat{E}_{au} + \widehat{E}_{ua})$$

Parametrization using the coefficients t_{pqrs} usually gives a very poorly conditioned equation system. This is addressed by defining new coefficients, according to

$$\Psi^{(1)} = \sum_{\alpha \alpha \alpha} c_{\alpha} \widehat{X}_{\alpha} \Psi^{(0)} \tag{3.7}$$

$$\widehat{X}_{\alpha} = \sum_{pqrs} T_{pqrs,\alpha} \widehat{E}_{pqrs} \tag{3.8}$$

$$t_{pqrs} = \sum_{\alpha} T_{pqrs,\alpha} c_{\alpha} \tag{3.9}$$

The transformation matrices have been determined such that the individual terms $\widehat{X}_{\alpha}\Psi^{(0)}$ in the first-order wave function are orthonormal, and thus non-interacting for the block-diagonal parts of $\widehat{H}^{(0)}$. The CASPT2 equation 3.3 then becomes a system of linear equations with coefficient matrix **A** and RHS (right-hand side) vector **v** whose elements are

$$A_{\alpha,\beta} = \left\langle \Psi^{(0)} \middle| \widehat{X}_{\alpha}^{\dagger} \left(\widehat{H}^{(0)} - E_0 \right) \widehat{X}_{\beta} \middle| \Psi^{(0)} \right\rangle$$
 (3.10)

$$v_{\alpha} = \left\langle \Psi^{(0)} \middle| \widehat{X}_{\alpha}^{\dagger} \left(\widehat{H}^{(0)} - E_0 \right) \middle| \Psi^{(0)} \right\rangle$$
 (3.11)

The equation matrix is not handled in full component form, but is represented by a number of factorized matrices and is strongly dominated by its diagonal, with couplings between submatrices handled iteratively by a preconditioned conjugate gradient (PCG) solver. Upon convergence, usually after about five to fifteen iterations, a solution for

$$\mathbf{A}\mathbf{s} = -\mathbf{v}, \quad \text{i.e.,} \quad \sum_{\beta} A_{\alpha,\beta} s_{\beta} = -v_{\alpha}$$
 (3.12)

is obtained which provides a solution to the original CASPT2 equation 3.3 in the form

$$\Psi^{(1)} = \sum_{\beta} s_{\beta} \widehat{X}_{\beta} \left| \Psi^{(0)} \right\rangle = \sum_{pqrs} \left(\sum_{\beta} T_{pqrs,\beta} s_{\beta} \right) \widehat{E}_{pqrs} \left| \Psi^{(0)} \right\rangle \tag{3.13}$$

Here s denotes the expansion coefficients of the first-order wave function in the orthonormal basis $\hat{X}_{\alpha}\Psi^{(0)}$. The equation system would be directly solved if the inactive-active, inactive-virtual, and active-virtual couplings were all zero. As these couplings are small, however, the direct solution of the diagonal part is a very efficient preconditioner of the full system.

3.2.2 The RASSCF/RASPT2 Method

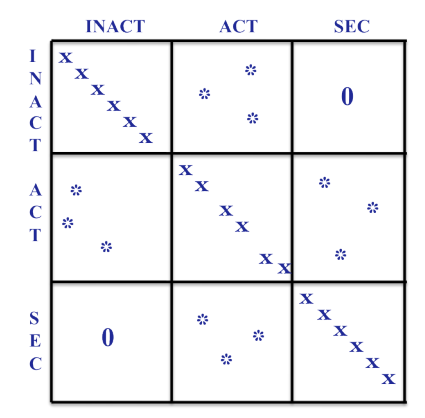
An alternative to the CASSCF method exists that has seen comparatively little use, namely, the Restricted Active Space (RAS) SCF method [24, 25]. In this model, the active subspace is itself divided into three distinct regions: RAS1, RAS2, and RAS3. The RAS2 region is identical to the active region in a CAS calculation, i.e., all possible spin- and symmetry-adapted CSFs that can be constructed from the orbitals in RAS2 are included in the multiconfigurational wave function. The RAS1 and RAS3 spaces, on the other hand, permit the generation of additional CSFs subject to the restriction that a maximum number of excitations may occur from RAS1, which otherwise contains only doubly occupied orbitals, and a maximum number of excitations may occur into RAS3, which otherwise contains only external orbitals.

Many different types of RAS wave functions can be constructed. For example, if one leaves RAS1 fully occupied and RAS3 empty, i.e., if the excitation maxima referred to above are both zero, then one obtains identically the CASSCF wave function for space RAS2. As another example, if the RAS2 space is defined to be empty, then the choice of excitation maxima delivers a RASSCF wave function that includes all single, double, etc. excitations within the RAS1/RAS3 window, i.e., a SDTQ etc. CI wave function. The formalism is clearly quite flexible. A key feature of the RASSCF wave function is that, provided the maximum number of RAS1/RAS3 excitations is relatively few, the number of CSFs associated with a given RAS protocol can be substantially smaller than for the CASSCF alternative defined over the

3.2. METHOD 53

same active space. The RASSCF model thus has the potential to permit multiconfigurational calculations with larger active spaces than can be employed with the CASSCF method. The challenge with a RASSCF wave function, however, is how to go about including the effects of dynamical electron correlation. In particular, second order perturbation theory is not equally straightforward to apply in the case of a RASSCF wave function.

In order to address this issue, we have proceeded in the following manner, which represents in some sense the simplest approach (possible improvements are discussed below in Section 3.4). In the current RASPT2 model, the effective Fock matrix is expanded from the 3 x 3 block structure of the CASPT2 model to a 5 x 5 block structure where the new blocks derive from separating the single CASPT2 active/active block into a 3 x 3 set of subblocks defined by the RAS1, RAS2, and RAS3 orbital spaces. This introduces a fundamental difference in the two PT2 implementations insofar as orbital rotations that couple different RAS spaces, i.e., RAS1 and RAS2, RAS1 and RAS3, and RAS2 and RAS3, are not allowed. Thus, the diagonalization of the active part of the Fock matrix is not complete in RASPT2, as it is in CASPT2, but instead non-zero elements may remain in the parts that couple different RAS spaces (See Figure 3.2). Some additional technical points must be addressed in formulating and diagonalizing the RASPT2 Fock matrix, some of which arise because the first-order interacting space S^{SD} is not as straightforwardly described in terms of orbital excitations, but also depends on the occupation numbers of the CSFs.



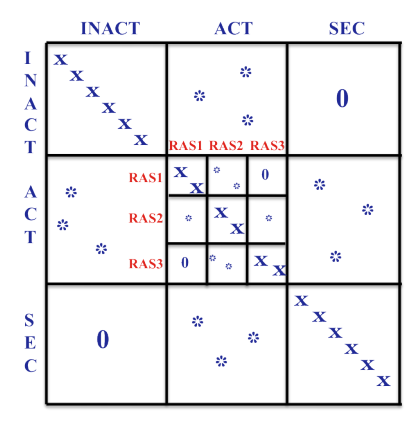


Figure 3.2: A schematic representation of the fock matrix after a CASSCF (left) and RASSCF (right) calculation.

We note that all except one of the CASPT2 excitation classes described above involve at least one active orbital. In the RASPT2 model, if an excitation creates an electron in a RAS3 orbital, or annihilates an electron in a RAS1 orbital, then a subset of the CSFs that are produced will fulfill the RAS restrictions, while the rest will not. However, in every case the excitation is combined with another excitation that either annihilates an electron in an inactive orbital or creates an electron in an external orbital, so all resulting CSFs will indeed belong to the first-order interacting space S^{SD} . Thus, as long as the remaining class of fully internal excitations is ignored, essentially the same formalism as in CASPT2 can be used, except that the active-active part of the Fock matrix is no longer fully diagonal. However, the matrix $\bf A$ as well as the right-hand side $\bf v$ of eq. (3.10), or rather, the data sets used to represent them in the actual calculations, involve reduced density matrices of only up to three particles (using active orbital indices only). These are computed using intermediate wave functions, which also must obey the RAS restrictions. By making use of conjugation and index permutation symmetries, all intermediate wave functions can be constrained to obey these restrictions.

3.3 Application to supported CuO_2 and Cu_2O_2 systems

We now examine the performance of the RASPT2 model for two challenging problems associated with the activation of O_2 by copper. Because of favorable combinations of covalency and oxidation/reduction potentials, the activation of molecular oxygen by its coordination to one or two supported (i.e., ligated) Cu(I) ions is common to a number of biological and inorganic catalytic processes [26, 27, 28, 29, 30, 31, 32, 33, 34, 35, 36, 37, 38, 39]. In the case of monocopper species $LCuO_2$, where L is a general ligand or ligands, one possible oxidation state that may be assigned to the complex is $LCu(II)O_2(-)$; thus, the copper atom has been oxidized by one electron and the O_2 fragment is formally a superoxide radical anion. Similarly, in the case of dicopper species ($LCu)_2O_2$, one possible oxidation state of the complex is formally $[LCu(II)]_2[(O_2)(2-)]$; in this instance each copper atom has been oxidized by one electron and the O_2 fragment is formally a peroxide dianion. In both of these cases, the resulting compounds with a variety of ligands can have singlet ground states that exhibit substantial biradical character because of the spin separation associated either with two d⁹ Cu(II) ions or one

such ion and a superoxide radical anion [40, 41, 42, 43, 44, 45, 46, 47, 48, 49, 50, 51, 52]. Wave function theories restricted to a single determinant are poorly suited to the description of such species since singlet biradicals are intrinsically two-determinantal [53, 54]. Moreover, even when oxidation states more likely to be characterized as closed-shell in nature are considered, e.g., $[LCu(III)]_2[O(2-)]_2$, computational studies have found that large contributions from dynamical correlation effects influence relative isomer energetics [40, 41, 42, 47, 48, 49, 51, 52].

In this section, we apply the RASPT2 method to two problems previously studied in considerable detail using a wide range of theoretical models (See Figure 3.3).

Figure 3.3: Molecular structures for $(C_3N_2H_5)CuO_2$ and $\{[Cu(NH_3)_n]_2O_2\}^{2+}$ isomerism.

The first case considers the singlet-triplet splitting in LCuO₂, L = 1,3-diketiminate [44, 52] while the second examines the relative energies of the isomeric peroxo and bis- μ -oxo forms of $\{[\text{Cu}(\text{NH}_3)_n]_2\text{O}_2\}^{2+}$ (n=0,1,2,3). In each case, our goal is primarily to compare the performance of different RASPT2 and CASPT2 protocols one to another, noting that in the latter case, i.e., the $\{[\text{Cu}(\text{NH}_3)_n]_2\text{O}_2\}^{2+}$ system, prior experience has indicated that it is impossible to choose a CAS active space sufficiently large to provide converged, balanced results for the CASPT2 energetics of the isomeric equilibrium [49]

3.3.1 Computational Details

For $(C_3N_2H_5)CuO_2$, structures for the lowest singlet and triplet state were obtained using B3LYP-DFT [55, 56, 57, 58] (making use of the Stuttgart pseudopotential and associated basis functions for Cu [59, 60], and 6-31G(d) basis sets [61] for other atoms. Both structures are planar, and have C_{2v} symmetry. They are positioned in the xy-plane, with the Cu-O₂ bonds bisected by the x-axis (i.e., the C_2 axis). All calculations on $\{[Cu(NH_3)_n]_2O_2\}^{2+}$ were performed on structures taken from ref. [49]. The molecules were positioned with the Cu_2O_2

core in the XY-plane, the two Cu atoms on the X-axis, and the two oxygen atoms on the Y-axis. As such, in both types of molecules the orbitals primarily involved in the Cu–O bonding are Cu $3d_{xy}$, O $2p_x$, O $2p_y$.

Two different basis sets were used in these calculations. The smallest basis set, denoted as BS1, consists of the Stuttgart pseudopotential and associated basis functions for Cu [59, 60], combined with ANO-L basis sets for the other atoms [62], contracted to [4s3p2d] for O and N and [2s1p] for H. The larger BS2 basis set is built from ANO-rcc basis sets [63, 64] on all atoms, contracted to [7s6p4d3f2g] for Cu, [4s3p2d1f] for N and O (all such atoms are directly coordinated to copper), [4s3p2d] for C (appearing only in $(C_3N_2H_5)CuO_2$, and not directly bound to copper), and [3s1p] for H. For the calculations with BS2, scalar relativistic corrections were included using a (standard second-order) Douglas-Kroll-Hess Hamiltonian. All calculations on $(C_3N_2H_5)CuO_2$ were performed with BS2. For $\{[Cu(NH_3)_n]_2O_2\}^{2+}$, most calculations were performed with BS1. This basis set was also used in previous studies ref. [49, 50] on $\{[Cu(NH_3)_n]_2O_2\}^{2+}$. Since we are also using the structures reported there, the present RASPT2 results are directly comparable to the DFT and completely renormalized coupled-cluster results (CR-CC) from that work. For $\{[Cu(NH_3)_2]_2O_2\}^{2+}$ and $\{[Cu(NH_3)_3]_2O_2\}^{2+}$, a number of RASPT2 results obtained with BS2 are also presented.

The largest RASSCF calculations performed included all valence electrons originating from occupied Cu 3d and O 2p atomic orbitals in an active space consisting of all valence orbitals and a second correlating orbital for each of them (i.e., Cu 3d,4d, and O 2p,3p). For $\{[Cu(NH_3)_n]_2O_2\}^{2+}$ this involves 28 electrons in 32 orbitals. For $(C_3N_2H_5)CuO_2$ 18 valence electrons were correlated in 21 orbitals, i.e., all Cu 3d,4d and O 2p,3p orbitals were included, except for one O 3p orbital corresponding to the unoccupied σ_y^* orbital of O_2^{2-} . Smaller active spaces were constructed as follows:

• for $(C_3N_2H_5)CuO_2$, by removing the O 3p orbitals, as well as the O $2p_z$ $\pi(b_2)$ orbital, which is not involved in the Cu-O₂ bonding and is doubly occupied in both considered states. The other O $2p_z$ orbital, $\pi^*(a_2)$, is depopulated in the 3B_2 state, and should therefore be active in all calculations. This reduced (16 in 15) active space still includes the static correlation effects connected to the Cu-O₂ bond as well as the Cu 3d double-shell effect [65, 66]. The latter effect is moved to the perturbation treatment by further reducing the active space to (8 in 6), now only containing the Cu $3d_{xy}$, O $2p_{x,y}$

combinations as well as the O $2p_z \pi^*(a_2)$ orbital.

• for $\{[Cu(NH_3)_n]_2O_2\}^{2+}$, by removing first the O $2p_z, 3p_z$ orbitals, giving rise to 24 electrons in 28 orbitals, and second by removing also the O $3p_{x,y}$ orbitals, resulting in a (24 in 24) active space, including important correlation effects related to the Cu-O bonds and the Cu 3d double-shell effect. Removing all Cu 4d as well as the doubly occupied Cu 3d orbitals further reduces this active space to a minimalist (8 in 6), i.e., the bonding and antibonding combinations of both Cu $3d_{xy}$ and the O $2p_{x,y}$ orbitals.

The calculations are denoted as RASPT2(n_{ae} in n_{ao})/(n_{ae2} in n_{ao2})/n, with n=2-5 indicating the maximum number of electrons excited from RAS1 or into RAS3, (n_{ae} in n_{ao}) describing the global RAS(1-3) active space, and (n_{ae2} in n_{ao2}) describing that part of the global active space assigned to RAS2, i.e., that part in which all possible symmetry-adapted excitations are considered. The RAS2 space was left empty in calculations on {[Cu(NH₃)_n]₂O₂}²⁺, but for (C₃N₂H₅)CuO₂ we considered either a (8 in 6) RAS2 space, as described above, or we left RAS2 empty for the singlet state, and populated it with the two singly-occupied orbitals for the 3 B₂ state. Calculations without a RAS2 space are denoted as RASPT2(n_{ae} in n_{ao})//n. Calculations on (C₃N₂H₅)CuO₂ with a (8 in 6) RAS2 space are only feasible for n=2, and for n=3 with the smaller global active spaces. Calculations with n=4-5, or with n=3 combined with the largest global active space were only possible when performed with the state-specific empty/(2 in 2) RAS2 space.

RASPT2 calculations were performed with the standard IPEA shifted $\widehat{H}^{(0)}$ operator [67] using an imaginary denominator shift (IS) of 0.1 a.u. For $(C_3N_2H_5)CuO_2$, intruder states appeared in some of the calculations with n=3. In those cases, the IS was increased to 0.20-0.25, taking the lowest value that gave rise to stable results. Two different types of RASPT2 calculations were performed. In the first, all core orbitals, including also the semi-core Cu 3s, 3p orbitals, were kept frozen, whereas in the second the latter four orbitals were included in the correlation treatment.

For $\{[Cu(NH_3)_n]_2O_2\}^{2+}$, a series of test calculations with different active spaces, basis sets, and a different number of correlated electrons were performed for the relative energy

Table 3.1: Relative energies (kcal mol⁻¹) of the $^3\mathrm{B}_2$ and $^1\mathrm{A}_1$ states in . $\Delta E_{ST}=E(^3\mathrm{B}_2)$ - $E(^{1}A_{1})$

active space	ΔE_{ST}
CASPT2(8 in 6)	17.8
CASPT2(16 in 15)	6.3
D 4 0D D 2 (1 5 1 1 1 1 1 1 1 1 1 1 1 1 1 1 1 1 1	
RASPT2(16 in 15)//2	-2.3
RASPT2 $(16 \text{ in } 15)/(8 \text{ in } 6)/2$	7.4
RASPT2(18 in 21)/(8 in 6)/2	15.5
RASPT2(16 in 15)// 3^a	3.3
RASPT2 $(16 \text{ in } 15)/(8 \text{ in } 6)/3$	9.0
RASPT2(18 in 21)/(8 in 6)/ 3^b	11.5
RASPT2(16 in 15)//4	7.7
RASPT2(18 in $21)//4$	11.2
aIS=0.20: $bIS=0.25$	

IS=0.20; IS=0.25

between the bis (\$\mu\$-oxo) and peroxo structures of {[Cu(NH_3)_2]_2O_2}^{2+} and {[Cu(NH_3)_3]_2O_2}^{2+}. For all four $\{[Cu(NH_3)_n]_2O_2\}^{2+}$ species, RASPT2(24 in 28)//4 calculations were performed for all structures (taken from ref. [49]) along the reaction path connecting the bis(μ -oxo) and peroxo structures. These calculations were performed with BS1 and without Cu 3s, 3pcorrelation, so that they could be compared to the CR-CC results from ref. [49] (which also did not include these electrons).

Singlet-triplet splitting in the $(C_3N_2H_5)CuO_2$ system 3.3.2

Table 3.1 shows the RASPT2 results obtained for the relative energy ΔE_{ST} between the ³B₂ and ¹A₁ states in (C₃N₂H₅)CuO₂ with different active spaces (BS2, Cu3s,3p included in RASPT2). The first two lines show the results obtained from CASPT2 calculations with an (8 in 6) and (16 in 15) active spaces. A difference of more than 10 kcal/mol is found between the CASPT2 results for ΔE_{ST} starting from a reference wave function which either does, (16) in 15), or does not, (8 in 6), include the Cu 3d double-shell effect. This clearly illustrates the importance of taking care of this type of correlation in the zeroth-order variational step.

With the (16 in 15) active space, two different types of RASPT2 calculations are presented, one in which the correlation effects on the Cu-O bonds are described by a full CI in the (8 in 6) RAS2 space, and a second in which these effects are, together with the Cu 3d-4d correlation, treated by up to double, triple or quadruple RAS1 \rightarrow RAS3 excitations. It is clear from the data in Table 3.1 that up to quadruple excitations are mandatory to describe the correlation effects on the Cu-O bonds. The differences between the results obtained from RAS(16 in 15)/n calculations with and without a (8 in 6) RAS2 space are a sizable 9.6 kcal/mol for n=2, and still 5.7 kcal/mol for n=3. On the other hand, the ΔE_{ST} value obtained with RAS(16 in 15)//4, 7.7 kcal/mol, is quite close the more complete CASPT2(16 in 15) result, 6.3 kcal/mol, indicating that the important nondynamical correlation effects in this system, both on the bonding interactions and the Cu 3d double-shell effect, may be captured by a (MC)SCF calculation including only up to quadruple excitations. Furthermore, the difference in ΔE_{ST} between RASPT2(16 in 15)/(8 in 6)/2 and CASPT2(16 in 15) is moderate, 1.1 kcal/mol. This suggests that for this mono copper system the 3d double-shell effect may already quite accurately be described by a RASSCF wave function including only up to double $3d\rightarrow 4d$ excitations.

By increasing the size of the active space from (16 in 15) to (18 in 21) oxygen 2p-3p correlation is introduced in the zeroth-order wave function. The effect is significant: 2.5-3.5 kcal/mol even with n=3 or 4. The final results obtained from either RAS(18 in 21)/(4 or RAS(18 in 21)/(8 in 6)/3 are similar, <math>11.2-11.5 kcal/mol, suggesting that this value is approaching convergence. On the other hand, including only up to double RAS1/RAS3 excitations obviously fails to suffice for an accurate description of the O 2p-3p correlation effects, leading to a result (15.5 kcal/mol) which is too high by about 4 kcal/mol.

3.3.3 Relative energy of peroxo and bis- μ -oxo isomers of $\{[Cu(NH_3)_n]_2O_2\}^{2+}$ $(n=0,\,1,\,2,\,3)$

Table 3.2 shows the RASPT2 results obtained for the relative energy ΔE_{bp} between the bis(μ -oxo) and peroxo structures of $\{[Cu(NH_3)_2]_2O_2\}^{2+}$ and $\{[Cu(NH_3)_3]_2O_2\}^{2+}$ with different active spaces, number of correlated electrons, and basis sets. Best estimates for this quantity based on prior many-body and DFT calculations for equivalent structures and basis sets [49]

are about -2 kcal/mol for n = 2 and 8 kcal/mol for n = 3.

Once again, correlation effects on bonding in the Cu_2O_2 core may be described by an (8 in 6) active space, but in this case including the description of the Cu 3d double-shell effect in the reference wave function requires a (24 in 24) active space, which is far too large for a CASSCF treatment. The lack of Cu 3d-4d correlation in the zeroth-order wave function is the main reason for the failure of the CASPT2 treatment in the original [41] and later [49, 47, 68] CASPT2 studies on this subject. All these studies were performed with moderately sized basis sets (comparable to BS1) and with active spaces starting from the (8 in 6) space used here, possibly extended with other valence (O 2s, O $2p_z$) or virtual (O 3p orbitals) orbitals. However, limitations on the size of the CAS space prevented the inclusion of the full set of Cu 3d, 4d orbitals, and this invariably led to erroneous CASPT2 results, grossly overestimating (more than 20 kcal/mol) the stability of the bis(μ -oxo) isomer relative to the peroxo isomer. As the results in Table 3.2 indicate, including the Cu 3d double-shell effect in the (24 in 24) active space leads to a relative stabilization of the peroxo structure by up to 14 kcal/mol for $\{[\text{Cu}(\text{NH}_3)_2]_2\text{O}_2\}^{2+}$ and up to 20 kcal/mol for $\{[\text{Cu}(\text{NH}_3)_3]_2\text{O}_2\}^{2+}$ (for the BS1 calculations).

As proved true for $(C_3N_2H_5)CuO_2$, properly accounting for correlation effects on the Cu-O bonding requires inclusion in the reference wave function of excitations at least up to quadruples between the orbitals involved: the ΔE_{bp} values obtained from RASPT2(24 in (24)/(8in6)/n are systematically larger than those from corresponding RASPT2(24 in 24)//n calculations, by 2-3 kcal/mol for $\{[Cu(NH_3)_2]_2O_2\}^{2+}$ and by 5-7 kcal/mol for $\{[Cu(NH_3)_3]_2O_2\}^{2+}$. However, as compared to $(C_3N_2H_5)CuO_2$, a more significant increase (3 kcal/mol) of ΔE_{bp} is in this case obtained by including the Cu 3d double-shell effect by up to triple rather than up to double RAS1 \rightarrow RAS3 excitations. Of course, this increase is a priori to be expected for size extensivity reasons, since we are now dealing with two instead of only one copper center. Furthermore, it should be noted that the ΔE_{bp} values obtained from RASPT2(24 in $\frac{24}{4}$ are systematically lower than those obtained from RASPT2(24 in $\frac{24}{6}$)/(8 in 6)/3 or from RASPT2(24 in 24)//5 when Cu semi-core orbitals are included (see below). This suggests that with RASPT2(24 in 24)//4 the description of correlation effects on the Cu-O bonds may not yet be fully converged with respect to the excitation level in the active space, and that RASPT2(24 in 24)/(8 in 6)/4 would give ΔE_{bp} values that are higher by 3-5 kcal/mol. Unfortunately, such a calculation exceeds the practical limits of our current

RASPT2 implementation. However, even with a remaining uncertainty of this magnitude, it is clear that the results obtained from the present (24 in 24) RASPT2 protocol represent a considerable improvement over all previous CASPT2 calculations.

A further significant (3-5 kcal/mol) increase of the ΔE_{bp} values is obtained by extending the active space from RAS(24 in 24)//4 to RAS(24 in 28)//4 by including correlating O 3p orbitals for the O $2p_{x,y}$ orbitals involved in the Cu–O bonds. Including also the O $2p_z, 3p_z$ couples (28 in 32) has a minor effect: 1 kcal/mol or less with BS1, and becoming slightly negative with BS2. As such, we believe that the present calculations are converged with respect to the size of the total active space.

Finally, we consider the effect of Cu 3s, 3p semi-core correlation (columns 2 and 4 of data in Table 3.2) and basis set effects. Starting from the CASPT2(8 in 6) active space, adding the Cu 3s, 3p electrons to the correlation treatment has a significant effect on the relative energies of the two structures, stabilizing the $bis(\mu-oxo)$ structure by 3 kcal/mol for $\{[Cu(NH_3)_2]_2O_2\}^{2+}$, and by 5 kcal/mol for $\{[Cu(NH_3)_3]_2O_2\}^{2+}$. However, the effect is reduced in the RASPT2 results obtained with larger active spaces, and in some of these calculations even reverses its sign. This seems to indicate that transition-metal semi-core correlation effects may in fact be overestimated by CASPT2 based on a too small active space. A similar phenomenon, although less pronounced, is observed when comparing the results obtained with different basis sets. Increasing the basis sets to BS2 significantly stabilizes the bis(μ -oxo) structure with respect to the peroxo structure for both $\{[Cu(NH_3)_2]_2O_2\}^{2+}$ and $\{[Cu(NH_3)_3]_2O_2\}^{2+}$. However, the effect is again largest for the CASPT2(8 in 6) calculations, and is reduced when performing RASPT2 with larger active spaces. Still, we note that for $\{[Cu(NH_3)_3]_2O_2\}^{2+}$ the "best" result for ΔE_{BP} , obtained from RASPT2(24 in 28)//4, is reduced from 7.0 kcal/mol with BS1 to 1.8 kcal/mol with BS2, the latter number suggesting that both structures of this molecule are nearly degenerate in energy.

Prior studies of the bis(μ -oxo)/peroxo equilibrium have focused not only upon the relative energies of the two stationary points shown in Figure 3.4, but also on the reaction coordinate generated by a linear transformation of one structure into the other. Table 3.3 shows the relative energies predicted from RASPT2(24 in 28)//4 calculations for the different structures along this reaction coordinate where F indicates the percentage transformation from extreme F = 0 (bis(μ -oxo)) to extreme F = 100 (peroxo). In Figure 3.4 the RASPT2(24 in 28)//4 re-

sults for the particular case of $\{[Cu(NH_3)_3]_2O_2\}^{2+}$ are compared graphically to DFT and CR-CC results from one previous study [49] and MRCI results from another [47]. The RASPT2 reaction coordinate is in general in fair to good agreement with coordinates predicted from CR-CC, MRCI, and the pure BLYP density functional. While $\{[Cu(NH_3)_3]_2O_2\}^{2+}$ is a model system for which experimental results are not available, the good agreement between CR-CC, MRCI, and pure density functionals has been interpreted to suggest that these levels of theory are indeed accurate for this isomerization. Moreover, pure DFT functionals like BLYP have been shown to be quantitatively accurate for $bis(\mu-oxo)$ /peroxo equilibria that have been experimentally characterized [69, 51]; such cases involve support of the copper atoms by larger, synthetically convenient bi- and tridentate ligands. Thus, to aid in interpretation of Table 3.3, we report best estimate values for the isomerization coordinates of [Cu₂O₂]²⁺, $\{[Cu(NH_3)]_2O_2\}^{2+}, \{[Cu(NH_3)_2]_2O_2\}^{2+}, \text{ and } \{[Cu(NH_3)_3]_2O_2\}^{2+} \text{ that are taken from CR-CC} \}$ calculations in the first two instances and an average of CR-CC and pure DFT calculations in the latter two instances [49]. With respect to the RASPT2(24 in 28)//4 model, there is still a small systematic tendency to overestimate the stability of the $bis(\mu$ -oxo) isomer relative to the peroxo, but the situation is vastly improved compared to CASPT2 (see Figure 3.4), where the largest practical active space is (16,14) [49]. We note that hybrid density functionals like B3LYP also show substantial errors in their predictions for this isomerization, even after correcting for spin contamination using a broken-symmetry formalism (referred to as sum-bs in the inset legend of Figure 3.4) [49], but the error is in the opposite direction to that of CASPT2.

3.4 Discussion and Conclusions

Some dynamical correlation effects are not addressed within the current RASPT2 ansatz. When the RAS restrictions are used in order to allow large active spaces, the RAS1 and RAS3 subspaces should handle only dynamical correlation, and RAS2 should account for all non-dynamical correlation. However, the subdivision into dynamical and non-dynamical correlation is not well defined, and in addition the limited number of excitations allowed in the RAS1 and RAS3 subspaces can give significant size extensivity errors. The situation would be much improved by extending the model to include perturbative treatment of the

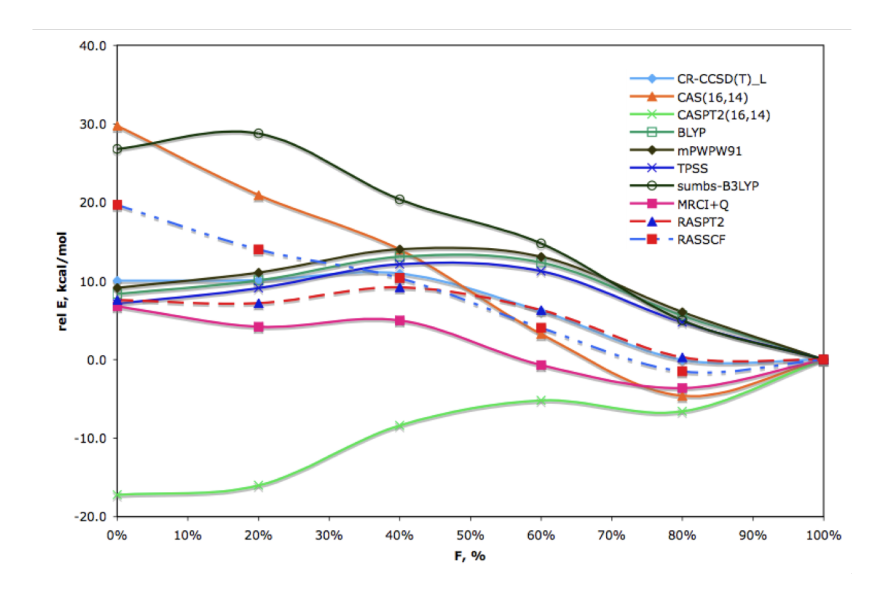


Figure 3.4: Relative energy (kcal mol⁻¹) predicted from various levels of theory for a reaction coordinate linearly connecting the $\{[Cu(NH_3)_3]_2O_2\}^{2+}$ bis $(\mu$ -oxo) (F=0%) and peroxo (F=100%) structures shown in Figure 3.2. The inset legend identifies the various theoretical models, which are discussed in more detail in the text and, completely, in Ref. [49].

fully internal excitations, i.e., excitations $\widehat{E}_{tuvx} - \widehat{E}_{utxv}$ from the RASSCF wave function. While such an improvement remains under consideration, implementation of these additional excitations is complicated because, while the right-hand side \mathbf{v} of the RASPT2 equations still requires only the use of three-body density matrices, $\widehat{H}^{(0)}$ would require fourth-order density matrices in the present formulation, and this is not practical with larger active spaces. Thus, the construction of this part of $\widehat{H}^{(0)}$ will need new approximations in order to be efficiently implemented.

In addition, the structure of the doubly internal subblock is different from those associated with other excitation classes, since a subset of the CSF's that are involved have already been used in the RASSCF wave function. It will likely prove important to distinguish between those excited CSFs that continue to fulfill the RAS restrictions and those that do not, as is presently done for the excitation classes that are not fully internal. In our view, regarding the calculation as strictly a single-reference calculation with an internally contracted root function, it will likely prove simpler to use antihermitian excitations of the form $\widehat{E}_{tuvx} - \widehat{E}_{utxv}$

and thus automatically produce linear combinations that are orthonormal to $\Psi^{(0)}$, rather than to use, e.g., additional projectors to separate out the interacting space. There will, of course, still be the additional problem of defining a suitable unperturbed Hamiltonian for the new excitations. However, even in the absence of this more complete implementation, the current RASPT2 model has proven valuable in the study of systems, like the supported copper complexes above, where a large active space is required but relatively few orbitals need to be assigned to the fully flexible RAS2 subspace. Using the RAS1 and RAS3 spaces in analogy to occupied and virtual spaces, respectively, and generating truncated CI wave functions at levels SD, SDT, or SDTQ, combines well with the subsequent perturbation theory accounting for additional electron correlation, and we anticipate that this model will prove useful in many cases where CASPT2 is not currently practical.

Table 3.2: Relative energies (kcal mol⁻¹) of the bis(μ -oxo) and peroxo structures of and . $\Delta E_{bp} = E(\text{bis}(\mu\text{-oxo}))$ - E(peroxo)

	C 2 2	21 C 2 2		'11 C 2 2	
active	no Cu $3s, 3p$	with $Cu3s, 3p$		with $Cu3s, 3p$	
space	correlated	correlated	correlated	correlated	
	Calculations with BS1				
CASPT2(8 in 6)	-18.0	-20.9	-8.8	-13.6	
RASPT2 $(24 \text{ in } 24)//2$	-10.2	-8.7	-3.5	-2.1	
RASPT2 $(24 \text{ in } 24)/(8 \text{ in } 6)/2$	-8.8	-6.5	3.6	3.9	
RASPT2 $(24 \text{ in } 28)/(8 \text{ in } 6)/2$	-6.9	-5.5	4.0	3.3	
RASPT2(28 in 32)/(8 in 6)/2	-4.8	-4.3	5.4	4.2	
, , , , , , , , , , , , , , , , , , , ,					
RASPT2 $(24 \text{ in } 24)//3$	-8.0	-5.5	0.6	2.9	
RASPT2(24 in 24)/(8 in 6)/3	-5.2	-3.6	6.8	7.1	
7/1 ()//					
RASPT2 $(24 \text{ in } 24)//4$	-6.6	-5.7	4.1	3.9	
RASPT2(24 in $28)//4$	-1.8	-1.2	7.6	7.0	
RASPT2(28 in $32)//4$	-0.7	-0.4	8.0		
7777					
RASPT2 $(24 \text{ in } 24)//5$	-6.6	-4.1			
	Calculations with BS2				
CASPT2(8 in 6)		-26.2		-20.6	
(/		-			
RASPT2(24 in $24)//4$		-4.5		-1.0	
RASPT2(24 in 28)//4		-2.6		1.8	
RASPT2(28 in $32)//4$		-3.3			

Table 3.3: Relative energies (kcal $\mathrm{mol^{-1}}$) of the $\mathrm{bis}(\mu\text{-oxo})$ and peroxo structures. RASPT2(24 in 28)//4 calculations without $\mathrm{Cu}3s, 3p$ correlated, compared to best estimates in parentheses, performed with BS1

	F					
molecule	0%	20%	40%	60%	80%	100%
	28.6	21.2	15.1	7.1	0.8	0.0
	(34)	(24)	(16)	(8)	(2)	(0)
	25.2	16.6	9.4	1.9	-3.5	0.0
	(30)	(20)	(12)	(3)	(-2)	(0)
	-1.8	-1.6	0.8	-0.8	-4.7	0.0
	(-3)	(-1)	(2)	(2)	(-2)	(0)
	7.6	7.2	9.2	6.3	0.3	0.0
	(8)	(9)	(12)	(10)	(4)	(0)

^aBest estimates are rounded to nearest unit. For the first two molecules they are CR-CC results, for the last two molecules they are an average of CR-CC results and (similar) DFT results from 3 pure density functionals. Full details of prior theoretical models are available in reference [49]

Bibliography

- [1] L. Gagliardi and B. O. Roos, Nature 433, 848 (2005).
- [2] L. Gagliardi, M. C. Heaven, J. W. Krogh, and B. O. Roos, J. Am. Chem. Soc. 127, 86 (2005).
- [3] L. Gagliardi, P. Pyykkö, and B. O. Roos, Phys. Chem. Chem. Phys. 7, 2415 (2005).
- [4] D. Hagberg, G. Karlström, B. O. Roos, and L. Gagliardi, J. Am. Chem. Soc. 127, 14250 (2005).
- [5] L. Gagliardi, Theor. Chim. Acta 116, 307 (2006). Witek:03
- [6] La Macchia G., M. Brynda, and L. Gagliardi, Angew. Chem. Int. Ed. 45, 6210 (2006).
- [7] B. O. Roos and L. Gagliardi, Inorg. Chem. 45, 803 (2006).
- [8] P. Celani, H. Stoll, H. J. Werner, and P. J. Knowles, Mol. Phys. 102, 2369 (2004).
- [9] K. Dyall, J. Chem. Phys. 102, 4909 (1995).
- [10] M. W. Schmidt and M. S. Gordon, Annu. Rev. Phys. Chem. 49, 233 (1998).
- [11] H. A. Witek, H. Nakano, and K. Hirao, J. Chem. Phys. 118, 8197 (2003).
- [12] C. Angeli, M. Pastore, and R. Cimiraglia, Theor. Chim. Acta 117, 743 (2007).
- [13] B. O. Roos, in Radiation induced molecular phenomena in nucleic acids, edited by M. K. Shukla and J. Leszczynski (Springer, Amsterdam, The Netherlands, 2008), pp. 125–156.

- [14] L. Gagliardi and B. O. Roos, Chem. Soc. Rev. 36, 893 (2007).
- [15] B. O. Roos, P. R. Taylor, and P. E. M. Siegbahn, Chem. Phys. 48, 157 (1980).
- [16] B. O. Roos, in Advances in Chemical Physics; Ab Initio Methods in Quantum Chemistry
 II, edited by K. P. Lawley (John Wiley & Sons Ltd., Chichester, England, 1987), chap.
 69, p. 399.
- [17] K. Pierloot, in Nondynamic Correlation effects in Transition Metal Coordination Compounds, edited by T. R. Cundari (Marcel Dekker, New York, 2000), chap. 5, pp. 123–158.
- [18] K. Pierloot, Mol. Phys. 101, 2083 (2003).
- [19] P. E. M. Siegbahn, A. Heiberg, B. O. Roos, and B. Levy, Physica Scripta 21, 323 (1980).
- [20] I. Huba c, P. Mach, and S. Wilson, Int. J. Quantum Chem. 89, 198 (2002).
- [21] B. O. Roos, P. Linse, P. E. M. Siegbahn, and M. R. A. Blomberg, Chem. Phys. 66, 197 (1982).
- [22] K. Andersson, P.-Å. Malmqvist, B. O. Roos, A. J. Sadlej, and K. Wolinski, J. Phys. Chem. 94, 5483 (1990).
- [23] K. Andersson, P.-Å. Malmqvist, and B. O. Roos, J. Chem. Phys. 96, 1218 (1992).
- [24] J. Olsen, B. O. Roos, P. Jørgensen, and H. J. A. Jensen, J. Chem. Phys. 89, 2185 (1988).
- [25] P.-Å. Malmqvist, A. Rendell, and B. O. Roos, J. Phys. Chem. 94, 5477 (1990).
- [26] K. D. Karlin and Y. Gultneh, Prog. Inorg. Chem. 35, 219 (1987).
- [27] E. I. Solomon and M. D. Lowery, Science 259, 1575 (1993). 22
- [28] K. D. Karlin and Z. Tyeklar, Adv. Inorg. Biochem. 9, 123 (1994).
- [29] P. L. Holland and W. B. Tolman, Coord. Chem. Rev. 192, 855 (1999).
- [30] N. Duran and E. Esposito, Appl. Catal. B 28, 83 (2000).

- [31] L. Que and W. Tolman, Angew. Chem. Int. Ed. 41, 1114 (2002).
- [32] C. Limberg, Angew. Chem. Int. Ed. 42, 5932 (2003).
- [33] L. M. Mirica, X. Ottenwaelder, and T. D. P. Stack, Angew. Chem. Int. Ed. 10'4, 1013 (2004).
- [34] E. A. Lewis and W. B. Tolman, Chem. Rev. 104, 1047 (2004).
- [35] T. Punniyamurthy, S. Velusamy, and J. Iqbal, Chem. Rev. 105, 2329 (2005).
- [36] S. Itoh, Curr. Opin. Chem. Biol. 10, 115 (2006).
- [37] J. P. Klinman, J. Biol. Chem. 281, 3013 (2006).
- [38] J. M. Bollinger, Curr. Opin. Chem. Biol. 11, 151 (2007).
- [39] C. J. Cramer and W. B. Tolman, Acc. Chem. Res. 40, 601 (2007).
- [40] C. J. Cramer, B. A. Smith, and W. B. Tolman, J. Am. Chem. Soc. 118, 11283 (1996).
- [41] M. Flock and K. Pierloot, J. Phys. Chem. A 103, 95 (1999).
- [42] C. J. Cramer, W. B. Tolman, K. H. Theopold, and A. L. Rheingold, Proc. Natl. Acad. Sci., USA 100, 3635 (2003).
- [43] P. E. M. Siegbahn, J. Biol. Inorg. Chem. 8, 577 (2003).
- [44] B. F. Gherman and C. J. Cramer, Inorg. Chem. 43, 7281 (2004).
- [45] N. W. Aboelella, S. Kryatov, B. F. Gherman, W. W. Brennessel, V. G. J. Young, R. Sarangi, E. Rybak-Akimova, K. O. Hodgson, B. Hedman, E. I. Solomon, et al., J. Am. Chem. Soc. 126, 16896 (2004).
- [46] C. R. Kinsinger, B. F. Gherman, L. Gagliardi, and C. J. Cramer, J. Biol. Inorg. Chem. 10, 778 (2005).
- [47] M. F. Rode and H. Werner, Theor. Chim. Acta 114, 309 (2005).

[48] B. F. Gherman, D. E. Heppner, W. B. Tolman, and C. J. Cramer, J. Biol. Inorg. Chem. 11, 197 (2006).

- [49] C. J. Cramer, M. Wloch, P. Piecuch, C. Puzzarini, and L. Gagliardi, J. Phys. Chem. A 110, 1991 (2006).
- [50] C. J. Cramer, A. Kinal, M. Wloch, P. Piecuch, and L. Gagliardi, J. Phys. Chem. A 110, 11557 (2006).
- [51] B. F. Gherman and C. J. Cramer, Coord. Chem. Rev. doi:10.1016/j.ccr.2007.11.018 (2008).
- [52] C. J. Cramer, J. R. Gour, A. Kinal, M. Wloch, P. Piecuch, A. R. M. Shahi, and L. Gagliardi, J. Phys. Chem. A in press (2008).
- [53] V. Bonacic-Koutecky, J. Koutecky, and J. Michl, Angew. Chem. Int. Ed. 26, 170 (1987).
- [54] C. J. Cramer, Essentials of Computational Chemistry: Theories and Models, 2nd edition (J. Wiley & Son, Chichester, 2004).
- [55] A. D. Becke, Phys. Rev. A 38, 3098 (1988).
- [56] C. Lee, W. Yang, and R. G. Parr, Phys. Rev. B 37, 785 (1988). 23
- [57] A. D. Becke, J. Chem. Phys. 98, 5648 (1993).
- [58] P. J. Stephens, F. J. Devlin, C. F. Chabalowski, and K. J. Frisch, J. Phys. Chem. 98, 11623 (1994).
- [59] Institut für Theoretische Chemie, Universität Stuttgart, http://www.theochem.uni-stuttgart.de/.
- [60] D. Andrae, U. Häussermann, M. Dolg, H. Stoll, and H. Preuss, Theor. Chim. Acta 77, 123 (1990).
- [61] W. J. Hehre, L. Radom, P. v. R. Schleyer, and J. A. Pople, Molecular Orbital Theory (Wiley, New York, 1986).

- [62] P.-O. Widmark, P.-Å. Malmqvist, and B. O. Roos, Theor. Chim. Acta 77, 291 (1990).
- [63] B. O. Roos, R. Lindh, P.-Å. Malmqvist, V. Veryazov, and P.-O-Widmark, J. Phys. Chem. A 109, 2851 (2005).
- [64] B. O. Roos, R. Lindh, P.-Å. Malmqvist, V. Veryazov, and P.-O-Widmark, J. Phys. Chem. A 109, 6575 (2005).
- [65] K. Andersson and B. O. Roos, Chem. Phys. Letters 191, 507 (1992).
- [66] M. Merchán, R. Pou-Amérigo, and B. O. Roos, Chem. Phys. Letters 252, 405 (1996).
- [67] G. Ghigo, B. O. Roos, and P.-A. Malmqvist, Chem. Phys. Letters 396, 142 (2004).
- [68] K. H. Marti, I. M. Ondik, G. Moritz, and M. Reiher, J. Chem. Phys. 128, 014104 (2008).
- [69] J. L. Lewin, D. E. Heppner, and C. J. Cramer, J. Biol. Inorg. Chem. 12, 1221 (2007).

Chapter 4

What Active Space Adequately Describes Oxygen Activation by a Late Transition Metal? CASPT2 and RASPT2 Applied to Intermediates from the Reaction of O_2 with a Cu(I)- α -Ketocarboxylate

Stefan Huber¹, Abdul Rehaman Moughal Shahi ¹, Francesco Aquilante¹, Christopher J. Cramer² and Laura Gagliardi¹, 2

Published in Journal of Chemical Theory and Computation, 5 (11) , 2009, p 2976 $\,$

¹Department of Chemistry, University of Geneva, 30 quai E. Ansermet, Geneva 1211, Switzerland

²Department of Chemistry and Supercomputing Institute, University of Minnesota, 207 Pleasant, St. SE. Minneapolis, Minnesota 55455-0431, USA

What Active Space Adequately Describes Oxygen Activation by a Late Transition Metal? CASPT2 and RASPT2 Applied to Intermediates from the Reaction of O_2 with a Cu(I)- α -Ketocarboxylate

Multiconfigurational second-order perturbation theory calculations based on a complete active space reference wave function (CASPT2) employing active spaces of increasing size are well converged at the level of 12 electrons in 12 orbitals for the singlet-triplet state energy splittings of three supported copper-dioxygen and two supported copper-oxo complexes. Corresponding calculations using the restricted-active space approach (RASPT2) offered similar accuracy with significantly reduced computational overhead provided an inner (2,2) complete active space was included in the overall RAS space to account for strong biradical character in most of the compounds. The effects of different active space choices and outer RAS space excitations are examined and conclusions drawn with respect to the general applicability of the RASPT2 protocol.

4.1 Introduction

In order better to understand the mechanistic details of substrate oxidations catalyzed by copper-containing metalloenzymes, considerable effort has been devoted to the synthesis and characterization of smaller copper coordination complexes capable of activating molecular oxygen. [1, 2, 3, 4, 5, 6, 7, 8, 9] In a recent example, Hong et al. [10] reported the preparation, structural characterization, and reactivities of related Cu(I)- α -ketocarboxylate complexes supported by iminopyridine ligands appended with arene substituents positioned so as to be susceptible to intramolecular attack by an activated oxygen species (Scheme 1). Using density functional theory (DFT) and multiconfigurational second-order perturbation theory based on a complete-active-space reference wave function (CASSCF/CASPT2), the microscopic details of the multistep mechanism for the observed oxidation reaction have been elucidated, [10] as has the sensitivity of the reaction path energetics to different ligand sets. [11]

$$\begin{array}{c|c}
 & 1. O_2, -80^{\circ}C \\
 & acetone \\
 & O \\
 & O \\
 & Ph
\end{array}$$

Scheme 1

As indicated in Scheme 2 (in which only the N atoms of the supporting ligand are shown), the reaction proceeds by initial coordination of molecular oxygen to the supported copper complex. Three isomeric structures were predicted at the DFT level, two of which were characterized by end-on coordination of the O₂ moiety, while the other exhibited side-on coordination. Following decarboxylation and subsequent cleavage of the O–O bond in an intermediate peroxybenzoate complex, two isomeric Cu(II)-oxyl species could be accessed, differing in the coordination geometry about the Cu center (square-planar (SP) vs. trigonal-bipyramidal (TBP); the literature alternatively sometimes refers to such species as formal Cu(III)-oxo complexes, but calculations make clear that a Cu(II)-oxyl formulation is more appropriate given the relevant electronic structures [10, 12, 13, 14, 15]. Both the peroxybenzoate and the Cu(II)-oxyl intermediates were determined to be highly reactive with respect to oxidation of the pendant arene ring in the iminopyridine ligand. Experimental investigations designed to isolate a Cu(II)-oxyl intermediate and to extend the reactivity of such species to external substrates continue to be actively pursued.

Scheme 2

Considering in more detail the theoretical modeling of these species, several key intermediates are well described as having biradical character. In particular, the initial oxygen adducts and the Cu(II)-oxyl intermediates. In the case of the oxygen adducts, whether viewed as complexes of molecular O₂ with Cu(I) or as Cu(II)-superoxide compounds, two electrons are effectively localized on distinct centers: the two O atoms in the former instance and the Cu(II) and one O atom in the latter. [16] The latter localization also prevails in the Cu(II)-oxyl intermediates. Such biradical character introduces challenges with respect to computing the properties of singlet electronic states based on single-determinant formalisms, like Kohn-Sham density functional theory (KS-DFT). [17] A proper spin and spatial wave function for a biradical singlet, also sometimes referred to as an open-shell singlet, formally requires a minimum of two determinants. Nevertheless, by invocation of a relationship between the eigenvalues of the Heisenberg-Slater-Dirac Hamiltonian [18, 19, 20, 21] and the energies obtained from broken-symmetry and high-spin single-determinant calculations, [22, 23, 24, 25] DFT models have been successfully employed to compute state-energy splittings in many open-shell coordination compounds. [9, 26, 27, 28]

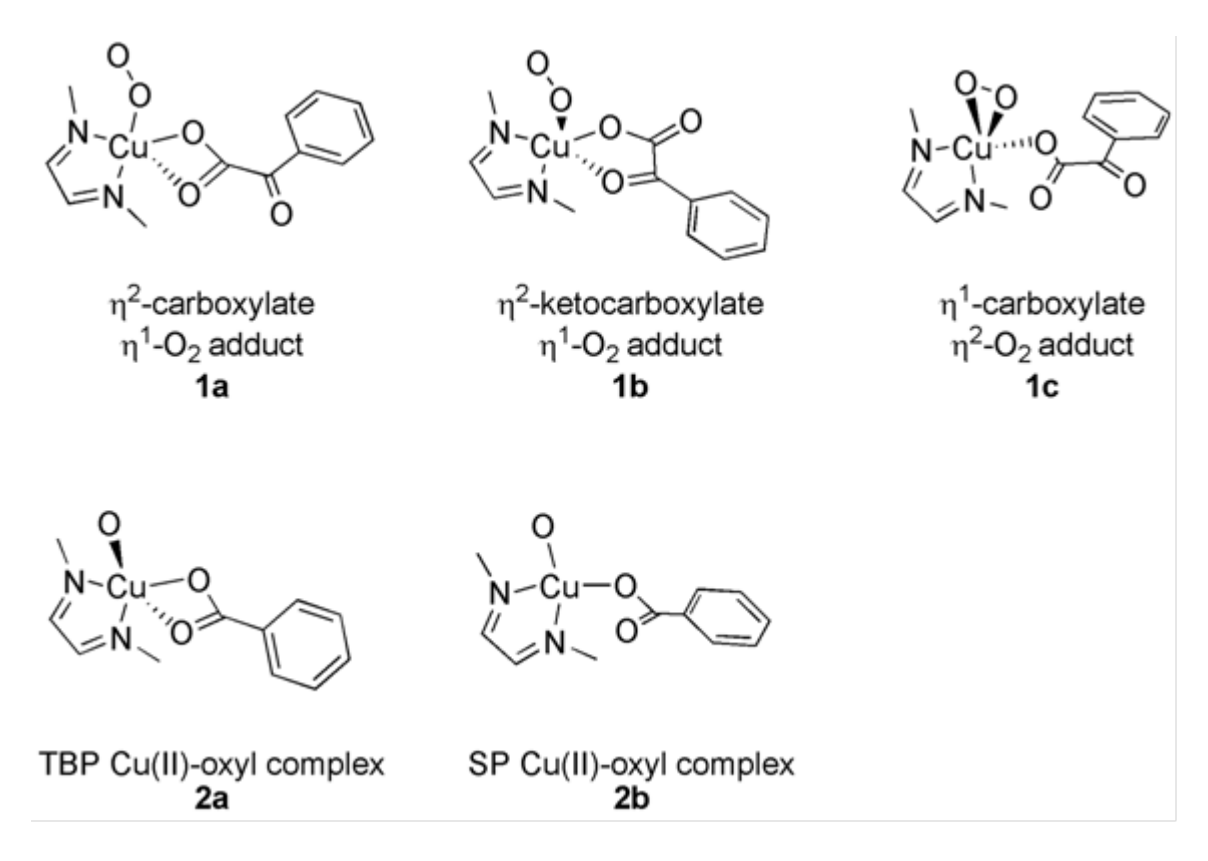
4.1. INTRODUCTION 77

However, this practical approach has a number of drawbacks, particularly insofar as no spin-pure wave function (or density) exists for states other than that of the highest spin, which can usually be well represented by a single determinant. Instead, the broken-symmetry states having S_z values below the S_{max} value for the high-spin state may be said to be spin-contaminated, and as such it is not clear how to evaluate properties other than the state energies. To be more precise, we should say that it is the Kohn-Sham determinant that is spin-contaminated—the wave function for the corresponding density is not known, so we cannot rigorously assess its spin expectation value, but, in practice, properties determined from broken-symmetry DFT calculations do appear to suffer from spin contamination.

In contrast to single-determinantal KS DFT, multideterminantal states are properly represented in multiconfigurational self-consistent field (MCSCF) theory. [29] The complete active space implementation of this theory, CASSCF, [30] constructs a wave function as a linear combination of all possible spin and spatially adapted determinants that may be formed from the distribution of a given number of "active" electrons in a given number of orbitals. The "active space" orbitals are typically chosen based on chemical analysis of the problem at hand, e.g., all bonding and antibonding orbitals associated with one or more bond making or bond breaking processes along a reaction coordinate. When supplemented by multireference second-order perturbation theory, CASSCF/CASPT2, [31] in order to account for dynamical electron correlation effects not included at the CASSCF level, accuracies on the order of 0.2 eV have been documented for state-energy splittings in molecules containing elements throughout the periodic table. [32, 33, 34, 35, 36, 37, 38, 39, 40, 41] In the particular case of the copper chemistry discussed above, Hong et al. [10] and Huber et al. [11] compared CASSCF/CASPT2 singlet-triplet splittings to those derived from broken-symmetry DFT calculations in order to assess the likely accuracy of the latter. The two models were in generally good agreement for the Cu(II)-oxyl species but agreement was less good for the initial oxygen adducts.

While such comparisons between broken-symmetry DFT and CASSCF/CASPT2 can be informative, the number of determinants in the CASSCF model increases factorially with increasing numbers of orbitals in the active space, leading to a practical limit of roughly 16

electrons in 16 orbitals. [17, 42] When larger active spaces are needed, e.g., in a trinuclear transition metal complex where a balanced active space might require three sets of valence d and s orbitals, the CASSCF/CASPT2 model cannot be applied in a practical fashion. In order to address this limitation, Malmqvist et al. [43] recently developed a second-order perturbation theory based on the restricted active space self-consistent-field method, namely, RASSCF/RASPT2. By subdividing the active space orbitals into three sets, one set entirely equivalent to a CAS space, one set consisting of occupied orbitals from which only a limited number of electrons may be excited, and one set consisting of virtual orbitals into which only a limited number of electrons may be excited, the number of orbitals and electrons that may be considered is substantially increased relative to the CASSCF/CASPT2 model. While initial results from studies of mono- and binuclear copper-oxygen adducts have been promising, much remains to be learned with respect to the question of how best to choose a RASSCF active space and excitation protocol. The aim of the present paper is to explore this question for biradical copper-oxygen adducts and Cu(II)-oxyl intermediates analogous to those already discussed above. In particular, we examine the predicted singlet-triplet splittings and relative isomer energies for the three adducts 1a-c and two intermediates 2a and 2b shown in Scheme 3. In order to facilitate this benchmarking study, the sterically demanding N-donor ligand shown in Scheme 1 is replaced by a simplified diimine ligand similarly characterized by two sp² hybridized donor nitrogen atoms. We begin with a discussion of the computational details, then present results designed to assess convergence in predicted energies with respect to methodological choices, and conclude with some general observations likely to prove useful in future applications of the RASSCF/RASPT2 model.



Scheme 3

4.2 Computational Details

Geometries of the structures in Scheme 3 were optimized at the M06-L [44] level of density functional theory adopting a broken-symmetry unrestricted formalism for the nominal singlet states. As we are interested here in comparing different RASSCF/RASPT2 protocols for given geometries, the choice of any particular geometry is arbitrary, but it is perhaps worth emphasizing that computed state-energy splittings in this work are vertical and not adiabatic. Geometry optimizations employed the Cu basis set and pseudopotential of Dolg et al. [45] augmented with three f functions having exponents of 5.10, 1.275, and 0.32; the 6-31G(d) basis set [46] was used for all other atoms.

Multiconfigurational calculations were accomplished according to a number of different protocols. In all cases, basis sets of ANO and ANO-RCC (for Cu) type [47, 48] were employed using contractions of 5s3p2d1f, 3s2p1d, 3s2p1d, 3s2p, and 1s for Cu, O, N, C and H, respectively. In prior work on the experimentally characterized system of Hong et al., (12,12) CAS spaces were adopted for CASSCF/CASPT2 calculations on the various species with the orbitals included based on a careful assessment of occupation numbers for different active space constructions. [10] These spaces inevitably contained orbitals formed from bonding and antibonding combinations of O 2p orbitals and Cu 3d orbitals, with the precise number of σ, π , and nonbonding orbitals being dictated by the chemical structure. The size of the active space was chosen based on consideration of 12 intermediates and transition-state structures along the reaction coordinate for the overall reaction indicated in Scheme 1. Our goal was to find an active space size that was consistent for all structures and was converged for predicted singlet-triplet energy splittings. The (12,12) space fulfilled these criteria. With respect to the convergence issue, calculations employing expanded (14,14) active spaces predicted very similar singlet-triplet splittings, e.g., 2.33 and 2.34 kcal/mol for structure 1b of the present study with (12,12) and (14,14) active spaces, respectively.

Those CAS(12,12) active space orbitals most relevant to the present study are illustrated in Figures 4.1 and 4.2; in particular, for each of the five structures discussed in this paper, two orbitals in the relevant active space had occupation numbers in the singlet state differing substantially from 2.0 or 0.0, consistent with varying degrees of biradical character, and these are shown in Figure 4.1. In addition, for the particular case of $\bf 1a$, the remaining 10 orbitals are shown in Figure 4.2. These orbitals are roughly representative of the analogous ones used for the various other structures, which, in the interest of brevity, are not depicted here. For $\bf 1a$ - $\bf c$, these orbitals involved π bonding and antibonding combinations of a Cu 3d orbital and an $\bf O_2$ π^* orbital, and the CAS(12,12) occupation numbers were 1.30, 0.70 ($\bf 1a$), 1.05, 0.95 ($\bf 1b$), and 1.78, 0.25 ($\bf 1c$). In the cases of $\bf 2a$ and $\bf 2b$, it was hybrid π orbitals from Cu 3d and O 2p orbitals that had occupation numbers of 1.16, 0.85 ($\bf 2a$), and 1.11, 0.89 ($\bf 2b$). All of these orbitals had occupation numbers of 1.0 in the corresponding triplet states. The other orbitals of the (12,12) active space included all remaining Cu 3d orbitals and a second shell of Cu d orbitals for correlation. When forming smaller (10,10) and (8.8) active spaces, as

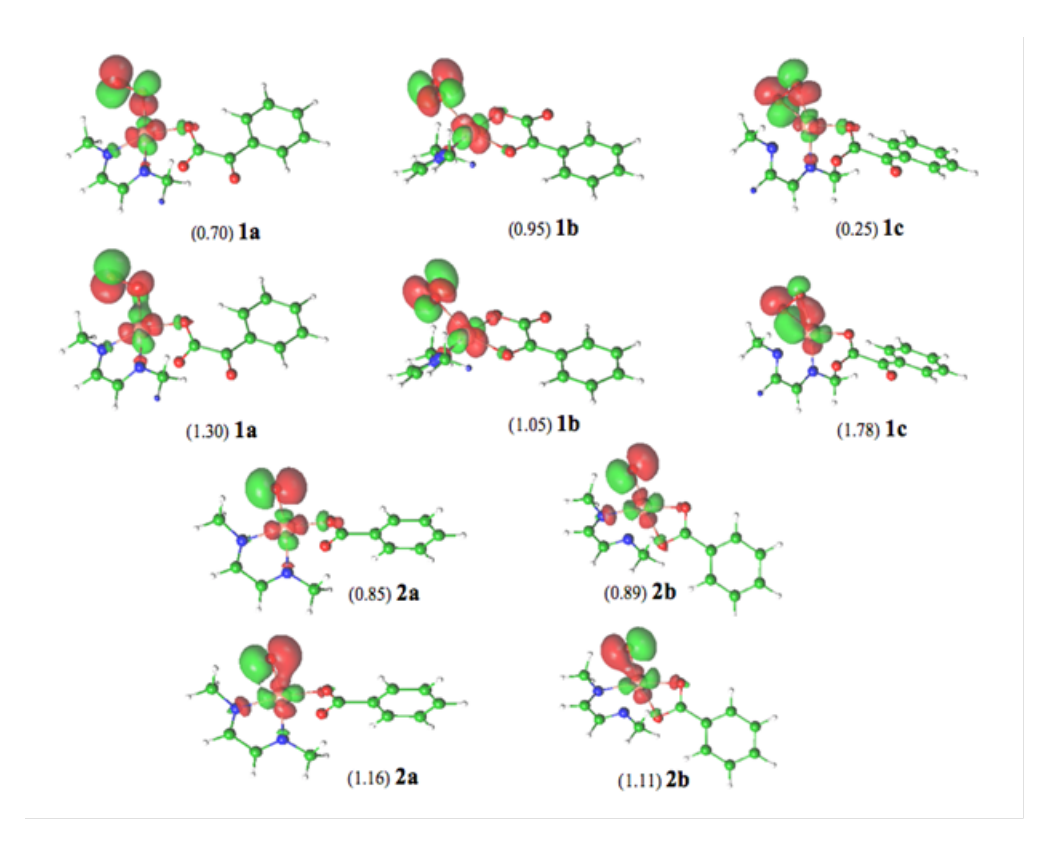


Figure 4.1: Isodensity surfaces (0.04 a.u.) and occupation numbers for the two active space orbitals with occupation numbers closest to 1.0 from CAS(12,12) calculations for **1a**-**1c** and **2a** and **2b**. Pairs of orbitals are ordered above and below one another (see also Scheme 3 for isomer ordering). Atomic colors are white (H), green (C), blue (N), red (O), and bronze (Cu).

described below, hybrid orbitals having substantial Cu d character were sequentially removed based on the degree to which their occupation numbers were very near 2.0 or 0.0 for occupied and virtual orbitals, respectively.

In the RASSCF model, the active subspace is divided into three distinct regions: RAS1, RAS2, and RAS3. The RAS2 region is identical to the active region in a CASSCF calculation, i.e., all possible spin- and symmetry-adapted configuration state functions, CSFs, that can be constructed from the orbitals in RAS2 are included in the multiconfigurational wave function. The RAS1 and RAS3 spaces, on the other hand, permit the generation of addi-

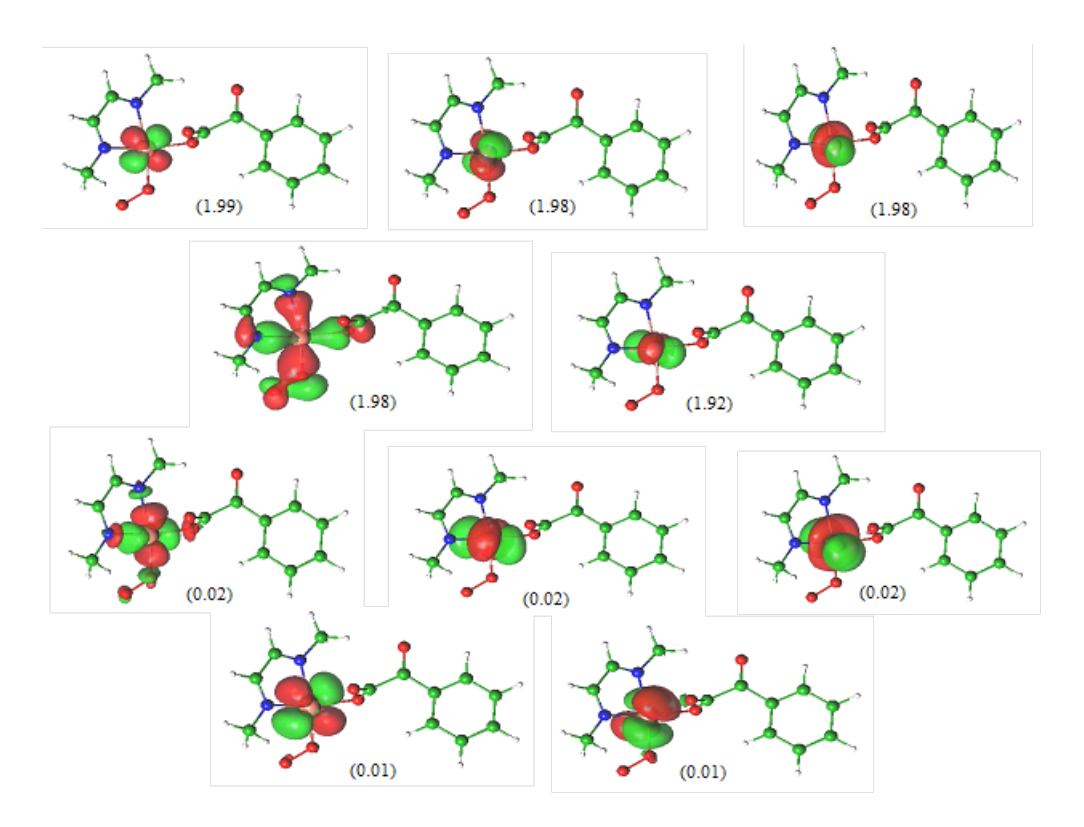


Figure 4.2: Isodensity surfaces (0.04 a.u.) and occupation numbers for the remaining 10 active space orbitals that are not shown in Figure 1 from a CAS(12,12) calculation for **1a**. Atomic colors are white (H), green (C), blue (N), red (O), and bronze (Cu).

tional CSFs subject to the restriction that a maximum number of excitations may occur from RAS1, which otherwise contains only doubly occupied orbitals, and a maximum number of excitations may occur into RAS3, which otherwise contains only external orbitals. There are various ways in which one can select the orbitals. In the present case, the maximum size of the full active space was kept at 12 orbitals, in analogy with the CASSCF calculations. Only the two orbitals with an occupation number significantly different from two and zero (see figure 4.2) were placed in RAS2, with the remaining occupied (mostly 3d) orbitals being in RAS1 and the unoccupied 4d orbitals (mostly) being in RAS3. Several levels of maximum excitation from RAS1 or into RAS3 were considered, namely up to double (SD), up to triple (SDT), and up to quadruple excitations (SDTQ). The general notation for a RASPT2 calculation is RASPT2(j,k)/(l,m)/n, where j is the number of electrons in RAS1 and RAS2,

k is the number of orbitals in all RAS spaces, l is the number of electrons in RAS2, m is the number of orbitals in RAS2, and n is the maximum level of excitation permitted out of RAS1 and into RAS3. Thus, for instance, a RASPT2(12,12)/(2,2)/3 calculation would have 10 electrons and 5 orbitals in RAS1, 2 electrons and 2 orbitals in RAS2, 5 orbitals in RAS3, and would permit up to triple excitations out of RAS1 or into RAS3.

In all calculations, Cholesky decomposition [49, 50] of the two-electron integrals was accomplished with a threshold of 10^{-5} a.u. Reduced-scaling evaluation of the Fock exchange matrices in the CASSCF and RASSCF calculations was accomplished by means of the Local-K (LK) screening approach [51] employing localized Cholesky orbitals. [52] M06-L calculations were done with MN-GFM, [53] a locally modified version of the Gaussian03 electronic structure program suite. [54] All CASSCF/CASPT2 and RASSCF/RASPT2 calculations were done with the MOLCAS 7.2 package. [42]

4.3 Results and Discussion

Singlet-triplet state-energy splittings.

We begin with an examination of the predicted singlet-triplet splittings at the CASSCF and RASSCF, and CASPT2 and RASPT2 levels, as a function of active space choice. Results from CASSCF and CASPT2 calculations are presented in Table 4.1.

A few trends merit discussion in the CASSCF/CASPT2 singlet-triplet splittings. First, at the CASSCF level, expanding the active space from (10,10) to (12,12) causes changes in the predicted splittings of 1 kcal/mol or less. At the CASPT2 level, the same change in active space size has an effect of roughly similar magnitude, with the exception of 1c where it is a somewhat larger 2.3 kcal/mol. In addition, the change in the splitting on going from the CASSCF level to the CASPT2 level is 0.4, 1.2, 6.3, 1.2, and 1.6 kcal/mol, respectively, for 1a–1c, 2a, and 2b. Dynamical correlation at the CASPT2 level favors the triplet state in every instance, but the change is small with the exception of 1c, which continues to be somewhat of an outlier. All of these observations suggest that the CASPT2(12,12) values

Table 4.1: Singlet-triplet state-energy splittings (kcal/mol) predicted at the CASSCF and CASPT2 levels for various active space choices.

	Structure					
Active space	1a	1b	1c	2a	2 b	
CASSCF						
(2,2)	0.4	0.4	-4.5	-4.5	2.1	
(8,8)	-11.7	-13.1	-23.0	-10.7	-10.1	
(10,10)	1.8	0.9	-8.8	3.2	3.6	
(12,12)	0.8	1.1	-9.4	4.0	4.4	
$\underline{\text{CASPT2}}$						
(2,2)	-0.1	0.4	-11.7	2.8	3.6	
(8,8)	8.1	7.8	-3.9	9.7	10.7	
(10,10)	2.5	1.8	-5.4	4.7	5.3	
(12,12)	1.2	2.3	-3.1	5.2	6.0	

may be considered to be reasonably well converged (and, as noted in the methods section, expanding to (14,14) in select instances led to negligible changes in predicted splittings). Thus, for future discussion purposes, we will consider the CASPT2(12,12) values to be reliable, with the possible exception of 1c, where a larger uncertainty exists.

With respect to smaller active spaces, it is noteworthy that the very simple (2,2) space offers quite reasonable accuracy in most instances, consistent with a fairly simple biradical description for the species under consideration. The exception is again 1c, but, as can be judged by the occupation numbers of the frontier orbitals for this structure in Figure 4.1, it is the least biradicaloid of the five compounds considered here, so one would not expect the (2,2) active space to capture as much nondynamical correlation as in the other instances. The (8,8) space leads to very poor predictions at the CASSCF level because it is difficult to find any clear distinction between different (8,8) spaces based on occupation numbers (cf. Figure 4.2 for the case of 1a), suggesting that either more orbitals or fewer orbitals leads to better balance. Including additional correlation effects at the CASPT2 level moderates the poor balance of the (8,8) spaces to some extent, but results remain poor compared to CASPT2(12,12).

To put into better perspective the efficiencies of different active spaces and the biradical

character of the singlet wave functions, we list in Table 4.2 the numbers of configuration state functions (CSFs) and dominant CSF weights for different active space choices. As the number of CSFs in the (2,2) spaces are about 5 orders of magnitude fewer than in the (12,12) spaces, the reasonable accuracy of the (2,2) predictions is certainly noteworthy from an efficiency standpoint. Inspection of the CSF weights makes clear that all triplets are essentially single determinantal, while most singlets have very high biradical character (defined as having roughly equal weights of the two dominant configurations) with 1c being the least biradical.

Table 4.2: Number of configuration state functions and dominant weights for various CASSCF active space choices.

			Dominant	CSF	weights	
Active space	No. CSFs	1a	1b	1c	2a	2b
(2,2)	3^a	$55/45^{b}$	51/49	79/21	56/44	54/46
	1	100	100	100	100	100
(8,8)	1764	59/39	51/48	83/15	61/37	58/40
	2352	99	99	98	98	98
(10,10)	19404	59/39	51/47	85/12	57/41	55/43
	29700	98	98	97	97	97
(12,12)	226512	63/34	51/46	85/10	56/41	54/43
	382239	97	97	97	96	96

^aSinglet above triplet. ^b Singlet above triplet; the weights of the two dominant CSFs are reported in the former case and the weight of the one dominant CSF in the latter case.

Turning next to the RASSCF and RASPT2 calculations, Table 4.3 lists the computed state energy splittings for various RAS protocols and Table 4.4 provides information on the numbers of CSFs and the weights of the dominant configurations associated with different active space choices. For convenience, in Table 4.3 the results from CASPT2(2,2) and CASPT2(12,12) calculations are recapitulated, and the same is true for CAS(12,12) in Table 4.4.

The first point to address is the very good performance of the RASPT2(12,12)/(2,2)/2 protocol. Compared to CASPT2(12,12), all state energy splittings are predicted to within a

mean unsigned error of 0.8 kcal/mol and a maximum unsigned error of 1.1 kcal/mol. Note in particular that this is better accuracy than CASPT2(2,2), suggesting that the additional excitations considered in the RAS protocol are important. With respect to dynamical correlation energy, the difference between the RASPT2(12,12)/(2,2)/2 and RASSCF(12,12)/(2,2)/2 state energy splittings is usually small (except for 1c it does not exceed 1.2 kcal/mol), but the RASPT2 model is in better agreement with CASPT2(12,12) in every instance, indicating the utility of the post-RASSCF PT2 calculation. Considering, as indicated in Table 4.4, that the number of CSFs is reduced by about 2 orders of magnitude on going from CASPT2(12,12) to RASPT2(12,12)/(2,2)/2, this is a particularly impressive level of accuracy.

As an additional measure of the importance of the orbital relaxation associated with RASSCF excitations outside the central (2,2) CAS space, we examined using the orbitals from a CASSCF(2,2) calculation as frozen orbitals for a subsequent RASPT2(12,12)/(2,2)/2 calculation. That is, we did not reoptimize any molecular orbital coefficients after the CAS(2,2) step, but instead only optimized the configuration interaction coefficients in the RAS(12,12)/(2,2)/2 wave function that was used as the multiconfigurational reference for the PT2. Such a calculation is computationally very inexpensive. However, the results were essentially the same as those obtained at the CASPT2(2,2) level, indicating that orbital relaxations associated with the RAS outer space excitations do improve the agreement with CASPT2 calculations using larger active spaces.

Turning to the consideration of triple and quadruple excitations in the outer RAS spaces, changes in predicted state-energy splittings tend to be small, but offer quantitative improvement in the agreement with CASPT2(12,12) values. At the RASPT2(12,12)/(2,2)/4 level, for which the number of CSFs is reduced by a factor somewhat larger than 4 compared to the CASPT2(12,12) level, the agreement averages within 0.1 kcal/mol for all structures other than 1c. For this latter structure, higher RAS excitations lead to progressively less good agreement with CASPT2(12,12). As already noted above, this structure is the one case where the (12,12) active space may not represent a sufficiently large space to be considered converged, and thus it may not be as meaningful to make a comparison for this least biradicaloid dioxo species. As a technical note, the current implementation of the RASPT2

Table 4.3: Singlet-triplet state-energy splittings (kcal/mol) predicted at the RASSCF and RASPT2 levels for various active space choices.

			Structure		
Active space	1a	1b	1c	2a	2 b
RASSCF					
(12,12)/(2,2)/2	0.7	0.9	-7.7	3.4	3.8
(12,12)/(2,2)/3	0.8	1.0	-8.5	3.8	4.2
(12,12)/(2,2)/4	0.8	1.1	-9.2	3.9	4.4
$(12,12)//2^a$	24.4	20.4	5.5	32.1	32.6
$(12,\!12)//3^a$	11.7	12.2	-4.7	17.8	14.7
$\underline{\text{RASPT2}}$					
(12,12)/(2,2)/2	0.8	1.5	-2.6	4.1	5.0
(12,12)/(2,2)/3	0.8	1.9	-2.1	4.8	5.8
(12,12)/(2,2)/4	1.6	2.3	2.0	5.3	6.0
$(12,12)//2^a$	22.9	25.6	5.3	25.8	25.4
$(12,12)//3^a$	2.3	3.0	-5.9	17.5	9.4
CASPT2					
(2,2)	-0.1	0.4	-11.7	2.8	3.6
(12,12)	1.2	2.3	-3.1	5.2	6.0
1 0 1 1		c 11	1 . 1		. 1

^aThe excitation level for the triplet state is formally one higher, since the generation of a triplet state from the starting set of six occupied RAS1 orbitals and six virtual RAS3 orbitals requires an initial single excitation.

model in MOLCAS is such that RASSCF convergence tends to be rapid when only double excitations are considered, and slows down considerably when higher levels of excitations are allowed. While future development efforts will be targeted to improve the convergence in the latter instance, the excellent accuracy of the RASPT2(12,12)/(2,2)/2 model for the present test set bodes well for future applications to other analogous biradicaloid transition-metal oxo species.

A curious feature of the outer-space RAS excitations that merits further study is the degree to which dominant configuration weights are reduced when excitations are limited to no more than triples. As seen in Table 4.4, in every instance the dominant configuration weights drop by 3-10% at the RASSCF(12,12)/(2,2)/3 level compared to the RASSCF(12,12)/(2,2)/2

Table 4.4: Number of configuration state functions and dominant weights for various RASSCF active space choices and excitation levels.

			Dominant	CSF	weights	
Active space	No.	1a	1b	1c	2a	2b
	CSFs					
$\overline{(12,12)/(2,2)/2}$	2028^{a}	$60/37^{b}$	51/46	84/13	56/41	54/43
	2891	97	97	97	97	96
(12,12)/(2,2)/3	14428	57/31	47/41	77/10	51/37	49/39
	22991	88	88	87	87	87
(12,12)/(2,2)/4	54678	62/33	51/44	84/9	55/40	53/42
	91091	95	95	95	94	94
$(12,\!12)//2^c$	703	90/d	90/a	89/6	82/15	84/13
	8991	97	97	97	97	97
$(12,\!12)//3^c$	6003	66/15	67/13	65/31	59/22	56/24
	45441	90	88	88	82	88
CAS(12,12)	226512	63/34	51/46	85/10	56 / 41	54 / 43
	382239	97	97	97	96	96

^a Singlet above triplet. ^b Singlet above triplet; the weights of the two dominant CSFs are reported in the former case and the weight of the one dominant CSF in the latter case. ^c The excitation level for the triplet state is formally one higher, since the generation of a triplet state from the starting set of six occupied RAS1 orbitals and six virtual RAS3 orbitals requires an initial single excitation. ^d No second singlet CSF has a weight of 5% or higher.

level. Of course, one might argue that as the number of possible CSFs increases to the full CI limit, one might naturally expect the weights of individual configurations to drop somewhat, but on going to the RASSCF(12,12)/(2,2)/4 level, i.e., including quadruples, the weights return to very near the RASSCF(12,12)/(2,2)/2 values, and are moreover almost identical to the CASSCF(12,12) values. Such oscillating behavior among even and odd levels of excitations is reminiscent of the convergence behavior of the correlation energy in Møller-Plesset perturbation theory, explored in detail by Olsen et al. [55, 56] and also by Luna et al. [57] This last reference [57] deserves special attention since it focuses on the problem of poor convergence with second order perturbation theory for ground state Cu(I) complexes.

In order to study this point further, one would have to monitor CSF weights for still higher

levels of excitation. For the present molecules, however, such calculations are prohibitively expensive. We will investigate this behavior for smaller test systems in the future.

We now consider an alternative protocol, which one might adapt in the absence of any knowledge of biradical character in the subject molecules. In particular, we examine RASPT2 protocols with a total of 12 electrons in 12 orbitals, but with no inner CAS(2,2) space, permitting up to double excitations from the occupied space to the virtual space. To be precise, it is the singlet state for which excitations up to double are allowed. For the triplet state, generation of a triplet wave function already requires a single excitation (with spin flip), so that the triplet state calculations actually permit up to triplet excitations in order to correspond properly with the singlet analogs. In any case, as shown in Table 4.3, the accuracy of the RASPT2(12,12)//2 approach is extremely poor, with errors as high as 23 kcal/mol. The direction of the errors indicates that the correlation energies predicted for the singlet states are considerably smaller than those for the triplet states. Inspection of the CSF weights (Table 4.4) indicates that the problem appears to be with the failure of the RAS(12,12)//2 protocol to adequately relax the orbitals such that the weight of a formally doubly excited configuration becomes fairly close to that of the reference configuration for the biradicaloid singlet states.

In addition to noting that this problem is least severe for 1c, which is the least biradicaloid of all of the singlets, inspection of the absolute electronic energies further illustrates the importance of this point. Triplet 1a, for example, has a predicted electronic energy at the CAS(2,2) level of -2598.57346. At the RAS(12,12)/(2,2)/2 level, the corresponding energy is -2598.73770, and at the RAS(12,12)//2, it is -2598.73794; thus, the two are very close, as might be expected. For the singlet state, on the other hand, the CAS(2,2) electronic energy is -2598.57290, and the RAS(12,12)/(2,2)/2 energy is -2598.73662, but the RAS(12,12)//2 energy is -2598.69905, the final value being 37 mE_h more positive than the RAS(12,12)/(2,2)/2 reference. This failure to adequately rotate the most important occupied and virtual orbital(s) in the SCF procedure of the RAS(12,12)//2 calculations will merit further attention but suggests that strong non-dynamical correlation effects should still be addressed with inner CASSCF spaces when possible.

The situation improves somewhat when the RASSCF excitation level is increased. Examining the state-energy splittings and CSF weights for the RASPT2(12,12)//3 level, the former are in reasonable agreement with CASPT2(12,12) results (except for 2a), but are not as good as the state-energy splittings predicted at the RASPT2(12,12)/(2,2)/2 level, where fewer CSFs are required. Interestingly, the CSF weights are again depressed upon the inclusion of triple excitations; the amount of that depression for the most dominant CSF in the singlet is coincidentally about equal to the degree to which single-configurational character is overemphasized by the failure to include an interior CASSCF(2,2) space, but consideration of the minor singlet CSF or the dominant triplet CSF clearly illustrates the phenomenon. The trend on going from the RASPT2(12,12)//2 to the RASPT2(12,12)//3 level suggests that good results might be expected from the RASPT2(12,12)//4 level. However, the final level requires formal quintuple excitations to generate quadruply excited triplet states, and we were not successful in converging such calculations, which in any case require a number of CSFs so large that there is little point in not simply carrying out a full CASPT2 calculation.

Relative energies of different isomers.

In addition to state-energy splittings, we examined the differences in specific spin-state energies for the three dioxygen adduct isomers and the two copper-oxo isomers. These results are presented in Table 4.5 for the triplet states and Table 4.6 for the singlet states. As we consider here only a single geometry for each species (see Methods section), and as we have already noted the relative performances of the various models for singlet-triplet energy differences, in principle the data in Table 4.6 should be evident from consideration of Table 4.5 and the foregoing data, but it is helpful to see where errors cancel or reinforce in the isomer energies.

For the triplet states, there is good convergence in the CASPT2 relative energies as the active space is increased from (2,2) to (12,12) in size. Moreover, all of the RASPT2 protocols are in fairly good agreement with the CASPT2(12,12) predictions, with the best agreement given by the RASPT2(12,12)/(2,2)/3 model (the results are very nearly as good at the RASPT2(12,12)/(2,2)/4 level). While this agreement suggests that the RASPT2 approaches

Table 4.5: Triplet energies (kcal/mol) of **1b** and **1c** relative to **1a** and **2b** relative to **2a** computed at various levels of theory.

	Structure			
Theory	1b	1c	2 b	
RASPT2				
(12,12)/(2,2)/2	3.9	-12.9	-0.1	
(12,12)/(2,2)/3	4.3	-14.0	0.4	
(12,12)/(2,2)/4	4.4	-13.3	0.1	
$(12,\!12)//2^a$	3.8	-13.4	0.0	
$(12,12)//3^a$	3.2	-15.1	-2.4	
$\underline{\text{CASPT2}}$				
(2,2)	2.3	-12.6	1.3	
(8,8)	4.2	-12.8	1.2	
(10,10)	4.6	-13.6	1.1	
(12,12)	4.7	-13.8	1.3	
$\overline{\mathrm{DFT}}$				
M06-L	1.9	4.4	-0.7	

^a The excitation level for the triplet state is formally one higher, since the generation of a triplet state from the starting set of six occupied RAS1 orbitals and six virtual RAS3 orbitals requires an initial single excitation.

are doing as good a job as CASPT2, the latter model itself may not be particularly accurate for the isomer energies. For comparison, we computed the M06-L relative energies for the same geometries, and these, too, are listed in Table 4.5. For the copper-oxo isomerization, the multireference models and M06-L are in fair agreement, while M06-L predicts the **1b-1a** energy difference to be smaller by about 3 kcal/mol than computed at the multireference levels. Finally, there is a very large discrepancy between the two types of theory for the **1c-1a** energy difference, with the multireference models predicting the side-on geometry to be much more stable than either end-on copper oxygen complex, and M06-L predicting the opposite.

As for which, if either, level of theory is more likely to be correct, various considerations suggest that the M06-L predictions are likely more trustworthy, at least for the **1c-1a** energy difference, where the discrepancy is largest. First, the triplets are all well described by single

determinants, in which instance DFT is generally quite robust for conformational analysis. [17] Second, consideration of a wide range of supported Cu(I)-dioxygen complexes suggests that the particular ligand set employed here would be more likely to favor an end-on coordination geometry to a side-on one. [6, 7, 16, 58] Third, and perhaps most importantly, were 1c to be as stable as is predicted at the RASPT2 and CASPT2 levels, the activation energy associated with the subsequent decarboxylation step (Scheme 2) would be inconsistent with the experimental kinetics, where M06-L is consistent. [10] (A precise quantification of this point would require more attention to optimization of the geometries for all relevant states, but the CASPT2/DFT discrepancy of 18.2 kcal/mol listed for 1c in Table 4.5 seems well outside the range of energies that might be associated with minor geometric relaxations in the triplet states).

Table 4.6: Singlet energies (kcal/mol) of **1b** and **1c** relative to **1a** and **2b** relative to **2a** computed at various levels of theory.

	Structure				
Theory	1b	1c	2 b		
RASPT2					
(12,12)/(2,2)/2	4.7	-16.3	-0.9		
(12,12)/(2,2)/3	5.4	-16.9	-0.6		
(12,12)/(2,2)/4	5.0	-13.0	-0.6		
$(12,\!12)//2$	6.6	-31.0	0.4		
(12,12)//3	3.8	-23.3	5.8		
$\underline{\text{CASPT2}}$					
(2,2)	2.9	-24.2	0.5		
(8,8)	3.9	-24.8	0.1		
(10,10)	3.8	-21.5	0.5		
(12,12)	5.9	-18.0	0.4		

Thus, while we have established that the (12,12) active space is in all cases, with the possible exception of 1c, adequate to compute converged state-energy splittings, it would appear that it is not adequate to compute isomer energies when the active space is not perfectly converged for all structures considered, with 1c again being the most problematic case. The geometric differences between 2a and 2b are small enough that even the (12,12) space

4.4. SIGNIFICANCE 93

seems adequate. It would be interesting to examine whether a full valence active space, using a RAS protocol, would give better results, but such calculations remain outside our present capabilities.

With respect to the relative singlet energies, most trends identified for the triplet states remain the same: RASPT2(12,12)/(2,2)/3 shows the best agreement with CASPT2(12,12) with the double and quadruple excitation levels being nearly as good. However, the RASPT2(12,12)//2 and //3 models are less consistent. They are surprisingly good for **1b** and **2b**, considering that these levels do very poorly for state-energy splittings, suggesting that the failure to capture singlet correlation energy is quite consistent across geometric isomers. The exception is **1c**, where there is greater sensitivity to the excitation level. In this case, we do not compare to M06-L, as the computation of biradical singlet energies with DFT presents its own set of complications that go beyond our interests in the present work.

4.4 Significance

We have compared the CASPT2 and RASPT2 models for the determination of the singlet-triplet state-energy splittings of five intermediates associated with the formation and reaction of copper-oxo species derived from oxygenation of Cu(I)-α-ketocarboxylate complexes. Based on consideration of several active spaces, we determined that the CASPT2 model was well converged with a (12,12) active space, but that semiquantitative results could be obtained with a minimal (2,2) space in most instances. Certain intermediate active spaces failed to be balanced, e.g., no good (8,8) active space could be identified. At the RASPT2 level, results were quantitatively very accurate (compared to CASPT2(12,12)) when an inner (2,2) CAS space was included in a total (12,12) space. Including up to double excitations in the outer RAS spaces generated two orders of magnitude fewer configuration state functions than the full CASPT2(12,12) calculations but provided essentially equivalent accuracy. Adding additional excitations in the outer RAS spaces led to small but systematic improvements in accuracy.

RASPT2 calculations with a (12,12) space that did not include an inner (2,2) CAS space were less accurate in their predictions; such calculations suffer from the requirement that triplet states begin as single excitations (with spin flip) from the (12,12) starting configuration, so the number of triplet configuration state functions is artificially inflated when additional excitations are desired to be consistent with singlet state wave functions. While it was not possible to include a sufficient number of excitations with this approach to demonstrate convergence, the trend in going from singles and doubles to singles, doubles, and triples suggests that it could be an effective strategy if efficient SCF convergence schemes are developed.

Neither CASPT2 nor similar RASPT2 isomer energies were judged to be especially accurate with (12,12) active spaces. This may reflect a greater demand on active space size for the computation of geometric energy differences in transition-metal complexes, or it may be specific to the systems under consideration here. This issue deserves further study in systems where full-valence active spaces may be accessible.

Overall, the RASPT2 model, when applied with careful attention to the most critical features associated with possible non-dynamical correlation, offers an efficient alternative to more demanding CASPT2 calculations with no loss in accuracy. These results seem particularly encouraging for the study of chemical systems having minimal balanced active spaces that are still so large that they are inaccessible to the conventional CASPT2 method.

Bibliography

- [1] Solomon, E. I.; Baldwin, M. J.; Lowery, M. D., Chem. Rev. 1992, 92, 521-542.
- [2] Mirica, L. M.; Ottenwaelder, X.; Stack, T. D. P., Chem. Rev. 2004, 104 (2), 1013-1045.
- [3] Lewis, E. A.; Tolman, W. B., Chem. Rev. 2004, 104 (2), 1047-1076.
- [4] Klinman, J. P., J. Biol. Chem. 2006, 281, 3013-3016.
- [5] Hatcher, L. Q.; Karlin, K. D., Adv. Inorg. Chem. 2006, 58, 131-184.
- [6] Itoh, S., Curr. Opin. Chem. Biol. 2006, 10 (2), 115-122.
- [7] Cramer, C. J.; Tolman, W. B., Acc. Chem. Res. 2007, 40 (7), 601-608.
- [8] Rolff, M.; Tuczek, F., Angew. Chem. Int. Ed. 2008, 47 (13), 2344-2347.
- [9] Gherman, B. F.; Cramer, C. J., Coord. Chem. Rev. 2009, 253, 723-753.
- [10] Hong, S.; Huber, S. M.; Gagliardi, L.; Cramer, C. J.; Tolman, W. B., J. Am. Chem. Soc. 2007, 129 (46), 14190-14192.
- [11] Huber, S. M.; Ertem, M. Z.; Aquilante, F.; Gagliardi, L.; Tolman, W. B.; Cramer, C. J., Chem. Eur. J. 2009, 15, 4886-4895.
- [12] Yamaguchi, K.; Takahara, Y.; Fueno, T., Ab-Initio Molecular Orbital Studies of Structure and Reactivity of Transition Metal-Oxo Compounds. In Applied Quantum Chemistry, Smith, V. H.; Schaefer, H. F.; Morokuma, K., Eds. Kluwer: Dordrecht, 1986; pp 155-184.

[13] Schroder, D.; Holthausen, M. C.; Schwarz, H., J. Phys. Chem. B 2004, 108 (38), 14407-14416.

- [14] Decker, A.; Solomon, E. I., Curr. Opin. Chem. Biol. 2005, 9, 152-163.
- [15] Gherman, B. F.; Tolman, W. B.; Cramer, C. J., J. Comp. Chem. 2006, 27 (16), 1950-1961.
- [16] Cramer, C. J.; Gour, J. R.; Kinal, A.; Wtoch, M.; Piecuch, P.; Moughal Shahi, A. R.; Gagliardi, L., J. Phys. Chem. A 2008, 112 (16), 3754-3767.
- [17] Cramer, C. J., Essentials of Computational Chemistry: Theories and Models. 2nd ed.; John Wiley & Sons: Chichester, 2004; p 385-427.
- [18] Heisenberg, W., Z. Physik 1928, 49, 619.
- [19] Dirac, P. A. M., Proc. R. Soc. London, Ser. A 1929, 123, 714.
- [20] Van Vleck, J. H., Rev. Mod. Phys. 1945, 17, 27.
- [21] Slater, J. C., Rev. Mod. Phys. 1953, 25, 199.
- [22] Ziegler, T.; Rauk, A.; Baerends, E. J., Theor. Chim. Acta 1977, 43, 261-271.
- [23] Noodleman, L., J. Chem. Phys. 1981, 74 (10), 5737-5743.
- [24] Yamaguchi, K.; Jensen, F.; Dorigo, A.; Houk, K. N., Chem. Phys. Lett. 1988, 149, 537-542.
- [25] Soda, T.; Kitagawa, Y.; Onishi, T.; Takano, Y.; Shigeta, Y.; Nagao, H.; Yoshioka, Y.; Yamaguchi, K., Chem. Phys. Lett. 2000, 319 (3-4), 223-230.
- [26] Ciofini, I.; Daul, C. A., Coord. Chem. Rev. 2003, 238, 187-209.
- [27] Neese, F., Coord. Chem. Rev. 2009, 253, 526-563.
- [28] Harvey, J. N., Struct. Bond. 2004, 112, 151-183.

- [29] Schmidt, M. W.; Gordon, M. S., Annu. Rev. Phys. Chem. 1998, 49, 233-266.
- [30] Roos, B. O.; Taylor, P. R.; Siegbahn, P. E. M., Chem. Phys. 1980, 48, 157-173.
- [31] Andersson, K.; Malmqvist, P.-Å.; Roos, B. O., J. Chem. Phys. 1992, 96 (2), 1218-1226.
- [32] Roos, B. O.; Malmqvist, P.-Å., Phys. Chem. Chem. Phys. 2004, 6, 2919-2927.
- [33] Azizi, Z.; Roos, B. O.; Veryazov, V., Phys. Chem. Chem. Phys. 2006, 8 (23), 2727-2732.
- [34] Gagliardi, L., J. Am. Chem. Soc. 2003, 125, 7504-7505.
- [35] Gagliardi, L.; La Manna, G.; Roos, B., Faraday Discuss. 2003, 124, 63-68.
- [36] Gagliardi, L.; Pyykkö, P., Angew. Chem. Int. Ed. 2004, 43 (12), 1573-1576.
- [37] Gagliardi, L.; Pyykkö, P.; Roos, B. O., Phys. Chem. Chem. Phys. 2005, 7 (2415-2417).
- [38] Gagliardi, L.; Cramer, C. J., Inorg. Chem. 2006, 45 (23), 9442-9447.
- [39] Roos, B. O.; Gagliardi, L., Inorg. Chem. 2006, 45, 803-807.
- [40] Roos, B. O.; Borin, A. C.; Gagliardi, L., Angew. Chem. Int. Ed. 2007, 46 (9), 1469-1472.
- [41] Gagliardi, L.; Roos, B. O., Chem. Soc. Rev. 2007, 36, 893-903.
- [42] Karlström, G.; Lindh, R.; Malmqvist, P.-Å.; Roos, B. O.; Ryde, U.; Veryazov, V.; Widmark, P. O.; Cossi, M.; Schimmelpfennig, B.; Neogrady, P.; Seijo, L., Comput. Matl. Sci. 2003, 28 (2), 222-239.
- [43] Malmqvist, P. Å.; Pierloot, K.; Moughal Shahi, A. R.; Cramer, C. J.; Gagliardi, L., J. Chem. Phys. 2008, 128, 204109.
- [44] Zhao, Y.; Truhlar, D. G., J. Chem. Phys. 2006, 125 (19), 194101.
- [45] Dolg, M.; Wedig, U.; Stoll, H.; Preuss, H., J. Chem. Phys. 1987, 86, 866-872.
- [46] Hehre, W. J.; Radom, L.; Schleyer, P. v. R.; Pople, J. A., Ab Initio Molecular Orbital Theory. Wiley: New York, 1986.

[47] Pierloot, K.; Dumez, B.; Widmark, P.-O.; Roos, B. O., Theor. Chim. Acta 1995, 90, 87.

- [48] Roos, B. O.; Lindh, R.; Malmqvist, P.-Å.; Veryazov, V.; Widmark, P.-O., J. Phys. Chem. A 2005, 109, 6575-6579.
- [49] Aquilante, F.; Malmqvist, P.-A.; Pedersen, T. B.; Ghosh, A.; Roos, B. O., J. Chem. Theor. Comput. 2008, 4, 694-702.
- [50] Aquilante, F.; Pedersen, T. B.; Lindh, R.; Roos, B. O.; de Meras, A. S.; Koch, H., J. Chem. Phys. 2008, 129 (2), 024113-8.
- [51] Aquilante, F.; Pedersen, T. B.; Lindh, R., J. Chem. Phys. 2007, 126 (19), 194106-11.
- [52] Aquilante, F.; Pedersen, T. B.; de Meras, A. S.; Koch, H., J. Chem. Phys. 2006, 125 (17), 174101-7.
- [53] Zhao, Y.; Truhlar, D. G., MN-GFM version 4.1. University of Minnesota: Minneapolis, 2008.
- [54] Frisch, M. J.; Trucks, G. W.; Schlegel, H. B.; Scuseria, G. E.; Robb, M. A.; Cheeseman, J. R.; Montgomery, J. A.; Vreven, T.; Kudin, K. N.; Burant, J. C.; Millam, J. M.; Iyengar, S. S.; Tomasi, J.; Barone, V.; Mennucci, B.; Cossi, M.; Scalmani, G.; Rega, N.; Petersson, G. A.; Nakatsuji, H.; Hada, M.; Ehara, M.; Toyota, K.; Fukuda, R.; Hasegawa, J.; Ishida, M.; Nakajima, T.; Honda, Y.; Kitao, O.; Nakai, H.; Klene, M.; Li, X.; Knox, J. E.; Hratchian, H. P.; Cross, J. B.; Adamo, C.; Jaramillo, J.; Gomperts, R.; Stratmann, R. E.; Yazyev, O.; Austin, A. J.; Cammi, R.; Pomelli, C.; Ochterski, J. W.; Ayala, P. Y.; Morokuma, K.; Voth, G. A.; Salvador, P.; Dannenberg, J. J.; Zakrzewski, V. G.; Dapprich, S.; Daniels, A. D.; Strain, M. C.; Farkas, O.; Malick, D. K.; Rabuck, A. D.; Raghavachari, K.; Foresman, J. B.; Ortiz, J. V.; Cui, Q.; Baboul, A. G.; Clifford, S.; Cioslowski, J.; Stefanov, B. B.; Liu, G.; Liashenko, A.; Piskorz, P.; Komaromi, I.; Martin, R. L.; Fox, D. J.; Keith, T.; Al-Laham, M. A.; Peng, C. Y.; Nanayakkara, A.; Challacombe, M.; Gill, P. M. W.; Johnson, B.; Chen, W.; Wong, M. W.; Gonzalez, C.; Pople, J. A., Gaussian 03, Revision D.01. Gaussian, Inc.: Wallingford, CT, 2004.

[55] Olsen, J.; Christiansen, O.; Koch, H.; Jorgensen, P., J. Chem. Phys. 1996, 105 (12), 5082-5090.

- [56] Christiansen, O.; Olsen, J.; Jörgensen, P.; Koch, H.; Malmqvist, P.-Å., Chem. Phys. Lett. 1996, 261 (3), 369-378.
- [57] Luna, A.; Alcamí, M.; Mó, O.; Yáñez, M., Chem. Phys. Lett. 2000, 320 (1-2), 129-138.
- [58] Maiti, D.; Fry, H. C.; Woertink, J. S.; Vance, M. A.; Solomon, E. I.; Karlin, K. D., J. Am. Chem. Soc. 2007, 129 (2), 264-265.

Chapter 5

Second-Order pertubation theory with complete and restricted active space reference functions applied to oligimeric hydrocarbons

Abdul Rehaman Moughal Shahi 1, Christopher J. Cramer 2 and Laura ${\rm Gagliardi}^{1,2}$

Published in Physical Chemistry Chemical Physics, 2009 (11) , 2009, p10964-10972

¹Department of Chemistry, University of Geneva, 30 quai E. Ansermet, Geneva 1211, Switzerland

²Department of Chemistry and Supercomputing Institute, University of Minnesota, 207 Pleasant, St. SE. Minneapolis, Minnesota 55455-0431, USA

Second-Order pertubation theory with complete and restricted active space reference functions applied to oligimeric hydrocarbons

Multiconfigurational second-order perturbation theory based on either a complete active space reference wave function (CASSCF/CASPT2) or a restricted active space reference wave function (RASSCF/RASPT2) has been applied to compute one-electron ionization potentials and vertical electronic energy differences of oligomers of length n formed from ethylene (n = 1–10), acetylene (n = 1–5), and phenylene (n = 1–3) subunits. The RASSCF/RASPT2 approach offers an accuracy similar to CASSCF/CASPT2 at significantly reduced computational expense (both methods show good agreement with experimental data where available). It is shown that RASPT2 extends the range of CASPT2-like approaches by permitting the use of larger active spaces.

5.1 Introduction

Electrically conducting and conjugated polymers have been the focus of considerable research in polymer science, condensed matter physics, materials science and related areas since the discovery of the conductivity of doped polyacetylene. [1] Extensive work has focused on the design of novel conjugated polymers having narrow band gaps, this being an essential property for high conductivity upon doping. [2]

One dimensional chains and rings of conjugated organic repeat units such as polyynes, polyenes, and polyphenylenes have generated substantial interest in molecular electronics as potential conductors, semi-conductors and opto-electronic devices. [3, 4, 5] Fully conjugated organic aromatic molecular wires are believed to be excellent candidates for the replacement, in emerging devices, of the Al and Cu wiring used in existing logic and memory architectures. [6] Model systems containing oligo(ethylene, acetylene, phenylene)-based components have been extensively investigated using various experimental methods [7] and synthetic work is ongoing. [8]

5.1. INTRODUCTION 103

When such π -conjugated systems are incorporated in solid-state devices, one important aspect from the electronic structure point of view is the nature of the coupling of the organic molecule to the electrode and the manner in which this affects charge injection into the wire. [9] In this context, properties like the ionization potential and band gap of the wire are important, and the ability to compare accurately calculated values and experimental values offers the potential to lead to a better understanding of the physical and chemical properties of conjugated polymers, [10, 11, 12, 13] particularly in as much as ionization potentials and band gaps in the organic wire can be modified by chemical substitution in much the same fashion as Fermi levels in solids may be modified by doping. [14, 15]

The accurate modeling of such polymers requires a theoretical method capable of describing electron correlation effects over very large conjugation lengths. Within multiconfigurational self-consistent field (MCSCF) theory, one of the most successful formalisms to treat electron correlation is the complete active space self-consistent field method, CASSCF. In the CASSCF approach, one constructs a wave function as a linear combination of all possible spin and spatially adapted determinants that may be formed from the distribution of a given number of active electrons in a given number of orbitals. When supplemented by multireference second-order perturbation theory, CASSCF/CASPT2, [16] so as to account for dynamical electron correlation effects not already included at the CASSCF level, accuracies on the order of 0.2 eV have been documented for state-energy splittings in molecules containing elements throughout the periodic table. [17, 18, 19, 20, 21, 22, 23, 24, 25] The major drawback of the CASSCF formalism is that the number of configuration state functions (CSFs) required for the multiconfigurational expansion increases factorially with the number of active electrons and active orbitals. Memory and disk storage limit the size of the active space in modern software packages to about 15 electrons in 15 orbitals, which is on the order of $1*10^6$ to $16*10^6$ CSFs depending on spin and spatial symmetry. When larger active spaces are needed, the CASSCF/CASPT2 model cannot be applied in a practical fashion.

Simplifying multiconfigurational wave function methods while preserving their accuracy is one of the major challenges in modern quantum chemistry (see ref. [26, 27, 28] and refer-

ences therein). Along this direction, Malmqvist and the present authors recently developed a second-order perturbation theory based on the restricted active space self-consistent-field method, namely, RASSCF/RASPT2. [29] By subdividing the active space orbitals into three sets, one set entirely equivalent to a CAS space, one set consisting of occupied orbitals from which only a limited number of electrons may be excited, and one set consisting of virtual orbitals into which only a limited number of electrons may be excited, the number of orbitals and electrons that may practically be considered is substantially increased relative to the CASSCF/CASPT2 model. It should be pointed out that several groups are making progress in density-matrix renormalization group techniques [27, 30, 31, 32] and in reduced density matrix techniques. [33] These approaches represent very interesting alternatives to the RASSCF and CASSCF schemes with respect to increasing the size of the active orbital space.

In initial studies, the RASSCF/RASPT2 approach has been employed for the study of oxygen activation by supported mono- and binuclear copper complexes. [29, 34] Compared to CASSCF/CASPT2, the more efficient RASSCF/RASPT2 model proved effective for the calculation of singlet-triplet splittings and relative isomer energies for various reactive intermediates implicated in the chemistry of the copper complexes. However, much remains to be explored with respect to the question of how best to choose a RASSCF active space and excitation protocol, and the aim of the present paper is to examine this question in the context of oligomeric conjugated species of increasing size. In particular, we here study the ionization potentials and vertical electronic energy differences of polyenes (n = 1-10, all s-trans), polyynes (n = 1-5) and polyphenylenes (n = 1-3), where n is the number of repeat units. (Figure. 5.1).

We begin with a discussion of the computational details, then present results designed to assess convergence in predicted energies with respect to methodological choices. We conclude with some general observations likely to prove useful in future applications of the RASSCF/RASPT2 model.

Figure 5.1: Polyene (left), polyyne (center), and polyphenylene (right).

5.2 Computational Details

Geometries of the structures of all systems were optimized at the PBE [35] level of density functional theory employing the resolution of the identity scheme to compute two-electron integrals and correlation-consistent triple-zeta basis set of Dunning on all atoms. [36]

The Turbomole software package version 5.10 [37] was employed. Subsequent single point CASSCF/CASPT2 and RASSCF/RASPT2 calculations were performed at these optimized geometries using atomic natural orbital (ANO)-L [38] basis sets on all the atoms, contracted to 4s3p2d for C and to 2s1p for H. The MOLCAS 7.3 package [39] was employed to perform these calculations. In all our calculations the IPEA approach (using the default value 0.25 au) for the CASPT2/RASPT2 zeroth order Hamiltonian was employed. [40] Cholesky decomposition [41] of the two-electron integrals was accomplished with a threshold of 10^{-5} a.u. Reduced scaling evaluation of the Fock exchange matrices in the CASSCF and RASSCF calculations was accomplished by means of the Local-K (LK) screening approach [42] employing localized Cholesky orbitals. [43]

In the RASSCF model, the active space is divided into three distinct subspaces: RAS1, RAS2, and RAS3. The RAS2 subspace is identical to the active space in a CASSCF calculation, i.e., all possible spin- and symmetry-adapted CSFs that can be constructed from the orbitals in RAS2 are included in the multiconfigurational wave function. The RAS1 and RAS3 subspaces, on the other hand, permit the generation of additional CSFs subject to the restriction that a maximum number of excitations may occur from RAS1, which otherwise contains only doubly occupied orbitals, and a maximum number of excitations may occur into RAS3, which otherwise contains only external orbitals. There are various ways in which

one can select the orbitals.

Since the systems studied here are π -conjugated systems, all π and π^* orbitals were included in the relevant active spaces. In CASSCF calculations, these orbitals were perforce assigned to the RAS2 space. In the RASSCF calculations on neutral (singlet) systems, the occupied π orbitals were included in RAS1 and the unoccupied and π^* orbitals in RAS3; RAS2 was left empty. For the radical cations, the singly occupied bonding π orbital and its corresponding antibonding π^* orbital were included in RAS2 (see next section for additional discussion). As an example, we show in Figure. 5.2 a schematic diagram of the active spaces employed for the acetylene dimer.

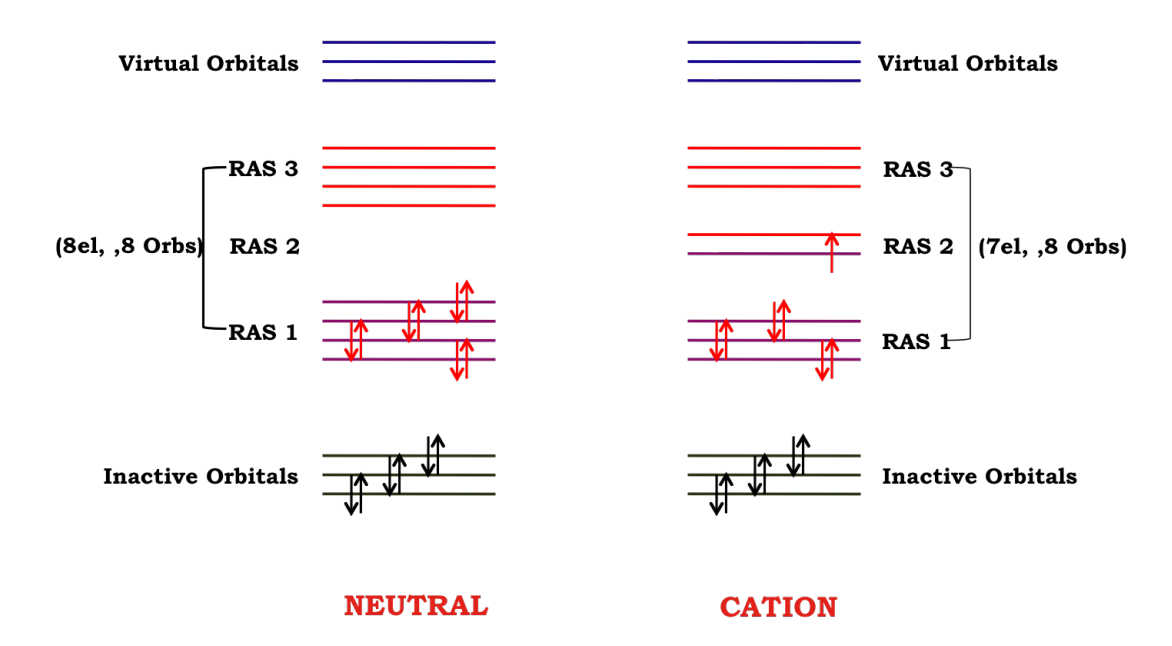


Figure 5.2: Schematic representation of the active space used for calculations of the acetylene dimer.

Several levels of maximum excitation from RAS1 and into RAS3 were considered, in particular up to double, up to triple, and up to quadruple excitations. The general notation for a RASSCF or RASPT2 calculation is (ae,ao)/(ae2,ao2)/max, where ae is the number of active electrons in RAS1 and RAS2 combined, ao is the number of active orbitals in all of the

RAS subspaces, ae2 is the number of active electrons in RAS2, ao2 is the number of active orbitals in RAS2, and max is the maximum number of excitations permitted out of RAS1 and into RAS3.

The number of electrons and number of orbitals in RAS2 are both 0 for all neutral systems, and are 1 and 2, respectively, for all cations. Thus, for instance, for the oligomer comprised of 10 ethylene subunits, calculations for the neutral system are designated as RASPT2/(20,20)//max, where max is equal to 2, 3, or 4 (the double solidus implies (0,0) for the RAS2 space) and calculations for the radical cation are designated as RASPT2(19,20)/(1,2)/max, where max again takes on values of 2, 3, or 4.

Table 5.1: RASSCF(ae,ao)/max vs CASSCF(ae,ao) ionization potentials (eV) for Polyene of length \mathbf{n} .

	Cation radical		RASSCF		
n (ae,ao)	electronic state	$\max = 2$	$\max = 3$	$\max = 4$	CASSCF
1(2,2)	${}^{2}\mathrm{B}_{3}(\mathrm{D}_{2})^{b}$	9.770	c	c	9.770
2(4,4)	2 A ₂ (C _{2v})	8.425	8.471	8.471	8.471
3(6,6)	$^2A(C_2)$	7.072	7.077	7.084	7.117
4 (8,8)	$^2\mathrm{B}(\mathrm{C}_2)$	7.005	6.978	7.119	7.127
5(10,10)	$^{2}\mathrm{A}_{u}(\mathrm{C}_{2h})$	6.422	6.377	6.431	6.434
6(12,12)	${}^2\mathrm{A}_g(\mathrm{C}_i)$	6.404	6.260	6.560	6.596
7(14,14)	2 A _u (C _i)	6.025	5.856	6.051	6.060
8 (16,16)	${}^2\mathrm{A}_g(\mathrm{C}_i)$	6.062	5.858	6.236	d
9 (18,18)	$^2\mathrm{A}(\mathrm{C}_2)$	5.802	5.583	5.886	d
10 (20,20)	$^2A(C_2)$	5.844	5.582	6.062	d

 $[^]a$ For uncharged precursors, the calculations are designated as RASSCF(ae,ao)/max vs CASSCF(ae,ao); for radical cations the proper designations are RASSCF(ae-1,ao)/(1,2)/max vs CASSCF(ae-1,ao). b The point group to which the optimized geometry of the radical cation belongs is indicated in parentheses. c There are only two active electrons for n = 1. d The number of active electrons/orbitals exceeds practical limits for a CASSCF calculation

The electronic ground states of all neutral species are totally symmetric singlets. The point groups and ground-state irreducible representations of the doublet cation radicals are reported in Tables 5.1–5.3 below.

Adiabatic ionization potentials (IPs) were determined as energy differences between optimized cations and neutral precursors. Vertical electronic energy differences were determined as energy differences between lowest singlet electronic excited states and precursor ground states. The irreducible representations of the lowest singlet electronic excited states are reported in Tables 5.7–5.9.

Table 5.2: RASSCF(ae,ao)/max vs CASSCF(ae,ao) ionization potentials (eV) for Polyene of length ${\bf n}.^a$

	Cation radical		RASSCF		
n (ae,ao)	electronic state	$\max = 2$	$\max = 3$	$\max = 4$	CASSCF
1(4,4)	$^{2}\mathrm{B}_{2u}(\mathrm{D}_{2h})^{b}$	10.345	10.345	10.421	10.421
2(8,8)	$^2\mathrm{B}_{1g}(\mathrm{D}_{2h})$	9.331	9.351	9.364	9.372
3(12,12)	$^{2}\mathrm{B}_{3g}(\mathrm{D}_{2h})$	8.773	8.623	8.737	8.744
4(16,16)	$^{2}\mathrm{B}_{2g}(\mathrm{D}_{2h})$	8.413	8.161	8.335	c
5(20,20)	$^2\mathrm{A}(\mathrm{C}_{2h})$	8.162	7.901	8.051	c

 $[^]a$ For uncharged precursors, the calculations are designated as RASSCF(ae,ao)/max vs CASSCF(ae,ao); for radical cations the proper designations are RASSCF(ae-1,ao)/(1,2)/max vs CASSCF(ae-1,ao). b The point group to which the optimized geometry of the radical cation belongs is indicated in parentheses. c The number of active electrons/orbitals exceeds practical limits for a CASSCF calculation.

Table 5.3: RASSCF(ae,ao)/max vs CASSCF(ae,ao) ionization potentials (eV) for polyphenylenes of length n.

	Cation radical		RASSCF		
n (ae,ao)	electronic state	$\max = 2$	$\max = 3$	$\max = 4$	CASSCF
1(6,6)	$^{2}\mathrm{B}_{3g}(\mathrm{D}_{2h})^{b}$	8.435	8.383	8.478	8.480
2(12,12)	$^2\mathrm{B}_3(\mathrm{D}_2)$	7.332	7.224	7.369	7.382
3(18,18)	$^2\mathrm{B}(\mathrm{C}_2)$	7.199	7.076	7.241	c

 $[^]a$ For uncharged precursors, the calculations are designated as RASSCF(ae,ao)/max vs CASSCF(ae,ao); for radical cations the proper designations are RASSCF(ae-1,ao)/(1,2)/max vs CASSCF(ae-1,ao). b The point group to which the optimized geometry of the radical cation belongs is indicated in parentheses. c The number of active electrons/orbitals exceeds practical limits for a CASSCF calculation.

5.3 Results and Discussion

The calculated IPs of polyenes, polyynes, and polyphenylenes are reported in Tables 5.1–5.6.

Before discussing our results for IPs, it should be noted that IPs can, in principle, be correctly determined also using a single configurational method, like MP2 (see, for example, the work of Deleuze and Ortis). [44, 45, 46, 47, 48] We have employed a multiconfigurational method because we wanted a method of general validity that could also determine electronic excitation energies with the same accuracy.

In the first three Tables, we compare RASSCF results with CASSCF results for the three different oligomers in order to assess the degree to which the two reference functions are similar. In the absence of accounting for additional dynamical correlation, these results are not expected to be particularly accurate, but it is instructive to evaluate the trends between the two models at the SCF level. In the next three tables, the RASPT2 and CASPT2 results, when the latter level is practicable, are compared to one another as well as to experiment and density functional predictions computed using the PBE functional.

Inspection of Tables 5.1–5.3 shows that the IPs calculated at the RASSCF level including only up to double excitations ($\max = 2$) are already in quite good agreement with the full CASSCF values and the agreement becomes even better as higher levels of excitations are included up to quadruples. The largest difference between any $\max = 4$ calculation and its CASSCF alternative is 0.036 eV for the n = 6 oligomer of ethylene, and the errors in the vast majority of instances are below 0.01 eV. With respect to trends in the predicted IPs as a function of n, a mildly curious feature is the oscillatory behavior of the IP between even and odd values of n in the oligoethylenes that is predicted at both the RASSCF and CASSCF levels of theory. Such oscillations are not present in the experimental data nor in the PT2 corrected multiconfigurational data (vide infra) and may perhaps be associated with variations in the number of symmetry adapted CSFs included in the active space as the C_2 symmetry axis bisects either a single or a double bond in the polyenes.

A different oscillatory behavior is also seen in the RASSCF data, namely that the IPs

Table 5.4: PBE, RASPT2(ae,ao)/max,	CASPT2(ae,ao), and experimental ionization poten-
tials (eV) for polyenes of length n. ^a	
DET	RASPT2

	DFT		RASPT2			
n (ae,ao)	PBE	$\max = 2$	$\max = 3$	$\max = 4$	CASPT2	Expt
1(2,2)	10.321	10.481	b	b	10.481	10.51^{c}
2(4,4)	8.877	9.262	9.492	9.176	9.175	9.09^{c}
3(6,6)	7.810	7.964	8.300	8.177	8.182	$8.29 – 8.45^d$
4 (8,8)	7.224	7.641	7.740	7.691	7.683	$7.8 – 8.1^e$
5(10,10)	6.810	7.285	7.362	7.329	7.314	
6(12,12)	6.498	6.963	6.973	7.044	7.040	
7(14,14)	6.253	6.780	6.844	6.852	6.874	
8 (16,16)	6.055	6.554	6.525	6.662	f	
9 (18,18)	5.895	6.445	6.450	6.555	f	
10 (20,20)	5.754	6.280	6.200	6.410	f	

^a For uncharged precursors, the multiconfigurational calculations are designated as RASPT2(ae,ao)/max vs. CASPT2(ae,ao); for radical cations the proper designations are RASPT2(ae-1,ao)/(1,2)/max vs. CASPT2(ae-1,ao). ^b There are only two active electrons.

oscillate as max increases from 2 to 4. Such oscillation has at least a superficial analogy with similar behavior observed in the convergence behavior of the correlation energy in Møller–Plesset perturbation theory as a function of level of excitation, as explored in detail by Olsen et al. [57, 58] In order to study this point further, we would have to monitor IPs for still larger values of max. For the present molecules, however, such calculations are not practical, although we hope to investigate this behavior for smaller test systems in the future. We note that in general results with max = 2 are within 0.1 eV of the predictions using max = 4, while results for max = 3 are generally only within about 0.2 eV of the max = 4 values. This suggests that there is little point in adding triple excitations in the absence of quadruple excitation, again in qualitative analogy to single-reference perturbation theory.

Considering now comparisons between RASPT2 and CASPT2 (Tables 5.4–5.6) and also considering DFT/PBE and experimental IP values, we see quite similar trends with respect to RASPT2/CASPT2 as those observed with RASSCF/CASSCF. In particular, results for RASPT2 with max = 4 are typically within 0.02 eV of the CASPT2 values, when computation of the latter are practical. Additionally, RASPT2 values with max = 2 are very nearly

Table 5.5: PBE, RASPT2(ae,ao)/max, CASPT2(ae,ao), and experimental ionization potentials (eV) for polyynes of length $n.^a$

	DFT		RASPT2			
n (ae,ao)	PBE	$\max = 2$	$\max = 3$	$\max = 4$	CASPT2	Expt
$\overline{1}$ (4,4)	11.245	11.254	11.254	11.290	11.290	11.4^{b}
2(8,8)	9.791	9.987	9.945	10.013	10.019	$10.2^{c,d}$
3(12,12)	8.932	9.345	9.272	9.312	9.322	9.5^{d}
4(16,16)	8.456	8.934	8.765	8.851	8.863	8.7^{d}
5 (20,20)	8.038	8.628	8.511	8.613	e	a

 $[^]a$ For uncharged precursors, the multiconfigurational calculations are designated as RASPT2(ae,ao)/max vs. CASPT2(ae,ao); for radical cations the proper designations are RASPT2(ae-1,ao)/(1,2)/max vs. CASPT2(ae-1,ao). b Ref. [52] c Ref. [53] d Ref. [54]. e The number of active electrons/orbitals exceeds practical limits for a CASSCF calculation

Table 5.6: PBE, RASPT2(ae,ao)/max, CASPT2(ae,ao), and experimental ionization potentials (eV) for polyphenylenes of length n.^a

	DFT		RASPT2			
n (ae,ao)	PBE	$\max = 2$	$\max = 3$	$\max = 4$	CASPT2	Expt
1 (6,6)	9.101	9.482	9.322	9.476	9.475	9.24^{b}
2(12,12)	7.768	8.141	8.171	8.137	8.128	7.95^{c}
3 (18,18)	7.150	7.973	7.992	7.968	d	7.78^{c}

 $[^]a$ For uncharged precursors, the multiconfigurational calculations are designated as RASPT2(ae,ao)/max vs. CASPT2(ae,ao); for radical cations the proper designations are RASPT2(ae–1,ao)/(1,2)/max vs.. CASPT2(ae–1,ao). b Ref. [55]. c Ref. [56]. d The number of active electrons/ orbitals exceeds practical limits for a CASSCF calculation.

as good as, or in certain cases somewhat better than, those with $\max=3$. Comparing to experiment, we see that all CASPT2 and RASPT2/ $\max=4$ values are within 0.2 eV of experiment. PBE predictions are also in reasonable accord with experiment and multireference predictions, but DFT systematically underpredicts the various IPs by a steadily increasing margin with increasing length n. Thus, for instance, in the oligoethylene series the separation between PBE and RASPT2/ $\max=4$ values increases from 0.2 to 0.7 eV as n goes from 1 to 10. The various theoretical and experimental results are compared graphically in Figure. 5.3–5.5

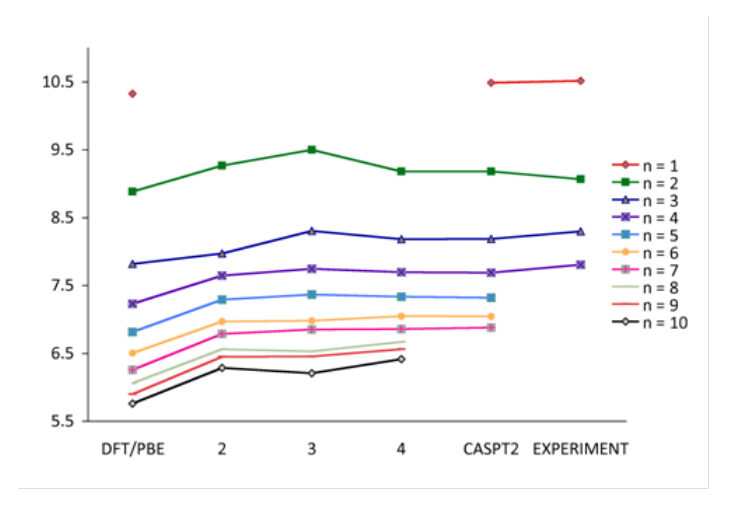


Figure 5.3: DFT/PBE, RASPT2 (max=2,3,4), CASPT2, and experimental ionization energies (eV) for polyenes of length n; RASPT2 values are indexed on the abscissa by value of max.

In Figure 5.6 we report the number of CSFs as a function of the level of theory for two representative systems studied here, namely the polyynes with n=3 and 4. It is clear that the increase in cost on going from RASPT2/max = 4 to CASPT2 is very large (note the logarithmic scale of the ordinate) and, given the agreement between RASPT2/max = 4 and full CASPT2, the former approach offers significant computational advantages. And, of course, many of the oligomers studied here had numbers of electrons and active spaces too large for practical study using CASPT2, in particular the oligomers of ethylene with n>7, those of acetylene with n>3, and those of phenylene with n>2. By contrast, using the RASPT2/max = 2 model, which shows quite good agreement with CASPT2 when the two can be compared, it would not be particularly challenging to extend these oligomers to substantially higher values of n.

We now consider the prediction of vertical electronic energy differences in the various oligomers. This is a truly multiconfigurational problem, for which methods like RASPT2 and CASPT2 are indispensable; Nakayama et al. were the first to use a multireference approach to correctly place the relative positions of low-lying, dark A_g states in polyenes. [59] RASSCF and CASSCF results are reported in Tables 5.7–5.9 and RASPT2 and CASPT2 in

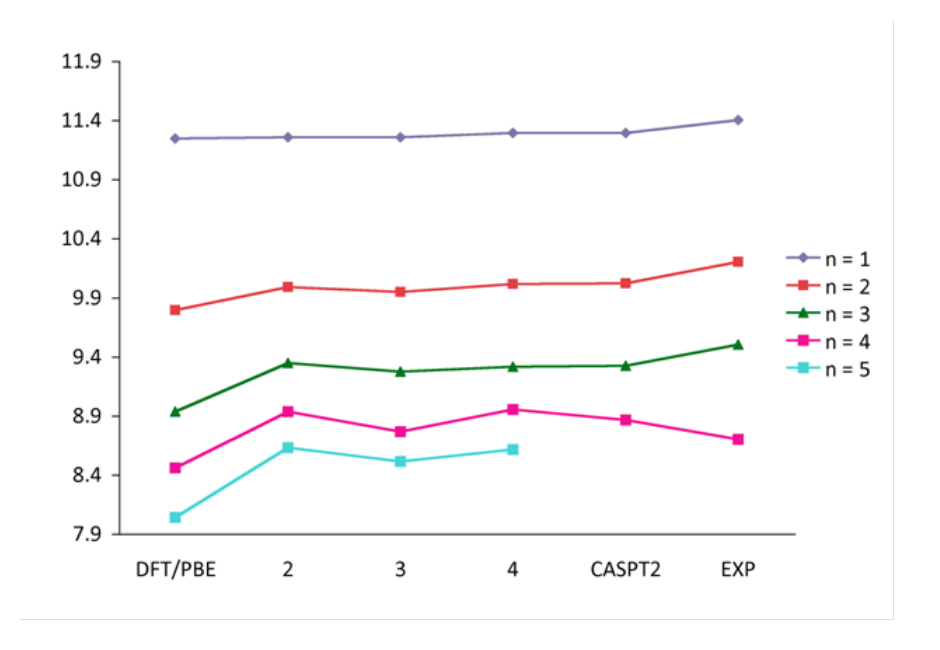


Figure 5.4: DFT/PBE, RASPT2 (max=2,3,4), CASPT2, and experimental ionization energies (eV) for polyynes of length n; RASPT2 values are indexed on the abscissa by value of max.

Tables 5.10–5.12. The latter set of tables also include DFT PBE and experimental values and the data in Tables 5.10–5.12 are summarized in graphical form in Figures. 5.7–5.9.

Comparing RASSCF and CASSCF, we see that for the ethylene and phenylene oligomers, the tendency is for the predicted vertical electronic energy difference to decrease monotonically with increasing values of max until max = 4, which gives generally good agreement with CASSCF—typically within 0.1 eV. In contrast with the situation for ionization potentials discussed above, proceeding to the inclusion of quadruple excitations is essential for good agreement with CASSCF values; vertical electronic energy differences predicted with max = 2 tend to be higher than the CASSCF targets by 1 eV or more. In the polyyne case, slightly different behavior is observed. In this case the vertical electronic energy difference does not decrease monotonically with increasing RAS excitation level, but instead oscillates, dropping sharply from max = 2 to max = 3, and then rising slightly with max = 4. Comparing to CASSCF values suggests that the oscillation is damped out for short oligomers, but

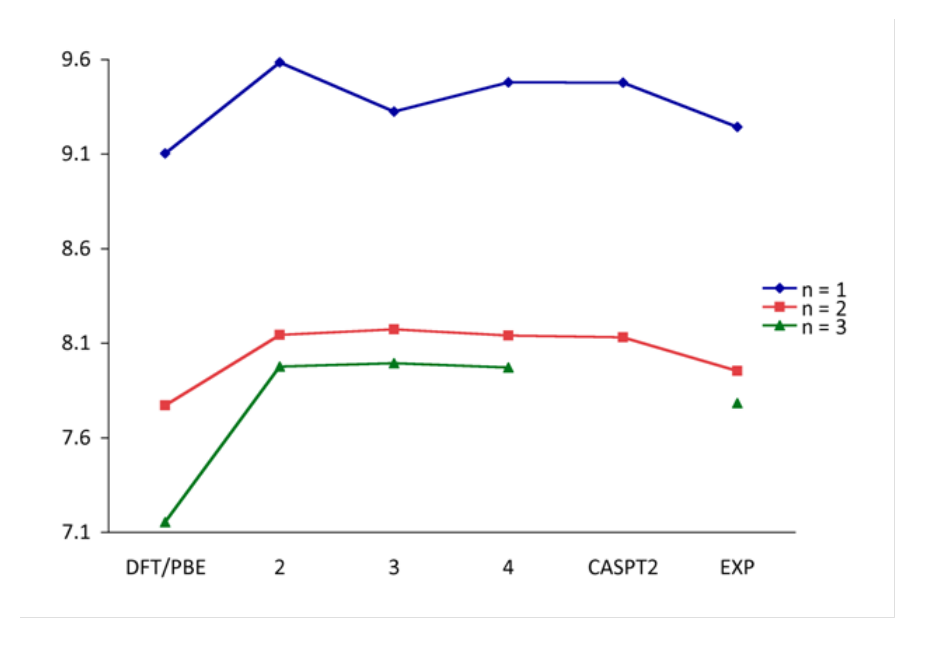


Figure 5.5: DFT/PBE, RASPT2 (max=2,3,4), CASPT2, and experimental ionization energies (eV) for polyphenylenes of length n; RASPT2 values are indexed on the abscissa by value of max.

that convergence in the RAS predictions is not yet complete with $\max = 4$ for n > 2. It is not obvious why the polyacetylene behavior is distinct in this case, although it is clearly the oligomer with the most concentrated number of active orbitals per atom.

In all three oligomers, the RASSCF/max = 2 vertical electronic energy differences are predicted to increase with increasing n after a certain length (in the case of phenylene this happens immediately). This is in contrast to the RASSCF/max = 4 predictions, which more sensibly smoothly decrease with increasing n for ethylene and acetylene. In the phenylene case, even the RASSCF/max = 4 predictions increase very slightly from n = 1 to 3 (0.1 eV).

When second-order perturbation theory is included in the vertical electronic energy difference predictions, there is a significant effect on longer oligomers, lowering their predicted gaps and establishing smooth trends, at least for $\max = 4$, where predicted excitation energies decrease with increasing n. RASPT2/ $\max = 4$ predictions agree to within 0.1 eV with CASPT2

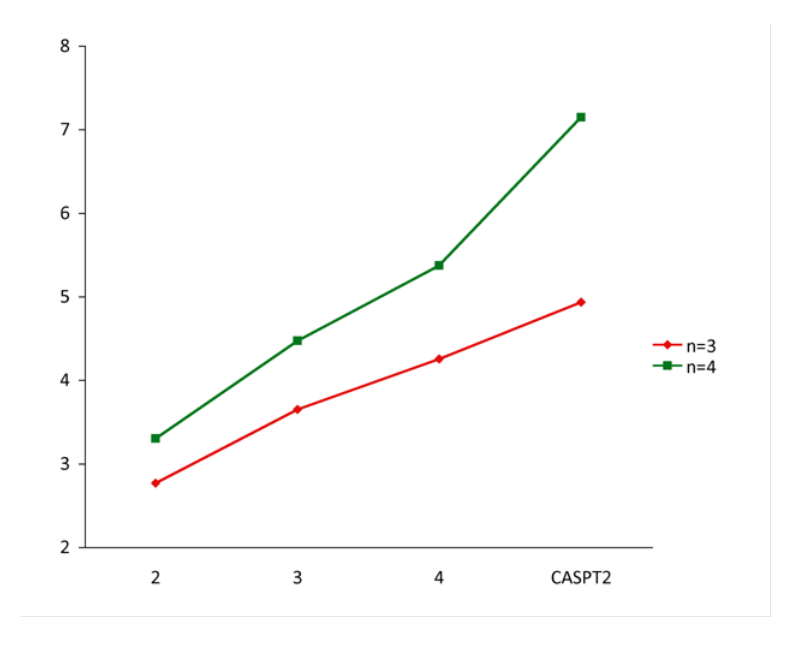


Figure 5.6: Log[CSFs] for RASPT2 (max=2, 3, 4) and CASPT2 for acetylene trimer (n=3) and tetramer (n=4)

predictions when the latter are practical. However, predictions at the RASPT2/max = 2 level are quite poor: for the longest oligomers the effect of increasing max from 2 to 4 can decrease the predicted gap by over 2 eV.

Given the good agreement between CASPT2 and RASPT2/max = 4, and the corresponding inference that the latter level of theory will maintain good accuracy in those instances where CASPT2 calculations cannot be carried out, we may consider a comparison to experiment. In general, we see quite good agreement with published experimental values. The ethylene case merits some additional discussion. We predict it to have an excitation energy of 8.3 eV. As reported by Serrano-Andrés et al., [60] its experimental electronic spectrum is dominated by an intense $\pi - \pi^*$ broad band with a maximum at 7.66 eV, which does not correspond to the vertical transition. A number of accurate theoretical studies have reported a final estimate of about 8.0 eV for the vertical transition energy, [69, 70, 71] and this is the value reported in Table 5.10 in the Experiment column, to which our CASPT2 result compares well. Moreover, the 0.23 eV discrepancy is related to the well-known valence-Rydberg

10(20,20)

101	poryenes or i	iengui n				
		Excited		RASSCF		
	n (ae,ao)	electronic state	$\max = 2$	$\max = 3$	$\max = 4$	CASSCF
	1(2,2)	$^{1}\mathrm{B}_{3u}$	8.795	a	a	8.795
	2(4,4)	$^{1}\mathrm{B}_{u}$	7.708	7.754	7.754	7.754
	3(6,6)	$^1\mathrm{A}_g$	6.042	5.917	5.920	5.920
	4(8,8)	$^1\mathrm{A}_g$	5.515	4.835	4.542	4.510
	5(10,10)	$^1\mathrm{A}_g$	5.260	4.462	4.172	4.131
	6(12,12)	$^{1}\mathrm{A}_{g}$	5.581	4.243	3.692	3.589
	7(14,14)	$^1\mathrm{A}_g^{}$	5.488	4.029	3.520	3.435
	8 (16,16)	$^1\mathrm{A}_g$	5.999	3.955	3.382	b
	9 (18.18)	$^{1}\mathrm{A}_{a}^{\circ}$	5.978	3.831	3.289	b

Table 5.7: RASSCF(ae,ao)/max vs. CASSCF(ae,ao) vertical electronic energy differences (eV) for polyenes of length n

6.556

3.825

3.342

mixing (present at some extent even if explicitly Rydberg functions are absent, because ANO basis sets are diffuse enough). To improve the value a multi-state (CASPT2 or RASPT2) treatment would be required. [72] The biphenyl case has also been previously studied using CASPT2. [73] This system, with its twisted structure, is complicated and, depending upon the environment, is found to have an excitation energy that varies from 4.3 eV to 4.6 eV.

Considering the performance of Time Dependent (TD)-DFT, we see that the PBE predictions are in poor accord with experiment for the very short oligomers, and become increasingly too small with increasing values of n. This behavior is expected, as PBE is a local functional and local functionals have a well known tendency to predict band gaps in polymeric and solid-state systems that are much too small. [74]

We close with some discussion of RAS active space choices and excitation levels. First, we note that in the calculation of ionization energies, we included a single electron in a RAS2 space of 2 orbitals. In the ground state of a high-spin open-shell system, the singly occupied orbitals must be included in RAS2 in order to permit them to be doubly occupied by an

^a There are only two active electrons for n=1. ^b The number of active electrons/orbitals exceeds practical limits for a CASSCF calculation.

Table 5.8: RASSCF(ae,ao)/max vs. CASSCF(ae,ao) vertical electronic energy differences (eV) for polyynes of length n

	Excited		RASSCF		
n (ae,ao)	electronic state	$\max = 2$	$\max = 3$	$\max = 4$	CASSCF
$\overline{1(4,4)}$	$^{1}\mathrm{B}_{1u}$	8.096	7.997	8.073	8.073
2(8,8)	$^{1}\mathrm{B}_{3u}$	7.134	6.438	6.530	6.524
3(12,12)	$^{1}\mathrm{B}_{1u}$	7.504	5.385	5.624	5.489
4(16,16)	$^{1}\mathrm{B}_{1u}$	7.987	4.749	5.183	4.848
5(20,20)	$^{1}\mathrm{B}_{1u}$	7.853	4.123	4.465	a

^a The number of active electrons/orbitals exceeds practical limits for a CASSCF calculation.

Table 5.9: RASSCF(ae,ao)/max vs. CASSCF(ae,ao) vertical electronic energy differences (eV) for polyphenylenes of length n

	Excited		RASSCF		
n (ae,ao)	electronic state	$\max = 2$	$\max = 3$	$\max = 4$	CASSCF
1(6,6)	$^{1}\mathrm{B}_{3u}$	5.505	4.994	4.974	4.968
2(12,12)	$^{1}\mathrm{B}_{3u}$	6.781	5.150	4.984	4.792
3(18,18)	$^{1}\mathrm{B}_{2}$	7.314	5.203	5.081	a

 $[^]a$ The number of active electrons/orbitals exceeds practical limits for a CASSCF calculation.

excitation out of RAS1 (because excitations can only occur into RAS2 or RAS3 orbitals). Thus, for instance, if the dominant configuration of a radical is $|a^2b^2c\rangle$ and another important CSF is $|a^2bc^2\rangle$, it will be impossible to generate the second CSF if orbital c and its resident electron are included in RAS1 instead of RAS2. In the case of the radical cations examined here, we also included an additional orbital, primarily because of the near degeneracies in the correlating π and π^* orbitals associated with the unpaired electron—such a requirement for an additional correlating orbital in RAS2 need not be operative in every case.

The first excited singlet states studied here provide some flexibility in terms of how they may be treated. If we consider the ground state to be represented by a dominant CSF $|a^2b^2c^2\rangle$ and the first excited state to be dominated by a CSF $|a^2b^2c^2\rangle$, one possibility would be to follow a prescription similar to that for the radical cation, i.e., treat orbitals c and d as

Table 5.10: RASPT2(ae,ao)/max, CASPT2(ae,ao), and experimental vertical electronic energy differences (eV) for polyenes of length n

	DFT		RASPT2			
n (ae,ao)	PBE	$\max = 2$	$\max = 3$	$\max = 4$	CASPT2	Expt
1(2,2)	5.701	8.229	a	a	8.229	$8.0^{b,c}$
2(4,4)	3.875	6.220	6.414	6.308	6.291	5.92^{d}
3(6,6)	2.935	4.863	5.551	5.222	5.159	$4.95^{e,f}$
4(8,8)	2.370	4.793	4.554	4.307	4.330	$4.41^{g,h}$
5(10,10)	1.990	4.372	4.089	3.771	3.783	3.71^{i}
6(12,12)	1.717	4.434	3.846	3.244	3.312	3.41^{i}
7(14,14)	1.515	4.241	3.560	3.055	3.013	3.18^{i}
8 (16,16)	1.358	4.509	3.416	2.847	j	3.02^{i}
9 (18,18)	1.232	4.432	3.294	2.615	j	2.82^{i}
10(20,20)	1.127	4.803	3.213	2.588	j	2.77^{i}

^a There are only two active electrons for n = 1. ^b Ref.[60]. ^c Ref.[61]. ^d Ref.[62] ^e Ref.[50]. ^f Ref.[63]. ^g Ref.[64]. ^h Ref.[50]. ⁱ Ref. [65]. ^j The number of active electrons/orbitals exceeds practical limits for a CASSCF calculation.

belonging to RAS2 and thus have a (2,2) RAS space. Such a choice ensures that CSFs like $|a^2bc^2d\rangle$ and $|a^2bcd^2\rangle$ can be generated, if such CSFs are relevant. However, both of these formal single excitations from the excited state dominant CSF can also be generated from the alternative RAS protocol that involves an empty RAS2 space. Thus, if all 6 electrons in the current example are placed in RAS1 with that space including orbitals a, b, and c, and RAS3 including orbital d, then $|a^2bc^2d\rangle$ is generated by a single excitation from orbital b to d and $|a^2bcd^2\rangle$ is generated as a double excitation from b and c into d. The distinction in these two approaches is that a higher number of excitations is required in the latter case to generate some of the determinants that are implicitly included when RAS2 is occupied. This point helps to rationalize why the RASPT2/max = 2 predictions of vertical electronic energy differences presented above are quite poor. In essence, the ground state has a reference wave function including all doubly-excited configurations involving RAS1 and RAS3 orbitals, while the excited-state singlet really only involves single excitations from its dominant CSF, since its dominant CSF is itself a single excitation from the RAS1 and RAS3 definitions. As illustrated above, including additional excitations ameliorates this apparent imbalance between

5.4. CONCLUSIONS 119

Table 5.11: PBE, RASPT2(ae,ao)/max, CASPT2(ae,ao), and experimental vertical electronic energy differences (eV) for polyynes of length n

	DFT		RASPT2			
n (ae,ao)	PBE	$\max = 2$	$\max = 3$	$\max = 4$	CASPT2	Expt
1 (4,4)	6.552	7.313	7.286	7.323	7.323	7.44^{a}
2(8,8)	4.624	5.860	5.590	5.358	5.485	5.36^{a}
3(12,12)	3.552	5.691	4.529	4.418	4.484	
4(16,16)	2.878	5.638	3.922	3.813	3.850	
5 (20,20)	2.436	5.702	3.540	3.397	b	

 $[^]a$ Ref. [66]. $^{\dot{b}}$ The number of active electrons/orbitals exceeds practical limits for a CASSCF calculation.

Table 5.12: PBE, RASPT2(ae,ao)/max, CASPT2(ae,ao), and experimental vertical electronic energy differences (eV) for polyphenylenes of length n.^a

	DFT		RASPT2			
n (ae,ao)	PBE	$\max = 2$	$\max = 3$	$\max = 4$	CASPT2	Expt
1 (6,6)	5.101	5.185	4.936	4.929	4.932	4.90^{a}
2(12,12)	3.817	5.614	4.862	4.440	4.376	4.92^{b}
3 (18,18)	3.280	5.982	4.926	4.112	\mathbf{c}	4.34^{b}

 $[^]a$ Ref. [67]. b Ref. [68]. c The number of active electrons/orbitals exceeds practical limits for a CASSCF calculation.

the ground and excited states. As the number of additional CSFs generated by increasing the value of max is quantitatively similar to the number generated by selecting a partially occupied RAS2 space, the adoption of one protocol vs. the other is of little consequence. However, the requirement to treat excited states and ground states in a balanced way should be borne in mind when selecting RAS spaces and excitation levels in general.

5.4 Conclusions

Based on analysis of the ionization potentials and vertical electronic energy differences of oligomers of length n formed from ethylene (n = 1-10), acetylene (n = 1-5), and pheny-

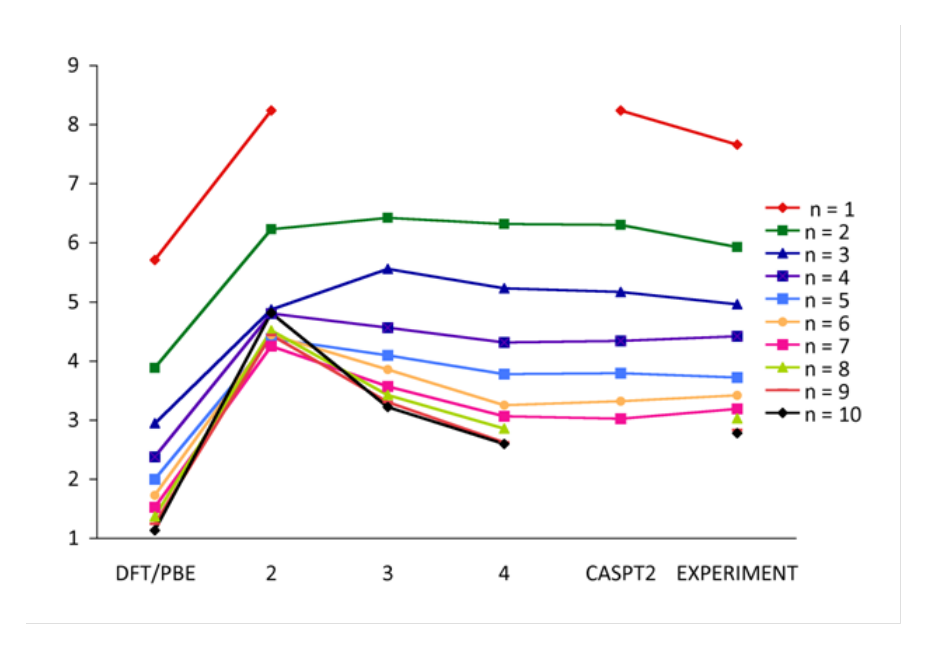


Figure 5.7: DFT/PBE, RASPT2 (max=2,3,4), CASPT2, and experimental vertical electronic energy differences for polyenes of length n; RASPT2 values are indexed on the abscissa by value of max.

lene (n = 1–3) subunits, multiconfigurational second-order perturbation theory based on a restricted active space reference wave function (RASSCF/RASPT2) offers an efficient alternative to the analogous theory based on a complete active space reference wave function (CASSCF/CASPT2). In all instances, predictions at the RASPT2 level agree with those at the CASPT2 level (and with experiment) to within about 0.1 eV and this agreement is achieved using from one to three orders of magnitude fewer configuration state functions. The RASSCF/RASPT2 approach thus offers an accuracy similar to CASSCF/CASPT2, but with substantially reduced computational overhead, permitting application of the RASSCF/RASPT2 model to systems where electron/active space combinations exceed the practical limits of the CASSCF/CASPT2 model. As such, the RASSCF/RASPT2 model shows considerable promise for future studies of highly correlated large systems.

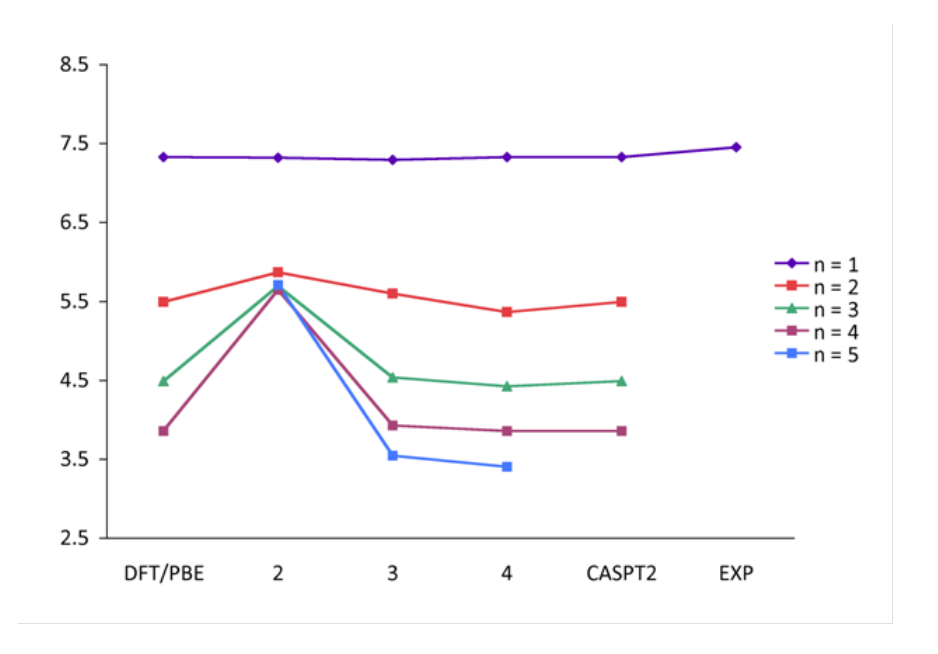


Figure 5.8: DFT/PBE, RASPT2 (max=2,3,4), CASPT2, and experimental vertical electronic energy differences for polyynes of length n; RASPT2 values are indexed on the abscissa by value of max.

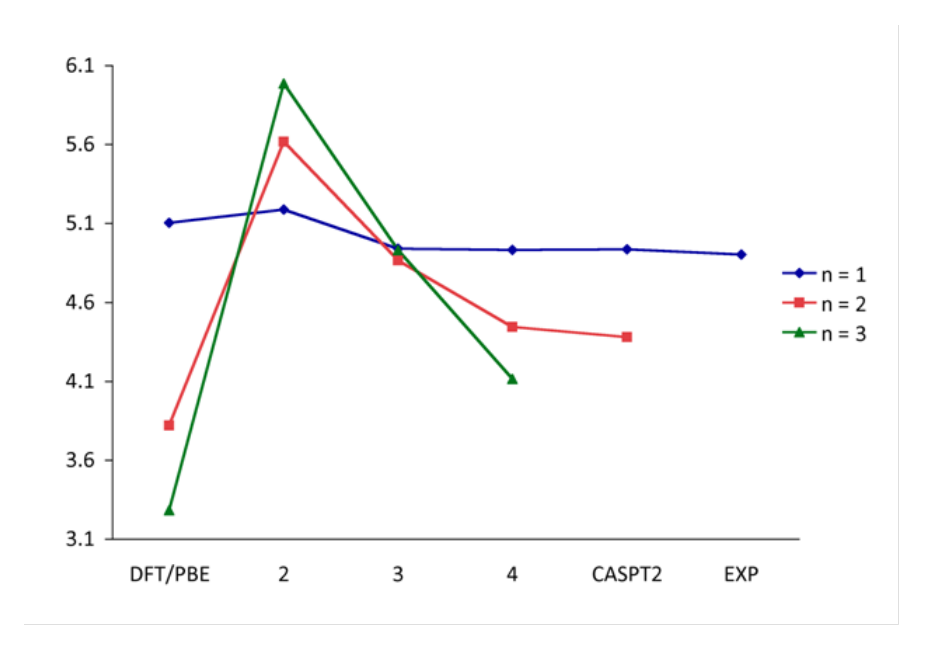


Figure 5.9: DFT/PBE, RASPT2 (max=2,3,4), CASPT2, and experimental vertical electronic energy differences for polyphenylenes of length n; RASPT2 values are indexed on the abscissa by value of max.

Bibliography

- [1] S. A. Jenekhe, Nature, 1986, 322, 345–347
- [2] J. Ma, S. H. Li and Y. S. Jiang, Macromolecules, 2002, 35, 1109–1115.
- [3] F. Diederich and L. Gobbi, in Carbon Rich Compounds II, 1999, vol. 201, pp. 43–79.
- [4] L. Lou and P. Nordlander, Phys. Rev. B: Condens. Matter Mater. Phys., 1996, 54, 16659–16662.
- [5] N. D. Lang and P. Avouris, Phys. Rev. Lett., 1998, 81, 3515–3518.
- [6] D. K. James and J. M. Tour, in Molecular Wires: From Design to Properties, 2005, vol. 257.
- [7] N. Robertson and C. A. McGowan, Chem. Soc. Rev., 2003, 32, 96–103.
- [8] C. S. Andersen and K. V. Gothelf, Org. Biomol. Chem., 2009, 7, 58–60.
- [9] Atomic and Molecular Wires, ed. J. L. Bredas, V. M. Geskin, D. A. das Santos, D. Beljonne and J. Cornil, Kluwer Academic, Boston, 1997.
- [10] J. L. Bredas, R. Silbey, D. S. Boudreaux and R. R. Chance, J. Am. Chem. Soc., 1983, 105, 6555–6559.
- [11] U. Salzner, J. B. Lagowski, P. G. Pickup and R. A. Poirier, Synth. Met., 1998, 96, 177–189.
- [12] H. Ding and J. P. Maier, J. Phys. Conf. Ser., 2007, 61, 252.

- [13] R. Zahradnik and L. Sroubkova, Helv. Chim. Acta, 2003, 86, 979–1000.
- [14] M. A. Reed, Proc. IEEE, 1999, 87, 652–658.
- [15] C. Weisbuch and B. Vinter, Quantum Semiconductor Structures, Academic Press, San Diego, 1991.
- [16] K. Andersson, P.-Å. Malmqvist and B. O. Roos, J. Chem. Phys., 1992, 96, 1218–1226.
- [17] L. Gagliardi and B. O. Roos, Chem. Soc. Rev., 2007, 36, 893–903.
- [18] L. Gagliardi, J. Am. Chem. Soc., 2003, 125, 7504–7505.
- [19] L. Gagliardi, Theor. Chem. Acc., 2006, 116, 307–315.
- [20] M. Brynda, L. Gagliardi and B. O. Roos, Chem. Phys. Lett., 2009, 471, 1–10.
- [21] I. Infante, L. Gagliardi, X. F. Wang and L. Andrews, J. Phys. Chem. A, 2009, 113, 2446–2455.
- [22] B. O. Roos, P. A. Malmqvist and L. Gagliardi, J. Am. Chem. Soc., 2006, 128, 17000–17006.
- [23] B. O. Roos and L. Gagliardi, Inorg. Chem., 2006, 45, 803–807.
- [24] G. La Macchia, L. Gagliardi, P. P. Power and M. Brynda, J. Am. Chem. Soc., 2008, 130, 5104–5114.
- [25] G. La Macchia, M. Brynda and L. Gagliardi, Angew. Chem., Int. Ed., 2006, 45, 6210–6213.
- [26] J. Hachmann, J. J. Dorando, M. Aviles and G. K. L. Chan, J. Chem. Phys., 2007, 127, 134309.
- [27] K. H. Marti, I. M. Ondik, G. Moritz and M. Reiher, J. Chem. Phys., 2008, 128, 014104.
- [28] L. Greenman and D. A. Mazziotti, J. Chem. Phys., 2009, 130, 184101.

[29] P. A. Malmqvist, K. Pierloot, A. R. Moughal Shahi, C. J. Cramer and L. Gagliardi, J. Chem. Phys., 2008, 128, 204109.

- [30] E. Neuscamman, T. Yanai and G. K. L. Chan, J. Chem. Phys., 2009, 130, 169901.
- [31] G. K. L. Chan, Phys. Chem. Chem. Phys., 2008, 10, 3454–3459.
- [32] T. Yanai, Y. Kurashige, D. Ghosh and G. K. L. Chan, Int. J. Quantum Chem., 2009, 109, 2178–2190.
- [33] D. A. Mazziotti, Phys. Rev. A: At., Mol., Opt. Phys., 1998, 57, 4219–4234.
- [34] S. M. Huber, A. R. Moughal Shahi, F. Aquilante, C. J. Cramer and L. Gagliardi, J. Chem. Theory Comput., 2009, DOI:10.1021/ct00282m, in press.
- [35] J. P. Perdew, K. Burke and M. Ernzerhof, Phys. Rev. Lett., 1996, 77, 3865–3868.
- [36] D. E. Woon and T. H. Dunning, J. Chem. Phys., 1994, 100, 2975–2988.
- [37] R. Ahlrichs, M. Bar, M. Haser, H. Horn and C. Kolmel, Chem. Phys. Lett., 1989, 162, 165–169.
- [38] P. O. Widmark, P. A. Malmqvist and B. O. Roos, Theor. Chim. Acta, 1990, 77, 291–306.
- [39] G. Karlström, R. Lindh, P.-Å. Malmqvist, B. O. Roos, U. Ryde, V. Veryazov, P.-O. Widmark, M. Cossi, B. Schimmelpfennig, P. Neogrady and L. Seijo, Comput. Mater. Sci., 2003, 28, 222–239.
- [40] G. Ghigo, B. O. Roos and P. A. Malmqvist, Chem. Phys. Lett., 2004, 396, 142–149.
- [41] F. Aquilante, P.-A. Malmqvist, T. B. Pedersen, A. Ghosh and B. O. Roos, J. Chem. Theory Comput., 2008, 4, 694–702.
- [42] F. Aquilante, T. B. Pedersen and R. Lindh, J. Chem. Phys., 2007, 126, 194106–194111.
- [43] F. Aquilante, T. B. Pedersen, A. S. de Meras and H. Koch, J. Chem. Phys., 2006, 125, 174101–174107.

- [44] M. S. Deleuze, J. Phys. Chem. A, 2004, 108, 9244.
- [45] M. S. Deleuze, J. Chem. Phys., 2002, 116, 7012.
- [46] M. S. Deleuze, A. B. Trofimov and L. S. Cederbaum, J. Chem. Phys., 2001, 115, 5859–5882.
- [47] J. V. Ortiz, J. Chem. Phys., 1998, 108, 1008–1014.
- [48] T. Ida and J. V. Ortiz, J. Chem. Phys., 2008, 129, 11.
- [49] K. Kimura, S. Katsumata, Y. Achiba, T. Yamazaki and S. Iwata, Handbook of HeI Photoelectron Spectra of Fundamental Organic Molecules, Halsted Press, New York, 1981.
- [50] R. J. Cave and E. R. Davidson, J. Phys. Chem., 1988, 92, 2173–2177.
- [51] R. J. Cave and E. R. Davidson, J. Phys. Chem., 1988, 92, 614–620.
- [52] T. Hayaishi, S. Iwata, M. Sasanuma, E. Ishiguro, Y. Morioka, Y. Iida and M. Nakamura, J. Phys. B: At. Mol. Phys., 1982, 15, 79–92.
- [53] S. G. Lias, J. E. Bartmess, J. F. Liebman, J. L. Holmes, R. D. Levin and W. G. Mallard, J. Phys. Chem. Ref. Data, 1988, 17, 1–861.
- [54] F. Brogli, E. Heilbronner, V. Hornung and E. Kloster-Jensen, Helv. Chim. Acta, 1973, 56, 2171.
- [55] L. A. Chewter, M. Sander, K. Mullerdethlefs and E. W. Schlag, J. Chem. Phys., 1987, 86, 4737–4744.
- [56] X. C. Cai, M. Sakamoto, M. Hara, S. Tojo, K. Kawai, M. Endo, M. Fujitsuka and T. Majima, J. Phys. Chem. A, 2004, 108, 9361–9364.
- [57] J. Olsen, O. Christiansen, H. Koch and P. Jorgensen, J. Chem. Phys., 1996, 105, 5082–5090.

[58] O. Christiansen, J. Olsen, P. Jorgensen, H. Koch and P. A. Malmqvist, Chem. Phys. Lett., 1996, 261, 369–378.

- [59] K. Nakayama, H. Nakano and K. Hirao, Int. J. Quantum Chem., 1998, 66, 157–175.
- [60] L. Serrano-Andrés, M. Merchán, I. Nebot-Gil, R. Lindh and B. O. Roos, J. Chem. Phys., 1993, 98, 3151–3162.
- [61] A. J. Merer and R. S. Mulliken, Chem. Rev., 1969, 69, 639.
- [62] O. A. Mosher, W. M. Flicker and A. Kuppermann, J. Chem. Phys., 1973, 59, 6502.
- [63] W. M. Flicker, O. A. Mosher and A. Kuppermann, Chem. Phys. Lett., 1977, 45, 492–497.
- [64] R. M. Gavin, C. Weisman, J. K. McVey and S. A. Rice, J. Chem. Phys., 1978, 68, 522–529.
- [65] W. Kutzelnigg, in Einfuhrung in die Theoretische Chemie, Verlag Chemie, Weinheim, 1978.
- [66] E. Kloster-Jensen, H. J. Haink and H. Christen, Helv. Chim. Acta, 1974, 57, 1731.
- [67] A. Hiraya and K. Shobatake, J. Chem. Phys., 1991, 94, 7700–7706.
- [68] A. F. Diaz, J. Crowley, J. Bargon, G. P. Gardini and J. B. Torrance, J. Electroanal. Chem., 1981, 121, 355–361.
- [69] C. Petrongolo, R. J. Buenker and S. D. Peyerimhoff, J. Chem. Phys., 1982, 76, 3655–3667.
- [70] L. E. McMurchie and E. R. Davidson, J. Chem. Phys., 1977, 66, 2959–2971.
- [71] R. Lindh and B. O. Roos, Int. J. Quantum Chem., 1989, 35, 813–825.
- [72] J. Finley, P. A. Malmqvist, B. O. Roos and L. Serrano-Andres, Chem. Phys. Lett., 1998, 288, 299–306.
- [73] M. Rubio, M. Merchan, E. Orti and B. O. Roos, Chem. Phys. Lett., 1995, 234, 373–381.

[74] E. N. Brothers, A. F. Izmaylov, J. O. Normand, V. Barone and G. E. Scuseria, J. Chem. Phys., 2008, 129, 011102.

Chapter 6

Multistate CASPT2 vs Multistate RASPT2

A benchmark set of 11 medium sized organic molecules (aromatic hydrocarbons and nucleobases) is chosen. Vertical excitation energies are computed for the valence excited states using multiconfigurational second order perturbation theory, based on the complete active space reference wave function (CASPT2) and restricted active space approach (RASPT2). The calculations are done at identical geometries obtained (DFT/B3LYP) and with the same basis set (TZVP). A systematic evaluation is done on the effects of different active space choices and the outer RAS space excitations. The RASPT2 results compare well with those obtained by CASPT2 method. The general applicability of the RASPT2 protocol to compute the excited states is discussed .

6.1 Introduction

The prediction of electronic spectra for organic molecules is important in organic photochemistry and it has been one of the challenges in the field of theoretical chemistry to accurately calculate the vertical excitation energies. It is often hard and impossible to obtain reliable and accurate experimental data for these because the observed band maxima do not exactly

correspond to the vertical excitation energy and often bands are found to overlap. Also, assignment of spectra may be uncertain and in some cases it is usually available only in solution and not in the gas phase. Therefore, high level *ab initio* theory becomes invaluable in obtaining the reference data computationally. In this respect, MultiState (MS) CASPT2 (complete active space second-order perturbation theory) [1, 2, 3] has become the standard *ab initio* method for calculating excited-state properties and many such CASPT2 results are available in the literature.

Recently, a multireference second-order perturbation theory using a restricted active space self-consistent wave function as a reference (RASPT2/RASSCF) has been developed [4]. Therein, it has been shown how this model extends the applicability of the well-known and accurate CASPT2 method to larger systems where the required active spaces need to be enlarged. Following it, this newly developed theory has been used in the determination of singlet-triplet state energy splitting of three supported copper-dioxygen and two supported copper-oxo complexes, in conjugation with CASPT2 method [5]. Furthermore, It has been shown how RASPT2 offers a similar accuracy when compared to CASPT2, at significantly reduced computational expense while computing one-electron ionization potentials and optical band gaps of ethylene, acetylene and phenylene oligomers. [6]

For the validation of any existing computational method or for the parameterization of improved approximate methods, a benchmark set of molecules with reliable reference data is a must. A benchmark set of medium-sized organic molecules has been chosen and comprehensively studied with various theoretical tools available by Thiel.et. al very recently. [7, 8, 9] In this present article, for the first time we test the MS-RASPT2 method to compute the excited states of a number of paradigmatic set of 11 medium-sized organic molecules (aromatic hydrocarbons and nucleobases) and thereby benchmark MS-RASPT2 level of theory against the MS-CASPT2 method in treating the electronically excited states, in particular the valence excited states at a uniform level, ie., using the same geometry, basis set and standard CASPT2 conventions. This allows us to check the consistency of the MS-RASPT2 results and it's performance for different types of excited states.

We are interested to answer the question of how best to choose a RASSCF active space and excitation protocol while computing electronically excited states.

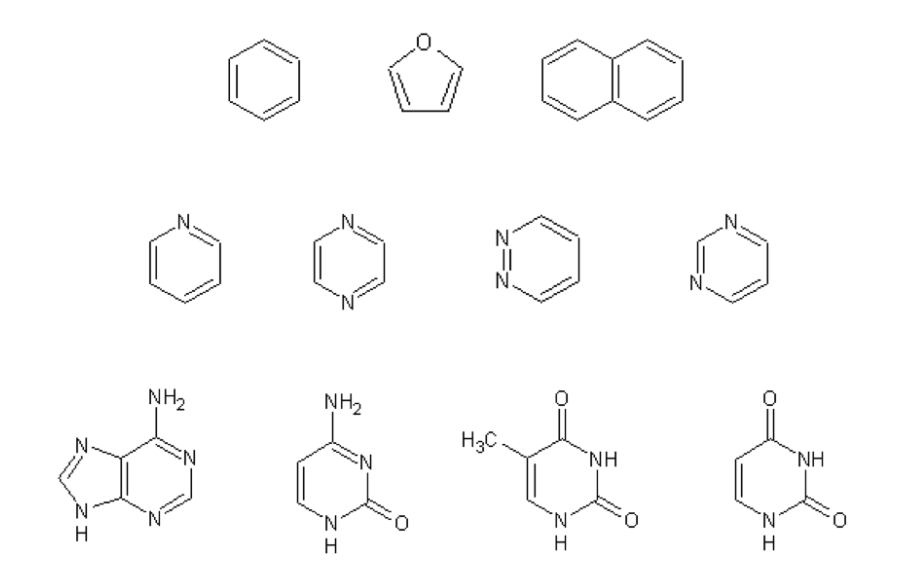


Figure 6.1: Benchmark set of molecules considered in this study.

We begin with a discussion of the computational details, and then present results designed to assess convergence in predicted energies with respect to methodological choices. We evaluate the capabilities and accuracy of the MS-RASPT2 method, which leads to us a better understanding of the active space partition that would better describe the electronic states. We conclude with some general observations likely to prove useful in future applications of the MS-RASPT2 model.

6.2 Computational details

Geometries of the structures of all systems were optimized at the B3LYP [10] level of density functional theory and triple-zeta valence polarized basis (TZVP) set on all atoms [11]. The Turbomole software package version 5.10 [12] was employed. Subsequent single point MS-CASSCF/CASPT2 and MS-RASSCF/RASPT2 calculations were performed at these op-

timized geometries using TZVP basis sets on all the atoms. The MOLCAS 7.3 package [13] was employed to perform these calculations. In all our calculations the IPEA approach (using the default value 0.25 au) for the CASPT2/RASPT2 zeroth order Hamiltonian was employed [14]. Cholesky decomposition [15] of the two-electron integrals was accomplished with a threshold of 10-5a.u. Reduced-scaling evaluation of the Fock exchange matrices in the CASSCF and RASSCF calculations was accomplished by means of the Local-K (LK) screening approach [16] employing localized Cholesky orbitals [17].

As mentioned, our aim is to treat the valence excited states of all benchmark molecules at a uniform level and therefore with the same standard basis set. Our benchmark set covers $\pi - \pi^*$ and $n - \pi^*$ excitations. It should be noted here that the TZVP basis set does not contain diffuse functions and thus are incapable to describe those excited states that are spatially extended and have rydberg character. Our focus is mostly on the low-lying valence excited states with compact electron density where the TZVP basis should be adequate. All the excitation energies reported here correspond to MS-CASPT2 and MS-RASPT2 energies.

The active space for the calculation of CASSCF (complete active space self-consistent field) reference function of any given system generally included π and π^* orbitals as well as any n orbitals involved. The number of active electrons was the total number of π electrons plus two electrons for each n orbital included.

In the RASSCF model, the active space is divided into three distinct subspaces: RAS1, RAS2, and RAS3. The RAS2 subspace is identical to the active space in a CASSCF calculation, i.e., all possible spin- and symmetry-adapted CSFs that can be constructed from the orbitals in RAS2 are included in the multiconfigurational wave function. The RAS1 and RAS3 subspaces, on the other hand, permit the generation of additional CSFs subject to the restriction that a maximum number of excitations may occur from RAS1, which otherwise contains only doubly occupied orbitals, and a maximum number of excitations may occur into RAS3, which otherwise contains only external orbitals. There are various ways in which one can select the orbitals. In all the cases studied here, the occupied π orbitals and the n orbitals were included in RAS1 and the unoccupied π^* orbitals in RAS3 with RAS2 space

empty. Few test cases were done where the RAS2 space was filled partially and these cases will be discussed individually.

Several levels of maximum excitation from RAS1 and into RAS3 were considered, in particular up to double, up to triple, and up to quadruple excitations. The general notation for a RASSCF or RASPT2 calculation is (ae,ao)/(ae2,ao2)/max, where ae is the number of active electrons in RAS1 and RAS2 combined, ao is the number of active orbitals in all of the RAS subspaces, ae2 is the number of active electrons in RAS2 ao2 is the number of active orbitals in RAS2, and max is the maximum number of excitations permitted out of RAS1 and into RAS3, where max takes on values of 2, 3, or 4 in this study.

6.3 Results and Discussion

The results of all the excited states considered are tabulated here. For every molecule studied, we have the table with the computed vertical excitation energies at different levels of excitations. The theoretical results obtained are compared to the experimental values (wherever available) graphically for each system. The active space chosen for each molecule is shown, below the table containing the results in parenthesis followed by the number of active electrons.

A total of 71 singlet and 32 triplet states have been evaluated. We now discuss individually each benchmark system, after which we will generalize the trends observed.

6.3.1 Benzene (Table 6.1, Fig 6.2 and 6.3)

In Table 6.1, we have tabulated the valence singlet and triplet excitation energies of benzene. These states considered are dominated by π - π^* single excitations and can thus be handled well by the CASPT2 method. As can be seen CASPT2 results agree well with the experimental numbers (typically by about 0.1 eV). Now, comparing the MS-RASPT2 with

MS-CASPT2, we can see that for all singlet and triplet states considered here the agreement is quite good (< 0.1 eV) at the triples and quadruple levels of excitation. However, at the doubles level we notice the deviations are higher (about 0.2 eV) and this more predominantly seen in the case of higher energy states. One needs to always keep in mind that we are truncating our wave function while doing a RASSCF method. Apart from this obvious approximation, at a given level of excitation it can happen that the ground state is being more accurately described than the excited state and vice versa, because the number of configuration state functions depend both on the spatial and spin symmetries of the wave function under consideration. This is the reason why one doesn't see a smooth trend as we increase level of excitations, going from doubles to quadruples. When we compare the results between RASPT2/max = 4 and CASPT2, we can see that the RASPT2 numbers are within 0.05 eV of CASPT2 (Fig. 6.2 & Fig. 6.3).

Table 6.1: Vertical excitation energies E (eV) of the singlet and triplet states of Benzene (D2h).

Exc.State	$\max = 2$	$\max = 3$	$\max = 4$	CASPT2	Expt
Ground State $(1^1A_g)RASPT2$					
Singlet states					
$\frac{1 {}^{1}\mathrm{B}_{3u}}{}$	5.280	5.021	5.018	5.023	4.90^{a}
$1~^1\mathrm{B}_{2u}$	6.390	6.236	6.337	6.352	6.20^{a}
$2~^1\mathrm{B}_{2u}$	7.187	6.811	6.778	6.892	6.94^{b}
$1~^1\mathrm{B}_{1g}$	8.157	7.613	7.616	7.612	7.8^{c}
Triplet states					
$-\frac{1 {}^{3}\mathrm{B}_{2u}}{}$	4.482	4.147	4.126	4.179	3.94^{d}
$1 {}^{3}\mathrm{B}_{3u}$	4.958	4.803	4.850	4.851	4.76^{d}
$2~^3\mathrm{B}_{3u}$	4.958	5.483	5.605	5.607	5.60^{d}
$2~^3\mathrm{B}_{1g}$	7.823	7.426	7.263	7.427	$7.24 - 7.74^e$

 a Ref.[18] b Ref.[19] c Ref.[20] d Ref.[21] e Ref. [22]

The active space is $(0\ 0\ 0\ 2\ 1\ 2\ 1)\ 6$. In parenthesis: the number of active orbitals of symmetry ag $b_{3u}\ b_{2u}\ b_{1g}\ b_{1u}\ b_{2g}\ b_{3g}\ a_{u}$ and the number of active electrons.

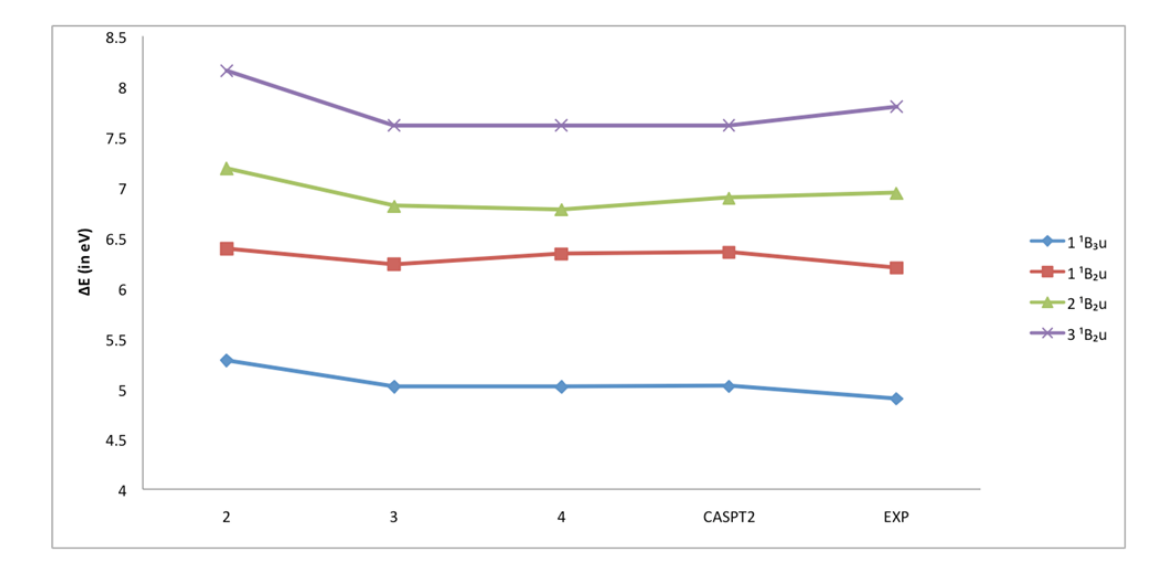


Figure 6.2: RASPT2 (max=2,3,4), CASPT2 and Experimental vertical excitation energies for the singlet states of Benzene.

6.3.2 Furan (Table 6.2, Fig. 6.4)

In Table 6.2, we have tabulated the valence singlet and triplet excitation energies of furan. The standard MS-CASPT2 approach gives the three lowest singlet valence excited states at 6.28 eV (1 1B1), 6.47 eV (2 A1), and 8.04 eV (3 1A1), i.e., about 0.25 eV higher than the experimental numbers. Similar to the benzene case, here too we see that RASPT2 numbers are within 0.05 eV of CASPT2 for the singlet states whereas the errors are about 0.2 eV for the 1 3B1 state (Fig. 6.5).

To understand better the trends seen here and in further systems we tabulate the number of CSFs for each state.

Looking carefully to the ratios in the Table 6.3, we notice that when the ratio of number of CSFs of the excited state to the ground state is closer to that of the CASPT2, the obtained excitation energy is also closer to the CASPT2 value. When the ratio is higher/lower than that seen in CASPT2, then the estimated energy difference seems to be higher/lower than the value obtained at CASPT2 level. This shows that both electronic states need to be described

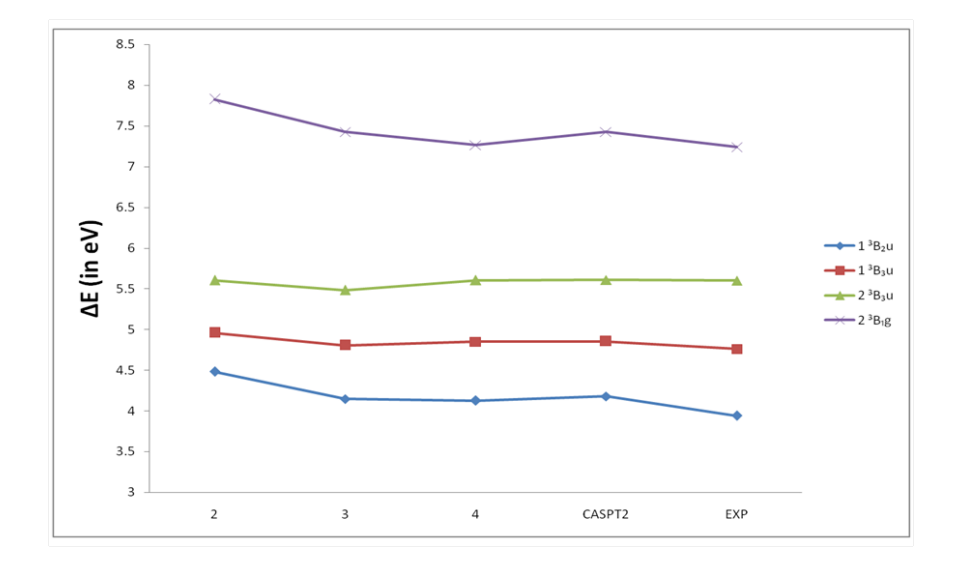


Figure 6.3: RASPT2 (max=2,3,4), CASPT2 and Experimental vertical excitation energies for the triplet states of Benzene.

in a balanced manner. One can see that with RASPT2/max = 4, we have close agreement between CASPT2 and RASPT2 results. This, along with inherent differences between the CASPT2 and RASPT2 implementations is the reason for the various trends that we see in this work.

6.3.3 Naphthalene (Table 6.4, Fig. 6.6 & 6.7)

Compared to the experimental results, the CASPT2 excitation energies are generally blue shifted, typically by 0.2 eV for singlet states. Larger blue shifts are encountered for singlet states with strong contributions from doubly excited configurations (3 $^{1}B_{3u}$). Still the results obtained with RASPT2/max = 4 give the numbers close to the CASPT2 results which is very encouraging. The large deviations for the higher energy states by CASPT2 could be an outcome of insufficient basis sets and they demand a better basis sets for their description.

	RASPT2				
Exc.State	$\max = 2$	$\max = 3$	$\max = 4$	CASPT2	Expt
Ground State (1^1A_1)					
Singlet states					
$1 {}^{1}\text{B}_{1}$	6.632	6.576	6.372	6.285	6.06^{a}
$2~^1\mathrm{A}_1$	6.629	6.635	6.490	6.474	-
$3~^1\mathrm{A}_1$	8.514	8.428	8.050	8.041	7.82^{a}
Triplet states					
$1 {}^{3}\mathrm{B}_{1}$	4.312	4.536	4.538	4.28	$4.02^{a,b}$
$1~^3\mathrm{A}_1$	5.634	5.790	5.561	5.533	5.22^{b}

Table 6.2: Vertical excitation energies E (eV) of the singlet and triplet states of Furan (C_{2v}) .

The active space is $(0\ 0\ 2\ 3)$ 6. In parenthesis: the number of active orbitals of symmetry a_1 b_1 a_2 b_2 and the number of active electrons.

6.3.4 Pyrrole, Pyridine, Pyrazine, Pyrimidine (Table 6.5 - 6.8, Fig. 6.7 - 6.15):

In these four heterocyclic compounds, CASPT2 method has a tendency to overestimate the excitation energies by 0.4-0.6 eV. For pyrrole, both CASPT2 method and RASPT2/max = (2, 3, 4) predict correct excitation energies when compared to the experimental results (Fig. 6.8) and as seen before the RASPT2/max =4 estimations are in about 0.5 eV range with those of CASPT2. For pyridine, both singlet and triplet states of $\pi - \pi^*$ character have been estimated rather well (Fig. 6.8 & 6.10) but large deviations of about 0.5 eV are seen in case of singlet $n\rightarrow\pi^*$ when compared to experimental results, while RASPT2/max = 4 underestimate the excitation energies by 0.1-0.3 eV for both singlet and triplet $n\rightarrow\pi^*$ states (Fig. 6.9 & 6.11). Similar trends are also evident from the results obtained for pyrazine and pyrimidine molecules as well (Figs. 6.12, 6.13, 6.14, 6.15).

^a Ref. [23] ^b Ref. [24]

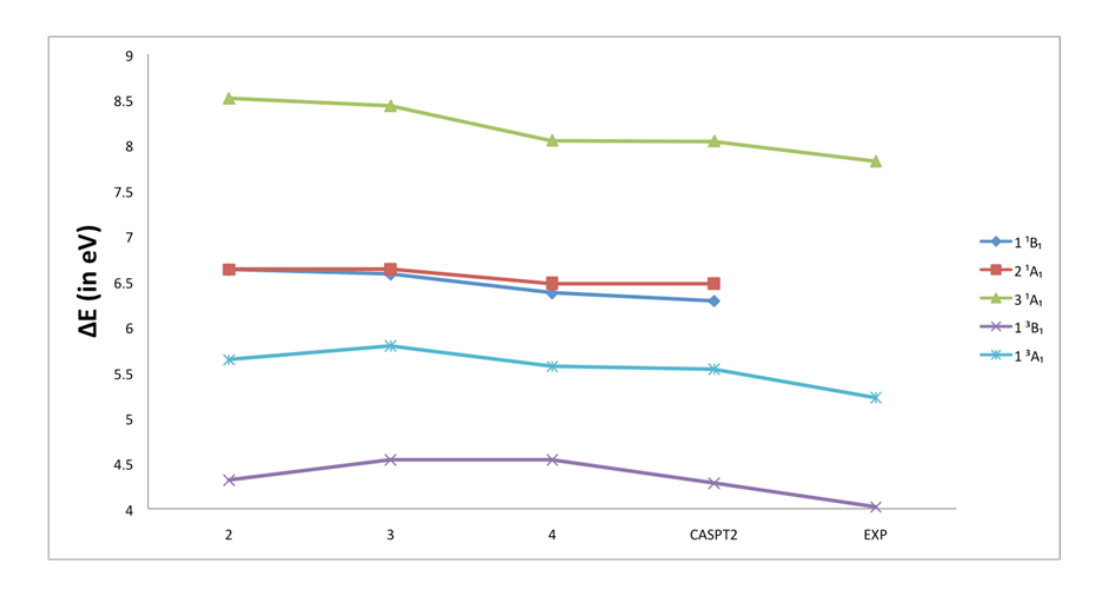


Figure 6.4: RASPT2 (max=2,3,4), CASPT2 and Experimental vertical excitation energies for the singlet and triplet states of Furan (C_{2v}).

Table 6.3: Number of CSFs required for the description of electronically excited state at different levels of excitation for Furan (C_{2v})

Exc.State	$\max = 2$	$\max = 3$	$\max = 4$	CASPT2
$1^{-1}A_{1}$	16	24	28	28
$1 {}^{1}{ m B}_{1}$	12	20	22	22
$1 {}^{3}A_{1}$	11	20	21	21
$1 {}^{3}{ m B}_{1}$	13	22	24	24
Ratio $({}^{1}B_{1}/{}^{1}A_{1})$	0.75	0.83	0.78	0.78
Ratio $({}^{3}A_{1}/{}^{1}A_{1})$	0.68	0.83	0.75	0.75
Ratio $(^3\mathrm{B}_1/^1\mathrm{A}_1)$	0.81	0.91	0.85	0.85

Table 6.4: Vertical excitation energies E (eV) of the singlet and triplet states of Naphthalene (D_{2h})

(216)		RASPT2			
Exc.State	$\max = 2$	$\max = 3$	$\max = 4$	CASPT2	Expt
Ground State (1^1A_g)					
Singlet states					
$1^{-1}\mathrm{B}_{2u}$	4.541	4.288	4.235	4.261	$3.97^a, 4.0^b$
$1 {}^{1}{ m B}_{3u}$	4.929	4.688	4.608	4.622	$4.45^a , 4.7^b$
$2~^1\mathrm{A}_g$	6.727	6.025	6.005	6.054	5.50^{c} c, 5.52^{d}
$2 {}^{1}{ m B}_{2u}$	6.856	5.979	6.203	6.048	$5.28c^c, 5.22^c$
$1 {}^{1}{ m B}_{1q}$	6.340	5.835	5.869	5.937	$5.63^d, 5.55^e, 5.89^a$
$3~^1\mathrm{A}_g^{^2}$	7.407	6.815	6.660	6.719	
$2~^1\mathrm{B}_{3u}$	6.487	6.209	6.120	6.128	$6.14^a, 6.0^b$
$2~^1\mathrm{B}_{1g}$	7.033	6.786	6.349	6.336	$6.01^c, 6.05^d$
$3~^1\mathrm{B}_{2u}$	8.007	8.112	7.474	7.782	
$3 {}^{1}{ m B}_{3u}$	8.218	7.979	8.913	8.926	$7.7^c, 7.6^b, 7.4^e$
Triplet states					
$1 {}^{3}\mathrm{B}_{3u}$	3.871	3.263	3.212	3.264	
Energies w.r.t to the B_{3u} stat	e				
$1~^3\mathrm{B}_{2u}$	0.905	0.943	0.896	0.965	
$1~^3\mathrm{B}_{1g}$	1.446	1.265	1.233	1.275	
$2~^3\mathrm{B}_{3u}$	1.502	1.363	1.414	1.382	
$1 {}^3\mathrm{A}_q$	2.319	2.264	2.253	2.279	2.25_q
$2 {}^{3}{ m B}_{1a}$	2.755	2.723	2.724	2.689	$3.12_h, \ 3.0_i$
$2 {}^{3}\mathrm{A}_{q}$	3.061	3.074	3.041	3.029	2.93_{q}
$3~^3\mathrm{A}_g^3$	3.247	3.194	3.142	3.172	J
$3~^3\mathrm{B}_{1g}^{^3}$	3.611	3.459	3.402	3.394	
a Rof [25] b Rof [26] c Rof [27] d	Rof [28] e B	of [20] f	Rof [30] g E	of [32] h	Rof [31] <i>i</i> Rof

 a Ref. [25] b Ref. [26] c Ref. [27] d Ref. [28] e Ref. [29] f Ref. [30] g Ref. [32] h Ref. [31] i Ref. [33]

The active space is $(0\ 0\ 0\ 0\ 3\ 3\ 2\ 2)\ 10$. In parenthesis: the number of active orbitals of symmetry ag $b_{3u}\ b_{2u}\ b_{1g}\ b_{1u}\ b_{2g}\ b_{3g}\ a_{u}$ and the number of active electrons.

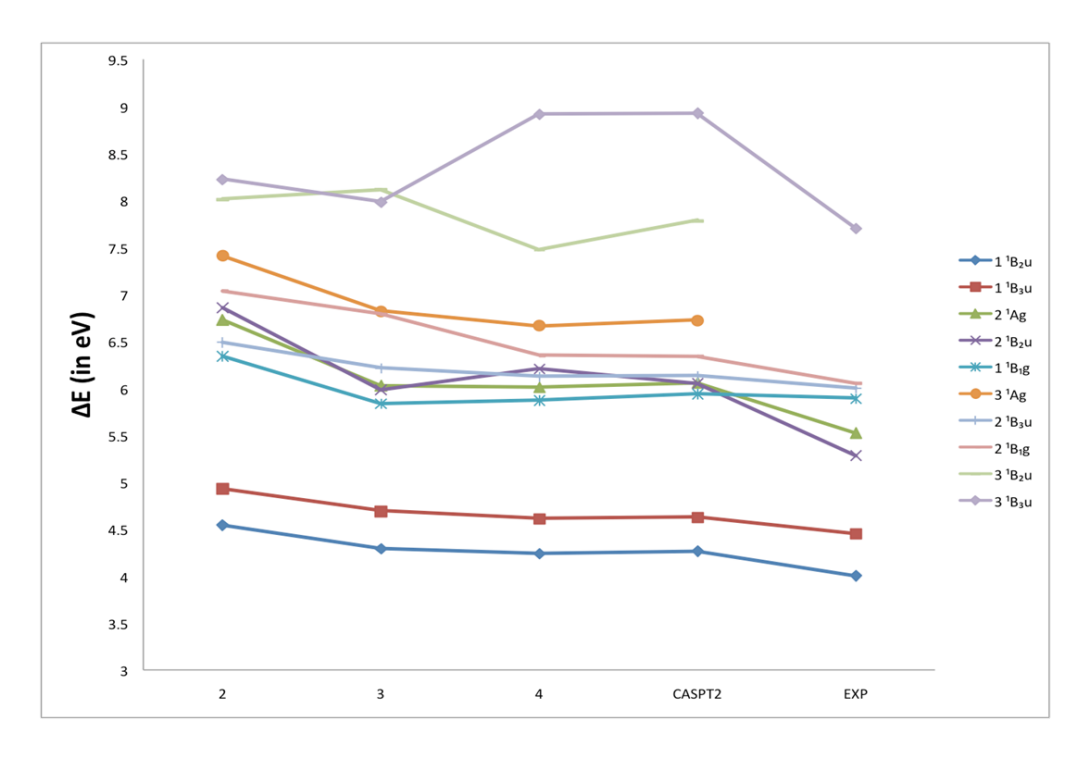


Figure 6.5: RASPT2 ($\max=2,3,4$), CASPT2 and Experimental vertical excitation energies for Naphthalene Singlet states.

Table 6.5: Vertical excitation energies E (eV) of the singlet and triplet states of Pyrrole(C_{2v}) RASPT2

Exc.State	max = 2	$\max = 3$	$\max = 4$	CASPT2	Expt
Ground State (1^1A_1)					
Singlet states					
$2 {}^{1}A_{1}$	6.480	6.539	6.303	6.277	
$1~^1\mathrm{B}_1$	6.812	6.958	6.668	6.619	$5.98^{a},^{b}$
$3~^1\mathrm{A}_1$	8.284	8.317	7.944	7.919	7.54^{a}
Triplet states					
$1~^{3}{ m B}_{1}$	4.449	4.778	4.500	4.475	$4.21^{a,c}$
$1~^3\mathrm{A}_1$	5.483	5.355	5.289	5.425	$5.10c^c$

 $[^]a$ Ref. [23] b Ref. [34] c Ref. [35] The active space is (0 0 2 3) 6. In parenthesis: the number of active orbitals of symmetry a_1 b_1 a_2 b_2 and the number of active electrons.

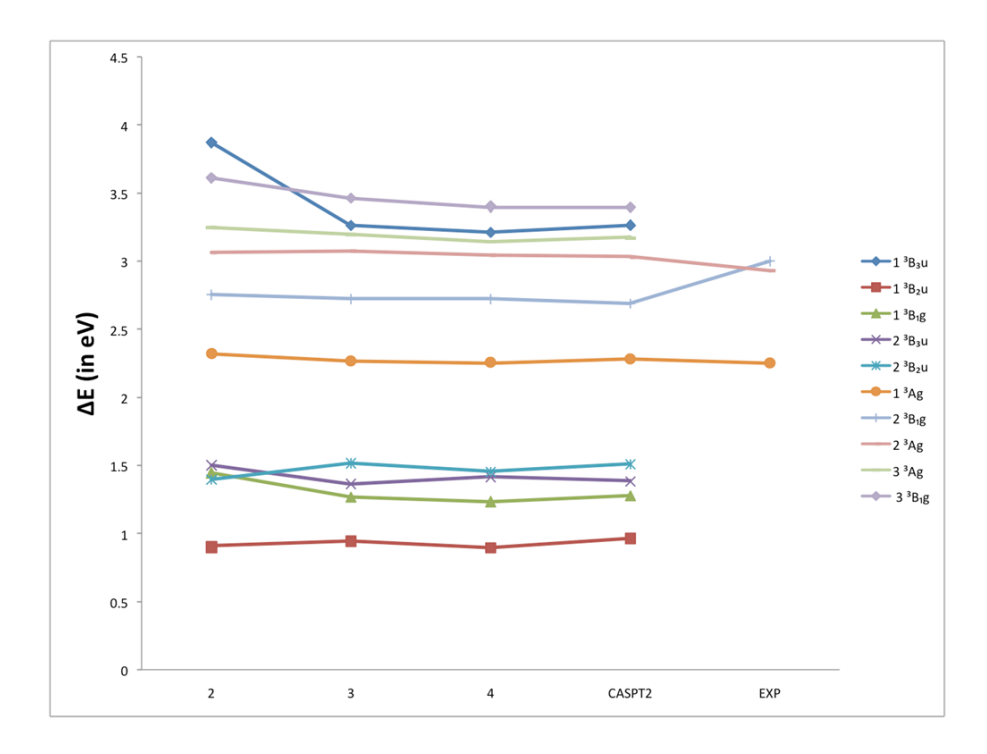


Figure 6.6: RASPT2 ($\max=2,3,4$), CASPT2 and Experimental vertical excitation energies for Naphthalene Triplet states.

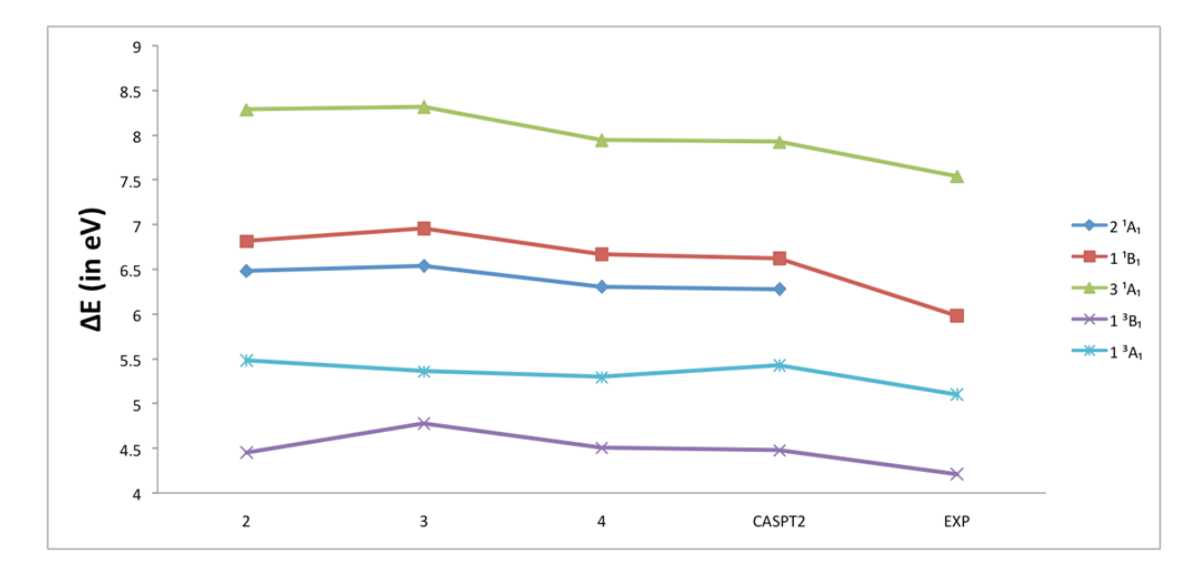


Figure 6.7: RASPT2 (max=2,3,4), CASPT2 and Experimental vertical excitation energies for the singlet and triplet states of Pyrrole

Table 6.6: Vertical excitation energies E (eV) of the singlet and triplet states of Pyridine (C_{2v})

		RASPT2			
Exc.State	$\max = 2$	$\max = 3$	$\max = 4$	CASPT2	Expt^a
Ground State (1^1A_1)					
Singlet states π - π *					
$1 {}^{1}\mathrm{B}_{1}$	5.426	5.030	5.262	5.099	4.99
$2 {}^{1}A_{1}$	6.573	6.680	6.709	6.573	6.38
$3 {}^{1}A_{1}$	7.120	7.489	7.477	7.120	7.22
$2 {}^{1}{\rm B}_{1}$	7.174	7.098	7.312	7.174	
$4~^1\mathrm{A}_1$	8.226	8.514	8.471	8.226	
$3 {}^{1}{\rm B}_{1}$	8.211	8.344	8.422	8.211	
Singlet states $n-\pi^*$					
$1 {}^{1}\mathrm{B}_{2}$	5.301	5.400	5.146	5.055	4.59
$1~^1\mathrm{A}_2$	5.339	5.706	5.417	5.352	5.43
Triplet states $(\pi - \pi^*)$					
$1 {}^{3}\text{A}_{1}$	4.708	4.674	4.440	4.32	4.10
$1~^3\mathrm{B}_1$	4.916	5.094	4.891	4.824	4.84
$2~^3\mathrm{A}_1$	5.220	5.336	5.175	5.015	
$2~^{3}\mathrm{B}_{1}$	6.143	6.738	6.638	6.695	
$3 {}^{3}A_{1}$	7.934	8.038	7.860	7.677	
$3~^3\mathrm{B}_1$	8.161	7.527	6.968	6.879	
Triplet states $(n-\pi^*)$					
$1 {}^3\mathrm{B}_2$	4.781	4.841	4.685	4.500	
$1~^3\mathrm{A}_2$	5.430	5.711	5.419	5.355	
[0.0]					

^a Ref. [36]

The active space is $(0\ 0\ 2\ 4)\ 6$. In parenthesis: the number of active orbitals of symmetry a_1 b_1 a_2 b_2 and the number of active electrons.

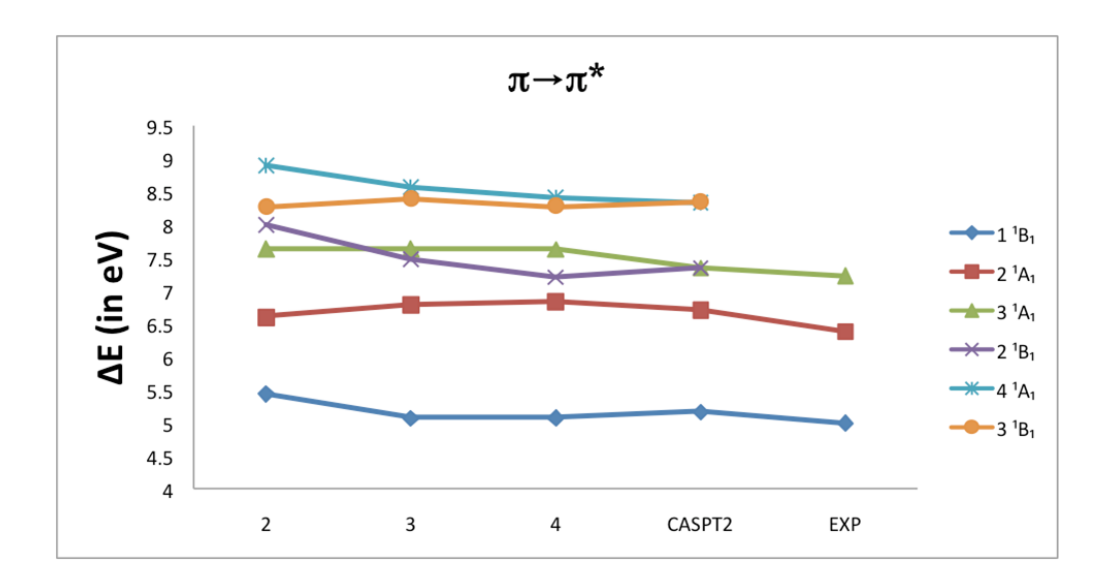


Figure 6.8: RASPT2 (max=2,3,4), CASPT2 and Experimental vertical excitation energies for Pyridine Singlet states $(\pi \rightarrow \pi^*)$

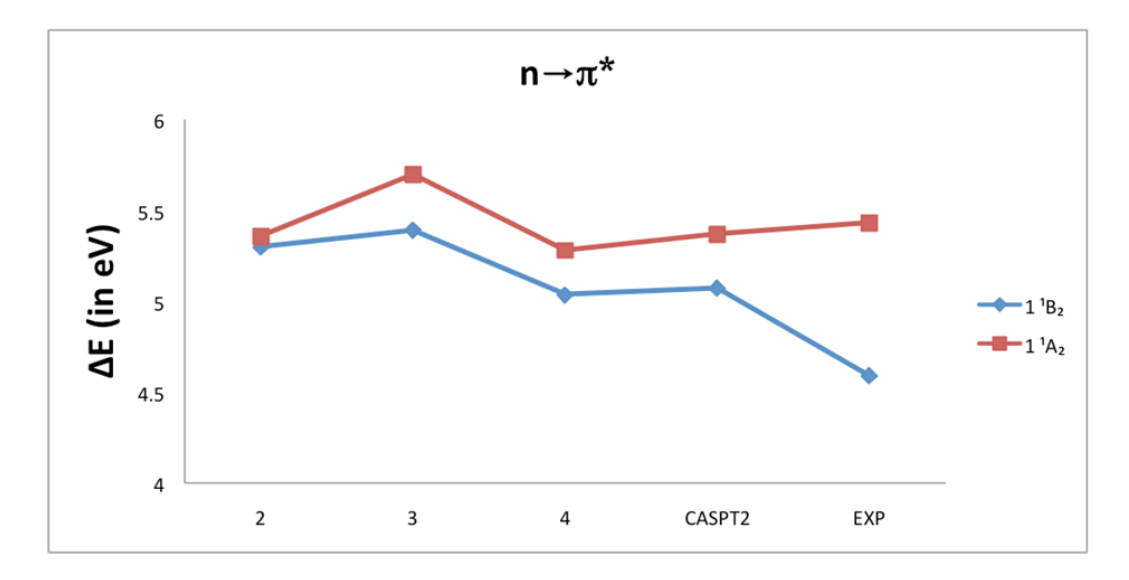


Figure 6.9: RASPT2 (max=2,3,4), CASPT2 and Experimental vertical excitation energies for Pyridine Singlet states ($n\rightarrow\pi^*$)

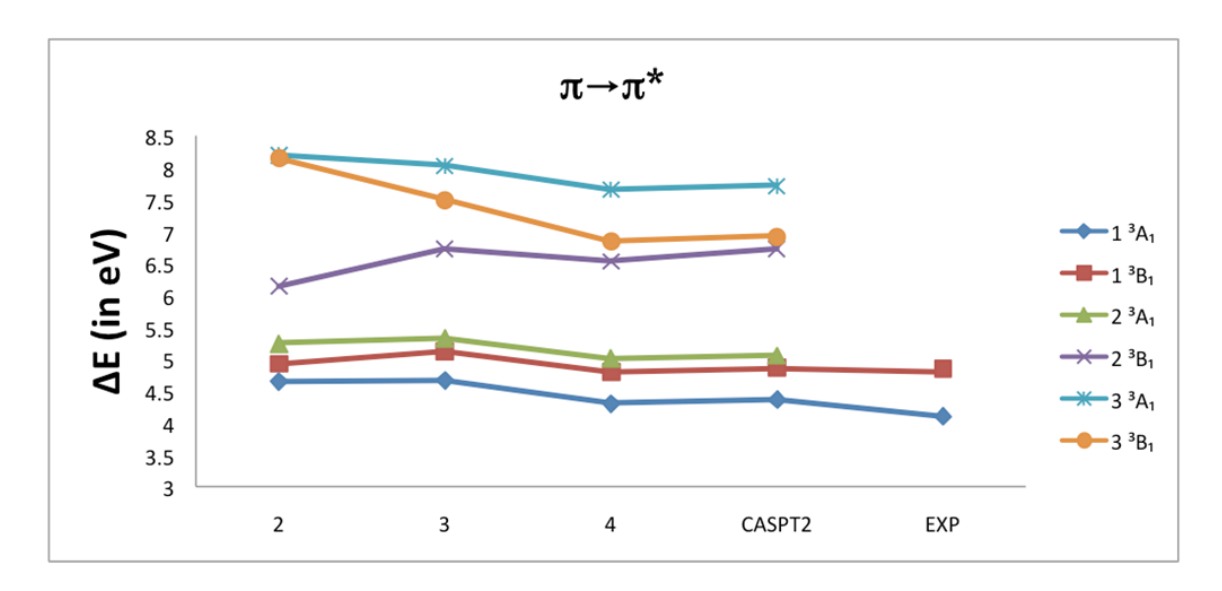


Figure 6.10: RASPT2 (max=2,3,4), CASPT2 and Experimental vertical excitation energies for Pyridine Triplet states $(\pi \rightarrow \pi^*)$

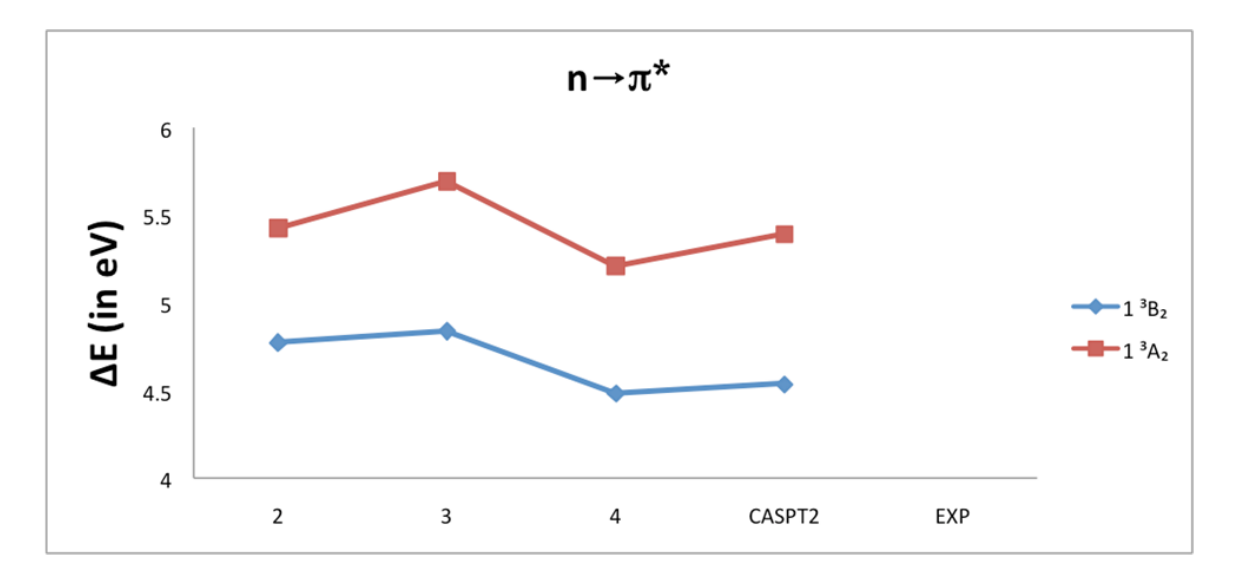


Figure 6.11: RASPT2 (max=2,3,4), CASPT2 and Experimental vertical excitation energies for Pyridine Triplet states (n $\rightarrow \pi^*$)

Table 6.7: Vertical excitation energies E (eV) of the singlet of Pyrazine (D_{2h}) RASPT2

		RASPIZ			
Exc.State	$\max = 2$	$\max = 3$	$\max = 4$	CASPT2	Expt^a
Ground State (1^1A_g)					
Singlet states $(\pi - \pi^*)$					
$1 {}^{1}\mathrm{B}_{2u}$	5.282	5.178	4.979	5.043	4.81
$1 {}^{1}{ m B}_{3u}$	6.853	6.770	6.426	6.685	6.51
$2 {}^{1}{ m B}_{3u}$	8.075	7.972	7.457	7.571	7.67
$1 {}^{1}\mathrm{B}_{2u}$	7.968	7.703	7.513	7.443	7.67
$1~^1\mathrm{B}_{1g}$	9.194	8.483	8.370	8.432	
$2~^1\mathrm{A}_g$	9.019	8.868	8.667	8.679	
Singlet states $(n - \pi^*)$					
$1 {}^{1}\mathrm{B}_{1u}$	4.384	4.213	3.948	4.091	3.83^{b}
$1 {}^{1}\mathrm{A}_{u}$	5.066	4.823	4.650	4.667	
$1~^1\mathrm{B}_{2g}$	6.002	5.708	5.392	5.554	5.46^{c}
$1 {}^{1}{ m B}_{3g}$	6.810	6.654	6.313	6.468	6.10^{d}
F					

 a Ref. [36] b Ref. [37] c Ref. [38] d Ref. [39]

The active space is $(0\ 0\ 1\ 1\ 2\ 2\ 1\ 1)\ 10$. In parenthesis: the number of active orbitals of symmetry ag $b_{3u}\ b_{2u}\ b_{1g}\ b_{1u}\ b_{2g}\ b_{3g}\ a_u$ and the number of active electrons.

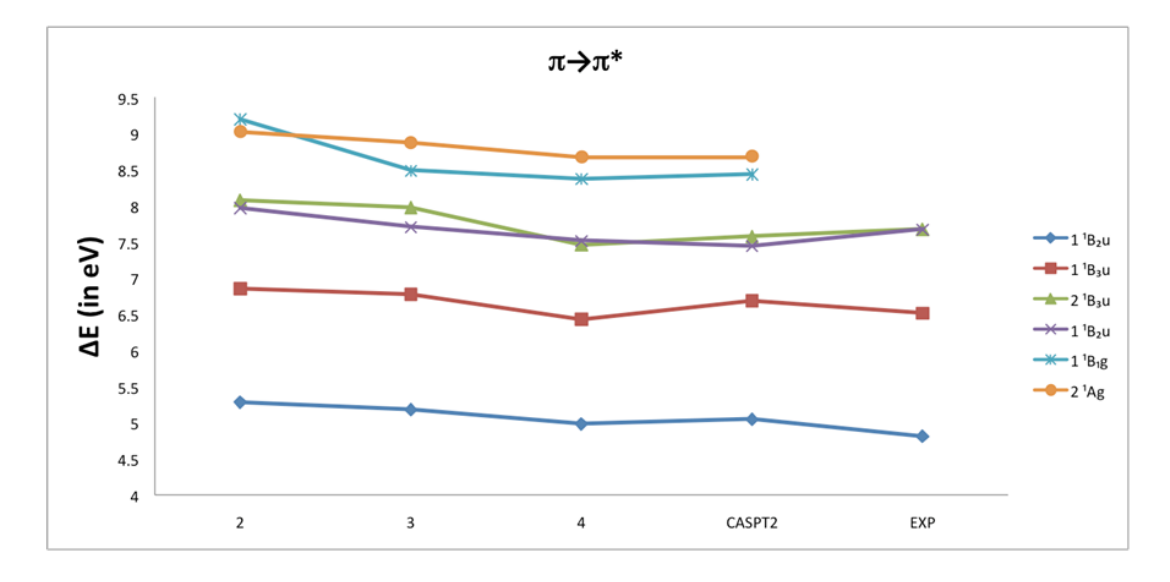


Figure 6.12: RASPT2 (max=2,3,4), CASPT2 and Experimental vertical excitation energies for Pyrazine Singlet states $(\pi \rightarrow \pi^*)$

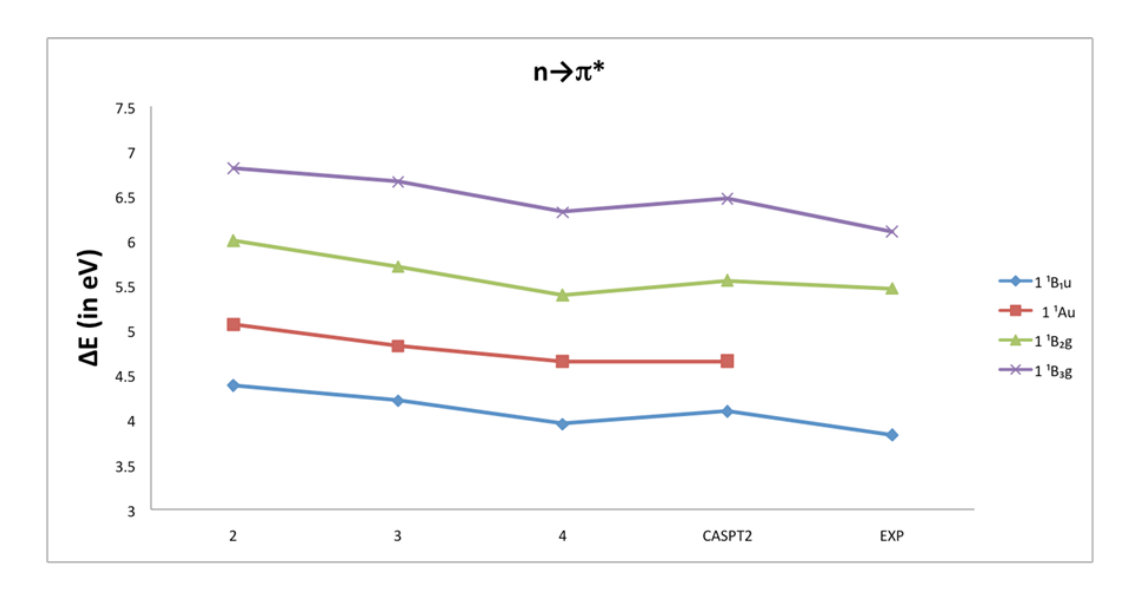


Figure 6.13: RASPT2 (max=2,3,4), CASPT2 and Experimental vertical excitation energies for Pyrazine Singlet states $(n\rightarrow\pi^*)$

Table 6.8: Vertical excitation energies E (eV) of the singlet of Pyrimidine (C_{2v})

RASPT2

		$\Lambda ASF 12$			
Exc.State	$\max = 2$	$\max = 3$	$\max = 4$	CASPT2	Expt^a
Ground State (1 ¹ A1)					
Singlet states $(\pi - \pi^*)$					
1 ¹ B	5.688	5.352	5.449	5.326	5.12
$2~^1\mathrm{A}_1$	6.953	7.044	6.963	6.957	6.7
$3 {}^{1}{ m A}_{1}$	8.110	8.078	7.751	7.543	7.57
$2 {}^{1}{ m B}_{1}$	7.772	7.604	7.574	7.366	7.57
$3 {}^{1}{ m B}_{1}$	9.158	8.998	8.805	8.757	
$4~^1\mathrm{A}_1$	8.421	8.224	7.821	7.857	
Singlet states $(n - \pi^*)$					
$1 {}^{1}{ m B}_{2}$	4.547	4.493	4.14	4.329	4.16^{b}
$1~^1\mathrm{A}_2$	5.025	4.945	4.550	4.708	4.62
_					

 a Ref. [36] b Ref. [39]

The active space is $(1\ 1\ 2\ 4)\ 10$. In parenthesis: the number of active orbitals of symmetry $a_1\ b_1\ a_2\ b_2$ and the number of active electrons.

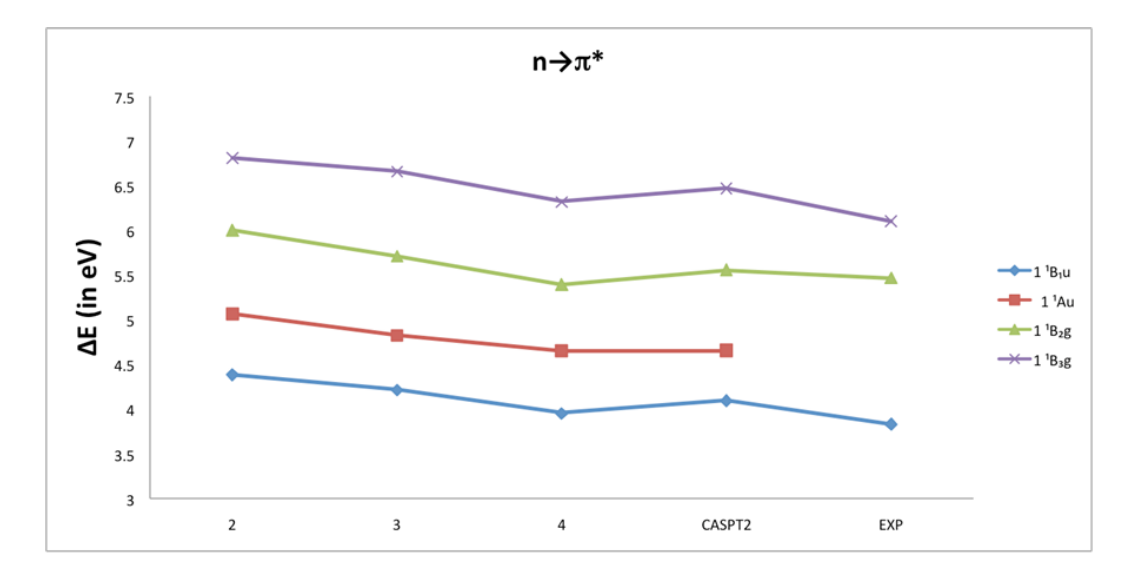


Figure 6.14: RASPT2 (max=2,3,4), CASPT2 and Experimental vertical excitation energies for Pyrimidine Singlet states $(\pi \rightarrow \pi^*)$

6.3.5 Adenine, Thymine, Uracil, Cytosine (Table 6.9 - 6.16, Fig. 6.16 -6.31):

The results obtained for the nucleobases are quite systematic. For Adenine molecule, CASPT2 method tends to overestimate the $\pi \to \pi^*$ excitation energies by about 0.2 - 0.4 eV, except for the 6 1 A' state in which case it underestimates by about 0.2 eV. The RASPT2 results converge to CASPT2 with the increase in the level of excitation and with RASPT2/max = 4, the results obtained are in very good agreement with those obtained by CASPT2 (Fig. 16). The trends change quite a bit when we look at the $n\to\pi^*$ states. As seen from Fig. 17, RASPT2/max = 4 excitation energies tend to be red shifted when compared to CASPT2 with a maximum deviation 0.9 eV in the case of 2 1 A" state. Similar kinds of trends are seen for the other three nucleobases as well (Figs. 6.20, 6.21, 6.24, 6.25, 6.28, 6.29). Furthermore, we have done similar kind of calculations by including 2 orbitals and 2 electrons in RAS2 subspace for these systems, in an attempt to see the effect and importance of RAS2 space in RASPT2 calculations. The results obtained are tabulated in Tables 6.10, 6.12, 6.14, 6.16. The general observation from all these is that the RASPT2/max = 2 gets corrected signifi-

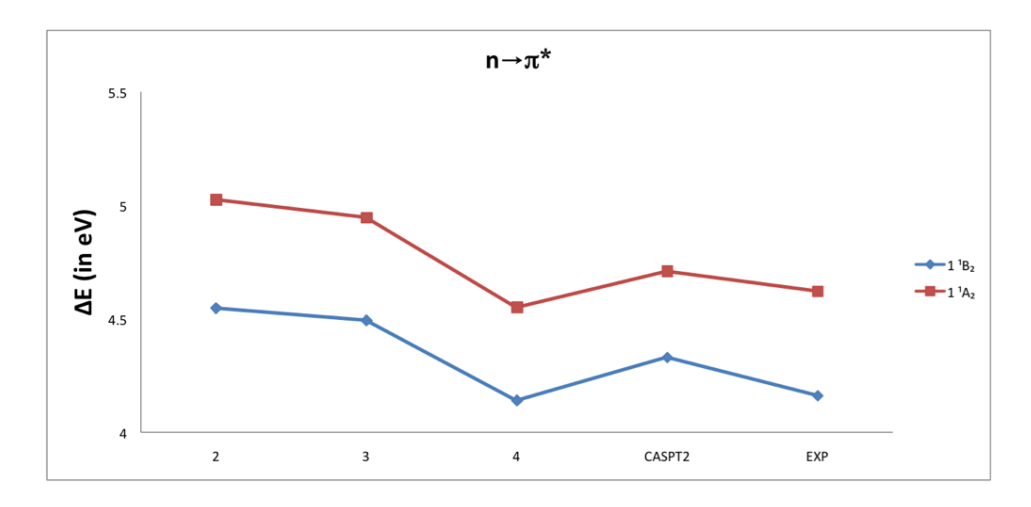


Figure 6.15: RASPT2 (max=2,3,4), CASPT2 and Experimental vertical excitation energies for Pyrimidine Singlet states ($n\rightarrow\pi^*$)

cantly (energy lowered by about 0.2 eV) and thereby already is in close agreement with the corresponding CASPT2 level (Figs. 6.18, 6.19, 6.22, 6.23, 6.26, 6.27, 6.30, 6.31). The same is also true for RASPT2/max = 3, 4 but the energy lowering is very little. However, we can notice that the trends get very regular with the inclusion of 2 orbitals and 2 electrons (those that correspond to the excitation generating a particular electronic state). While in terms of accuracy this is seen not to make much of a difference in the describing states generated from $\pi \rightarrow \pi^*$ excitations, it does make the significant difference in calculating the states generated from $n \rightarrow \pi^*$ excitations. So, this tells that if one knows the orbital excitations describing a particular electronic state apriori, it is very beneficial to include them in the RAS2 space. Of course, this in turn is going to increase computational overhead required for that particular calculation.

Table 6.9: Vertical excitation energies E (eV) of the singlet and triplet states of Adenine (C_s)

		RASP 12			
Exc.State	$\max = 2$	$\max = 3$	$\max = 4$	CASPT2	Expt
Ground State $(1^1A')$					
Singlet states					
$2^{1}A'(\pi - \pi^{*})$	5.632	5.183	5.142	5.097	4.63^{a}
$3 {}^{1}A'(\pi - \pi^{*})$	5.674	5.206	5.175	5.170	4.92^{b}
$1 {}^{1}A''(n-\pi^{*})$	5.756	5.146	4.974	5.147	5.4^c
$4^{1}A'(\pi - \pi^{*})$	6.885	6.427	6.425	6.407	5.99^{b}
$2 {}^{1}A''(n-\pi^{*})$	6.274	5.843	6.781	5.854	-
$5^{1}A'(\pi - \pi^*)$	6.982	6.478	6.471	6.481	6.33^{d}
$6 {}^{1}\text{A}'(\pi - \pi^{*})$	7.017	6.652	6.632	6.652	6.81^{e}

 $^a {\rm Ref.} \ [40]^b \ {\rm Ref.} \ [41]^c {\rm Ref.} \ [42]^d \ {\rm Ref.} \ [43]^e \ {\rm Ref.} \ [44]$

The active space is (0 10) 12. In parenthesis: the number of active orbitals of symmetry a' a' and the number of active electrons.

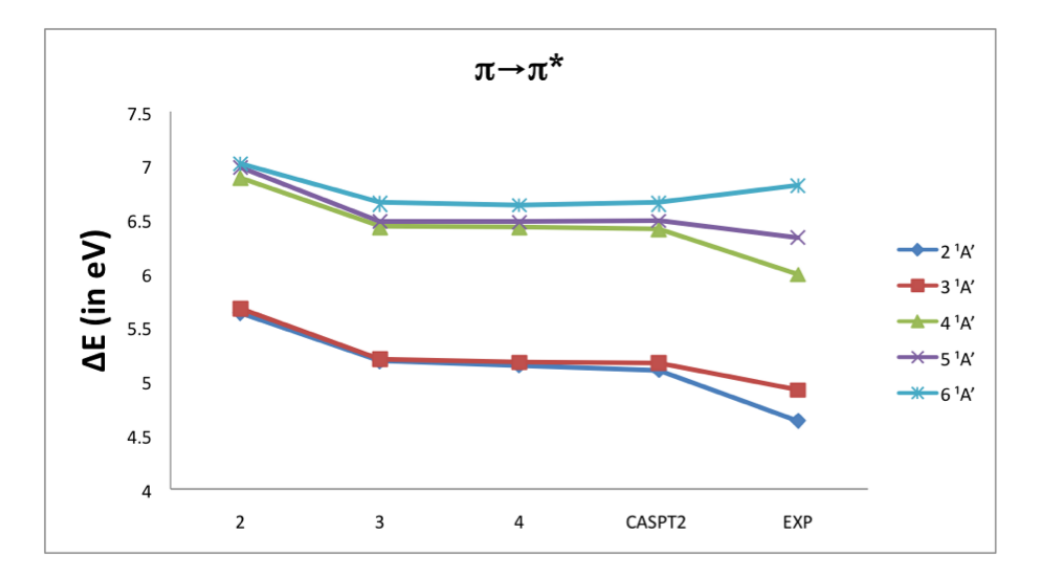


Figure 6.16: RASPT2 (max=2,3,4), CASPT2 and Experimental vertical excitation energies for Adenine Singlet states $(\pi \rightarrow \pi^*)$

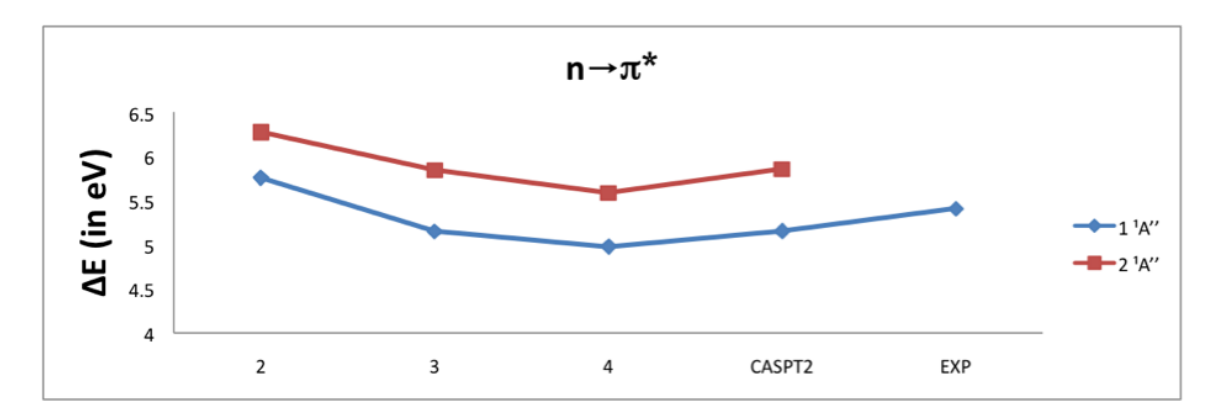


Figure 6.17: RASPT2 (max=2,3,4), CASPT2 and Experimental vertical excitation energies for Adenine Singlet states ($n\rightarrow\pi^*$)

Table 6.10: Vertical excitation energies E (eV) of the singlet and triplet states of Adenine (C_s) with RAS2

		RASPT2			
Exc.State	$\max = 2$	$\max = 3$	$\max = 4$	CASPT2	Expt
Ground State $(1^1A')$					
Singlet states					
$2^{1}A'(\pi - \pi^{*})$	5.111	5.012	4.984	5.097	4.63^{a}
$3 {}^{1}A'(\pi - \pi^{*})$	5.41	5.206	5.117	5.170	4.92^{b}
$1 {}^{1}A'(n-\pi^{*})$	5.361	5.116	4.817	5.147	5.4^c
$4^{1}A'(\pi - \pi^{*})$	6.622	6.505	6.385	6.407	5.99^{b}
$2 {}^{1}A'(n-\pi^{*})$	6.122	5.948	5.65	5.854	-
$5^{1}A'(\pi - \pi^*)$	6.731	6.517	6.386	6.481	6.33^{d}
$6^{1}A'(\pi - \pi^*)$	6.857	6.651	6.59	6.652	6.81^{e}

 a Ref. $[40]^{b}$ Ref. $[41]^{c}$ Ref. $[42]^{d}$ Ref. $[43]^{e}$ Ref. [44]

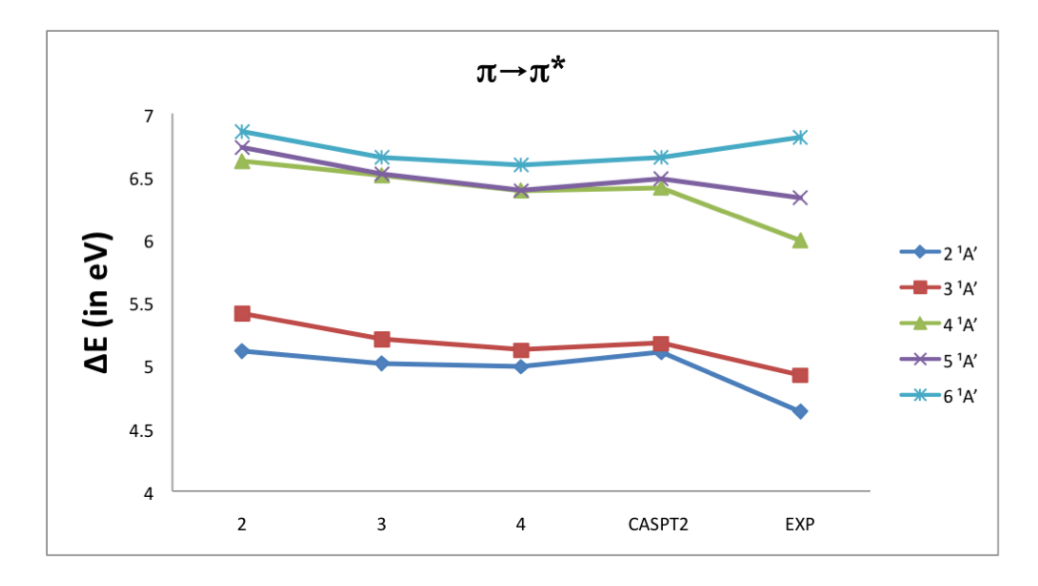


Figure 6.18: RASPT2 (max=2,3,4), CASPT2 and Experimental vertical excitation energies for Adenine Singlet states $(\pi \rightarrow \pi^*)$ with RAS2

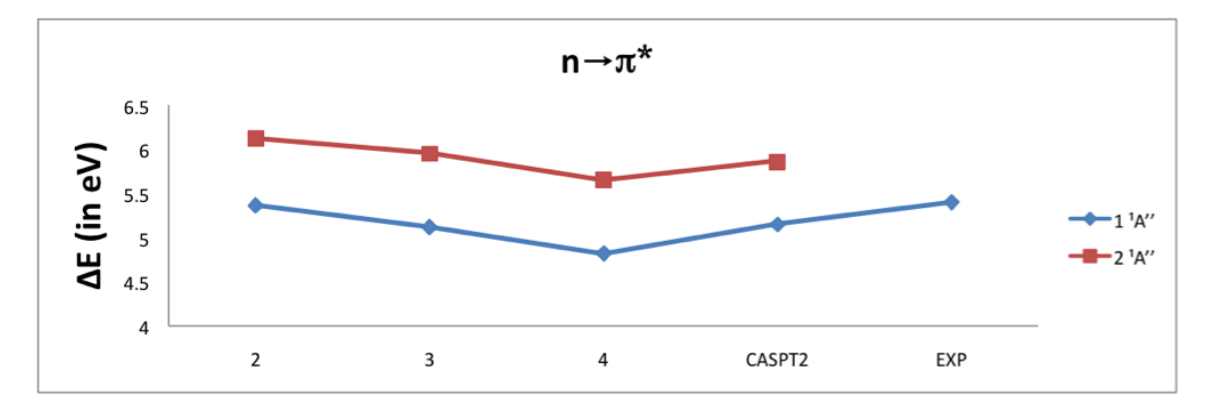


Figure 6.19: RASPT2 (max=2,3,4), CASPT2 and Experimental vertical excitation energies for Adenine Singlet states ($n\rightarrow\pi^*$) with RAS2

Table 6.11: Vertical excitation energies E (eV) of the singlet and triplet states of Thymine (C_s)

		RASPT2			
Exc.State	$\max = 2$	$\max = 3$	$\max = 4$	CASPT2	Expt
Ground State $(1^1A')$					
Singlet states					
$1^{1}A''(n-\pi^{*})$	5.618	5.289	5.091	5.24	$4.9 - 5.2^a$
$2 {}^{1}A'(\pi - \pi^{*})$	6.154	5.928	5.805	5.558	4.95^{b} , 4.8^{c}
$3 {}^{1}A'(\pi - \pi^{*})$	7.083	6.898	6.719	6.544	$6.2^{b}, 5.7^{c}$
$2 {}^{1}A''(n-\pi^{*})$	6.883	6.650	6.431	6.536	-
$4^{1}A'(n-\pi^{*})$	7.123	6.985	6.734	6.583	6.2^{c}
$3 {}^{1}A''(n-\pi^{*})$	7.817	7.770	7.237	7.403	-
$4^{1}A''(n-\pi^{*})$	8.293	7.825	7.802	7.887	-
$5^1 A''(\pi - \pi^*)$	7.967	7.875	7.383	7.194	$7.4^{b}, > 6.7^{c}$
$6^1 A'(\pi - \pi^*)$	9.181	9.298	9.068	8.808	-

 a Ref. $[45]^{b}$ Ref. $[46]^{c}$ Ref. [41]

The active space is $(0\ 9)\ 12$. In parenthesis: the number of active orbitals of symmetry a' a'' and the number of active electrons.

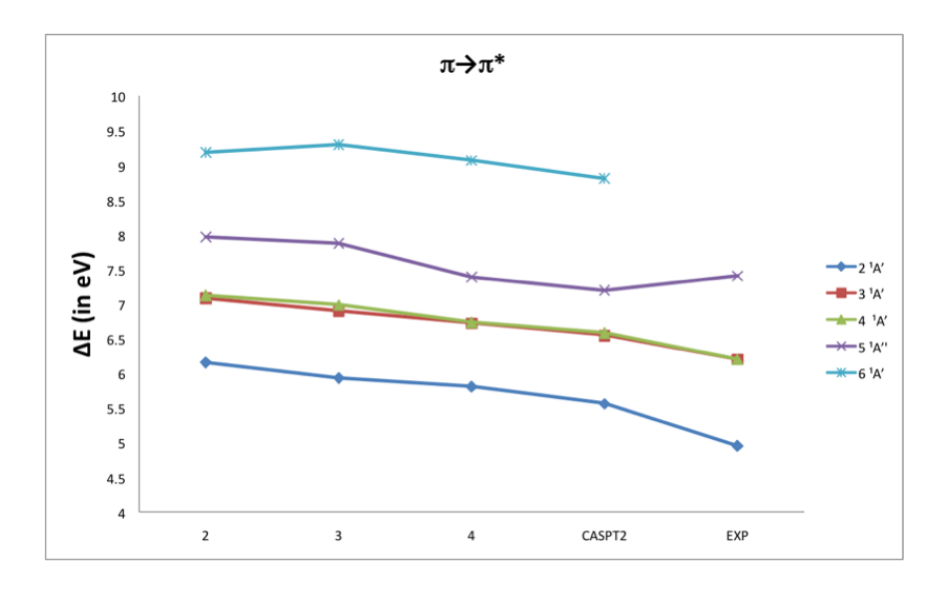


Figure 6.20: RASPT2 (max=2,3,4), CASPT2 and Experimental vertical excitation energies for Thymine Singlet states ($\pi \rightarrow \pi^*$)

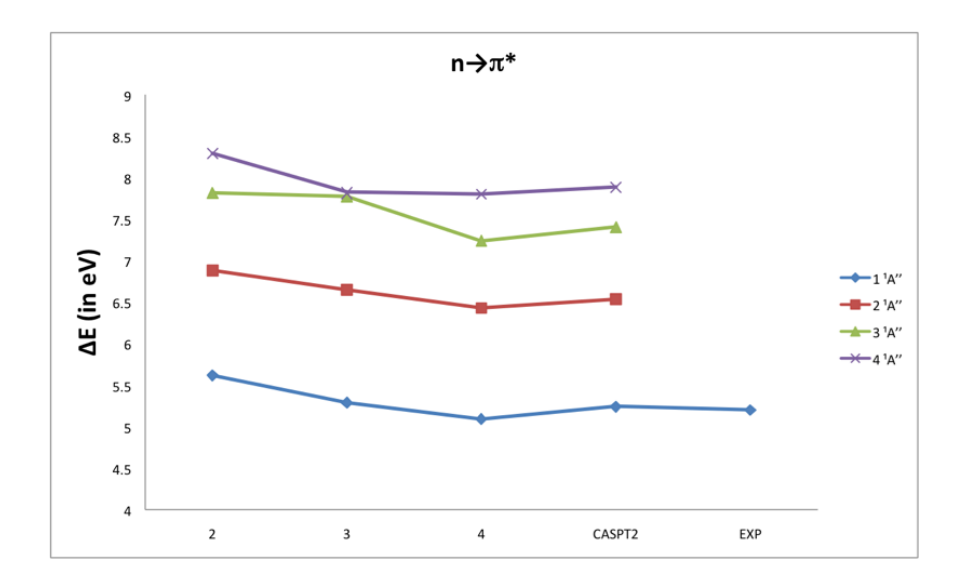


Figure 6.21: RASPT2 (max=2,3,4), CASPT2 and Experimental vertical excitation energies for Thymine Singlet states ($n\rightarrow\pi^*$)

Table 6.12: Vertical excitation energies E (eV) of the singlet and triplet states of Thymine (C_s) with RAS2

		RASPT2			
Exc.State	max = 2	$\max = 3$	$\max = 4$	CASPT2	Expt
Ground State $(1^1A')$					
Singlet states					
$1^{1}A''(n-\pi^{*})$	5.139	5.328	4.995	5.24	$4.9 - 5.2^a$
$2^{1}A'(\pi - \pi^{*})$	5.81	5.817	5.813	5.558	4.95^b , 4.8^c
$3 {}^{1}A'(\pi - \pi^{*})$	6.705	6.655	6.665	6.544	$6.2^{b}, 5.7^{c}$
$2^{1}A''(n-\pi^{*})$	6.485	6.734	6.334	6.536	-
$4 {}^{1}A'(\pi - \pi^{*})$	6.99	6.927	6.776	6.583	6.2^{c}
$3 {}^{1}A''(n-\pi^{*})$	7.626	7.439	7.102	7.403	-
$4^{1}A''(n-\pi^{*})$	8.105	8.184	7.887	7.887	-
$5^1 A''(\pi - \pi^*)$	7.739	7.724	7.339	7.194	$7.4^{b}, > 6.7^{c}$
$6^1 A'(\pi - \pi^*)$	9.158	9.149	9.051	8.808	-

 a Ref. $[45]^{b}$ Ref. $[46]^{c}$ Ref. [41]

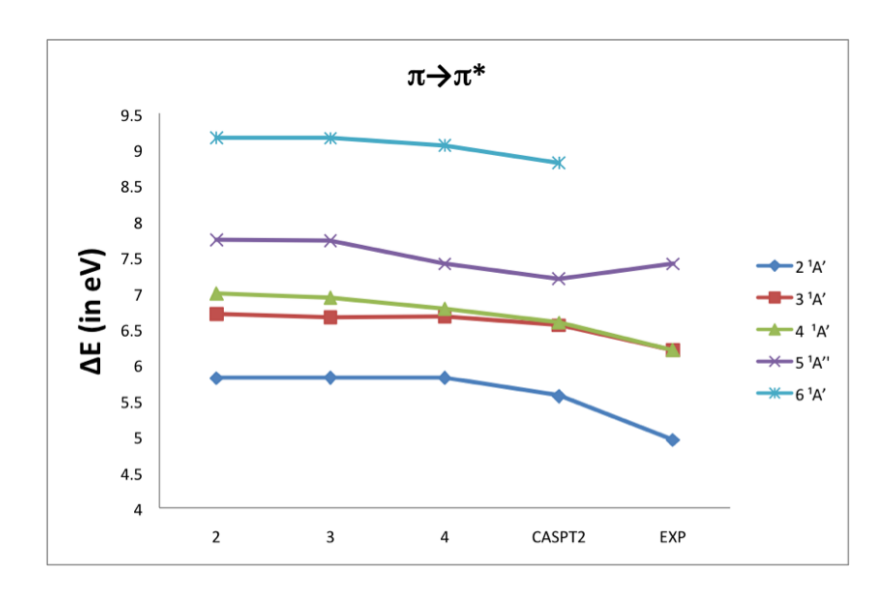


Figure 6.22: RASPT2 (max=2,3,4), CASPT2 and Experimental vertical excitation energies for Thymine Singlet states ($\pi \rightarrow \pi^*$) with RAS2

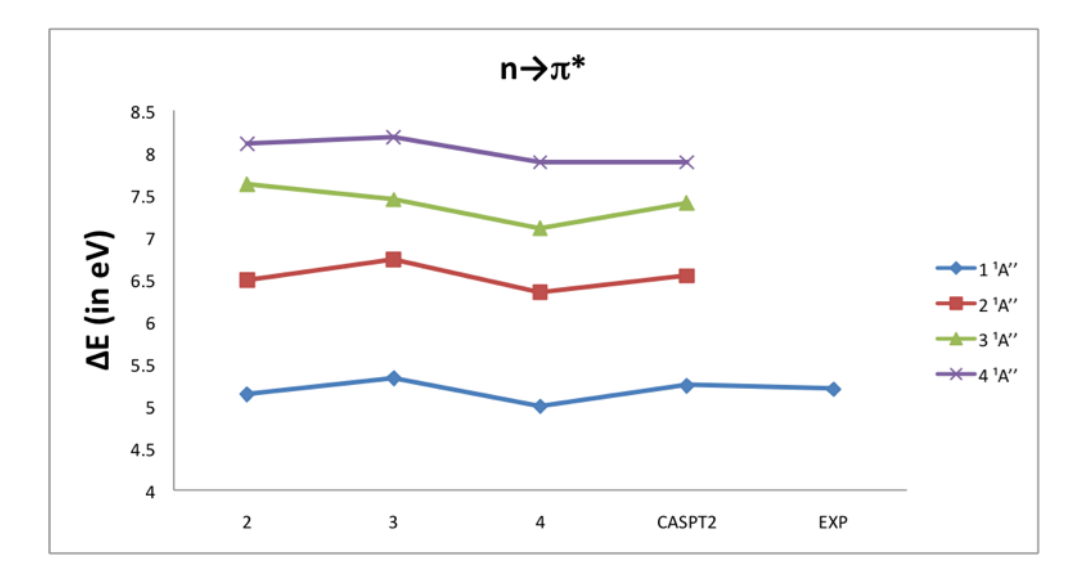


Figure 6.23: RASPT2 (max=2,3,4), CASPT2 and Experimental vertical excitation energies for Thymine Singlet states ($n\rightarrow\pi^*$) with RAS2

Table 6.13: Vertical excitation energies E (eV) of the singlet and triplet states of Uracil (C_s)
RASPT2

		10/10/1 12			
Exc.State	$\max = 2$	$\max = 3$	$\max = 4$	CASPT2	Expt
Ground State $(1^1A')$					
Singlet states					
$1^{1}A''(n-\pi^{*})$	5.534	5.364	5.558	5.428	$4.38^b, 4.9-5.2^c$
$2 {}^{1}A'(\pi - \pi^{*})$	6.267	6.011	5.935	5.896	5.1
$3 {}^{1}A'(\pi - \pi^{*})$	6.974	6.816	6.651	6.735	6.0
$2 {}^{1}A''(n-\pi^{*})$	6.874	6.805	6.898	6.785	-
$3 {}^{1}A'(n-\pi^{*})$	7.894	7.664	7.918	7.650	-
$4 {}^{1}A''(\pi - \pi^{*})$	7.238	6.956	6.867	6.935	6.6
$4^{1}A''(n-\pi^{*})$	8.138	7.911	8.162	7.668	-
$5^1 A''(\pi - \pi^*)$	7.930	7.750	7.384	7.476	6.9 - 7.0
a [:=1:== a [:=1					

 b Ref. [47] c Ref. [45]

The active space is (0.8) 10. In parenthesis: the number of active orbitals of symmetry a' a'' and the number of active electrons.

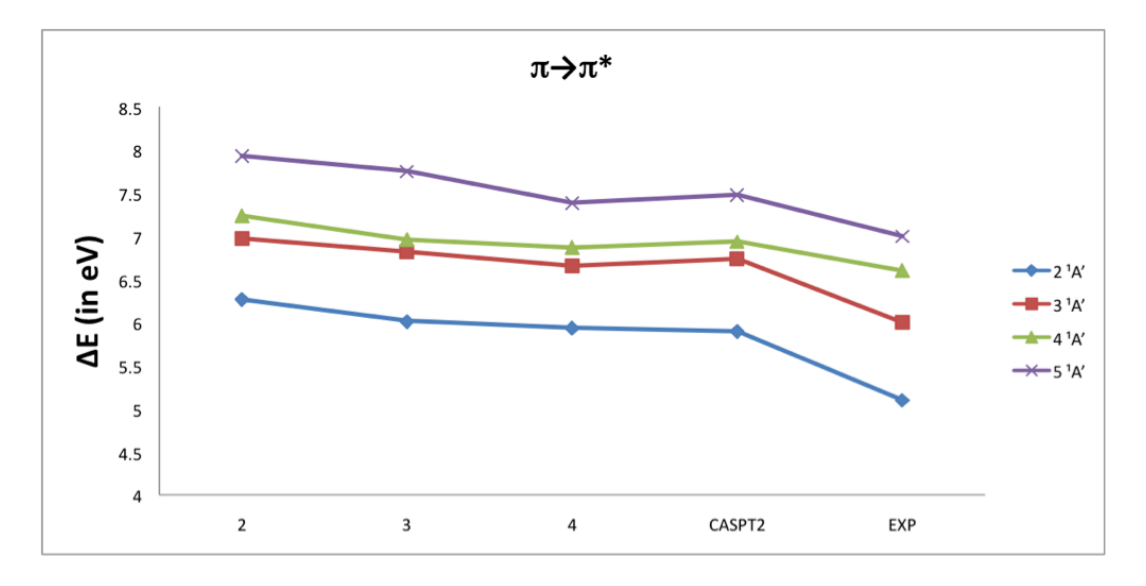


Figure 6.24: RASPT2 (max=2,3,4), CASPT2 and Experimental vertical excitation energies for Uracil Singlet states $(\pi \rightarrow \pi^*)$

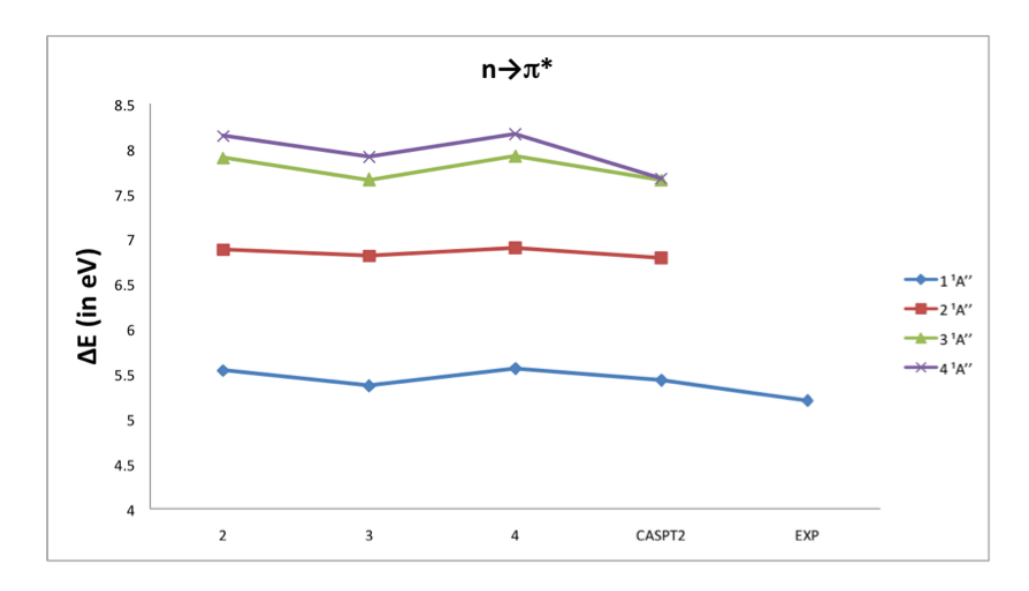


Figure 6.25: RASPT2 (max=2,3,4), CASPT2 and Experimental vertical excitation energies for Uracil Singlet states ($n\rightarrow\pi^*$)

Table 6.14: Vertical excitation energies E (eV) of the singlet and triplet states of Uracil (s) with RAS2

		RASPT2			
Exc.State	$\max = 2$	$\max = 3$	$\max = 4$	CASPT2	Expt
Ground State $(1^1A')$					
Singlet states					
$1^{1}A''(n-\pi^{*})$	5.095	5.387	5.112	5.428	$4.38^b, 4.9-5.2^c$
$2 {}^{1}A'(\pi - \pi^{*})$	5.913	5.893	5.894	5.896	5.1
$3 {}^{1}A'(\pi - \pi^{*})$	6.878	6.821	6.628	6.735	6.0
$2 {}^{1}A''(n-\pi^{*})$	6.51	6.903	6.457	6.785	-
$3 {}^{1}A'(n-\pi^{*})$	7.506	7.787	7.429	7.650	-
$4 {}^{1}A''(\pi - \pi^{*})$	6.908	6.957	6.854	6.935	6.6
$4^{1}A''(n-\pi^{*})$	8.337	7.843	7.466	7.668	-
$5^{1}A''(\pi - \pi^{*})$	7.785	7.835	7.427	7.476	6.9 - 7.0
b Ref. [47] c Ref. [45]					

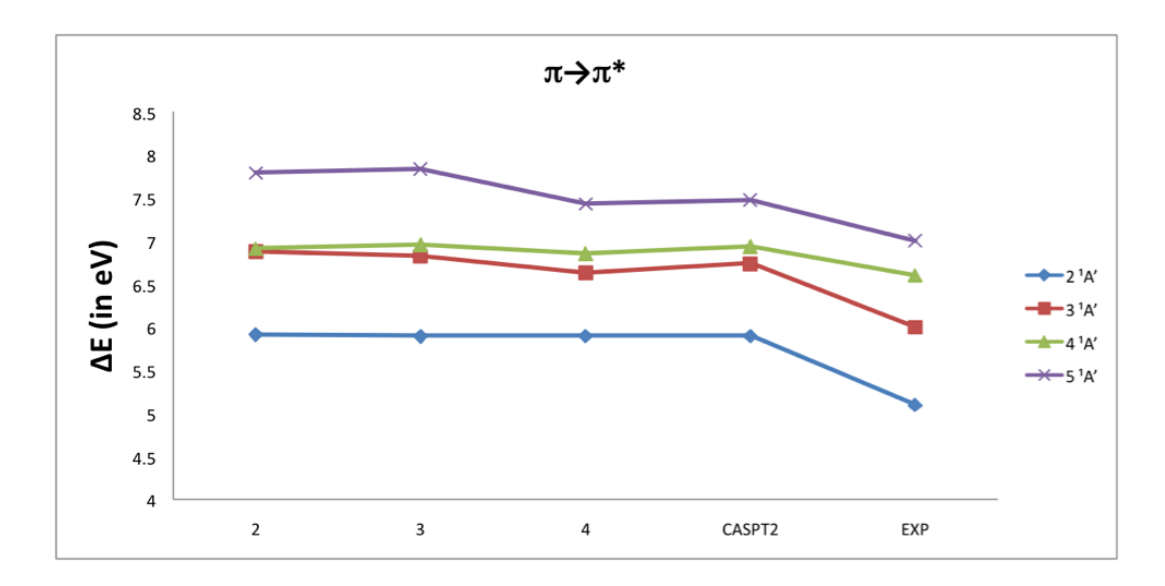


Figure 6.26: RASPT2 (max=2,3,4), CASPT2 and Experimental vertical excitation energies for Uracil Singlet states with RAS2 $(\pi \rightarrow \pi^*)$

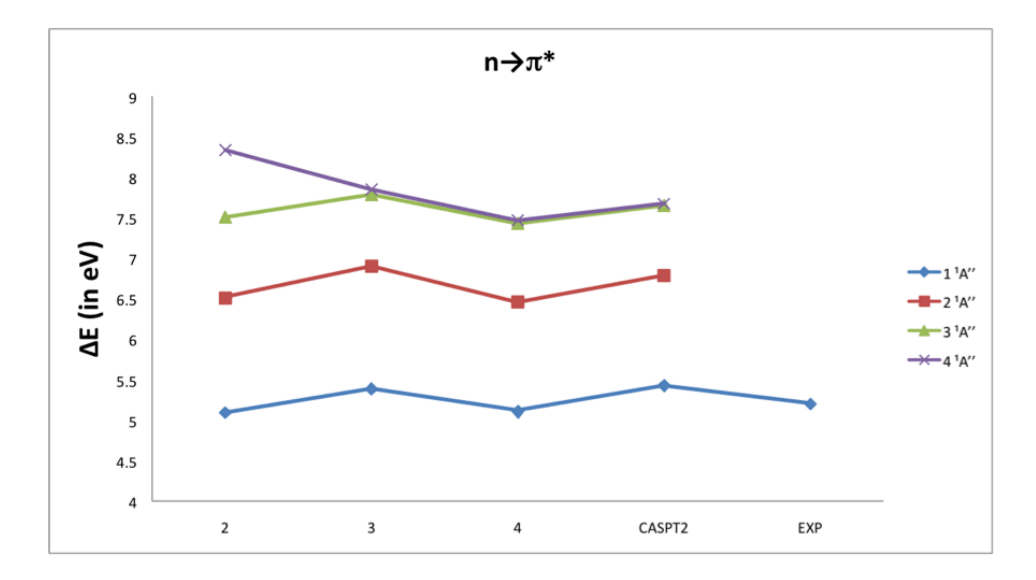


Figure 6.27: RASPT2 (max=2,3,4), CASPT2 and Experimental vertical excitation energies for Uracil Singlet states with RAS2 ($n\rightarrow\pi^*$)

		RASPT2			
Exc.State	$\max = 2$	$\max = 3$	$\max = 4$	CASPT2	Expt
Ground State $(1^1A')$					
Singlet states					
$2^{1}A'(\pi - \pi^*)$	5.078	4.959	5.042	4.721	$4.6^{a,b,c}$
$1 {}^{1}A''(n-\pi^{*})$	5.779	5.921	5.847	5.519	$5.0^b, 5.3^c$
$3 {}^{1}A'(\pi - \pi^{*})$	6.284	6.223	6.292	5.952	$5.4^a, 5.6^b, 5.8^c$
$4^{1}A'(\pi - \pi^*)$	7.025	7.175	7.302	6.852	$6.1^a, 6.2^c, 6.4^b$
$2 {}^{1}A''(n-\pi^{*})$	5.989	6.149	6.028	5.735	-
$5^{1}A'(\pi - \pi^*)$	7.548	7.435	7.374	7.000	$6.7^a, 7.1^c$
$6^1 A' (\pi - \pi^*)$	8.605	8.489	8.597	8.221	-

Table 6.15: Vertical excitation energies E (eV) of the singlet and triplet states of Cytosine (C_s)

 a Ref. [48] b Ref. [49] c Ref. [43]

The active space is (0.8) 10. In parenthesis: the number of active orbitals of symmetry a' a'' and the number of active electrons.

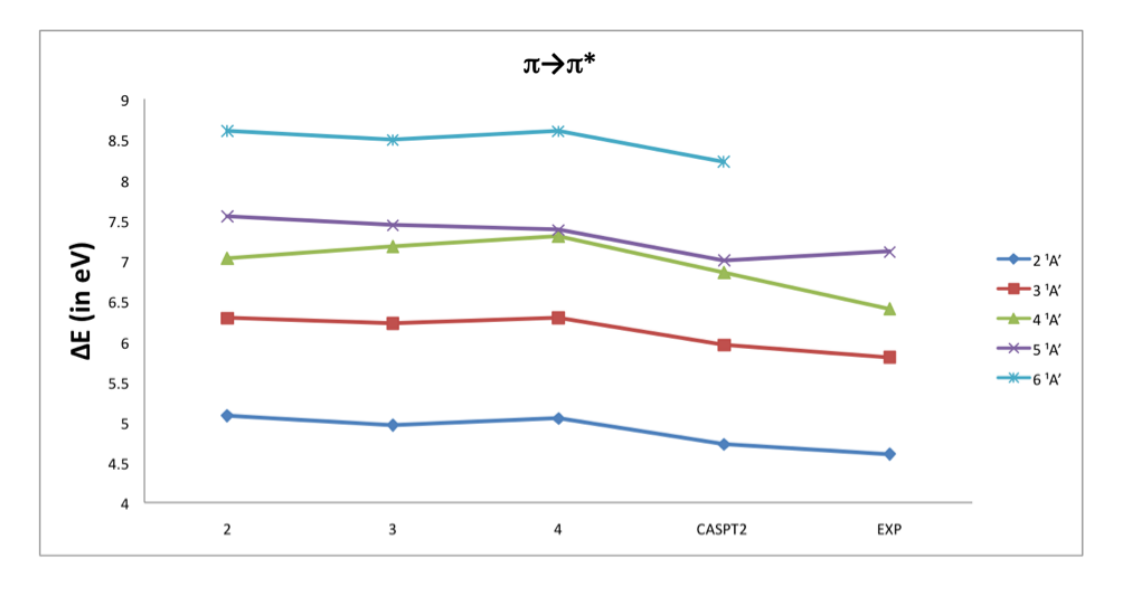


Figure 6.28: RASPT2 (max=2,3,4), CASPT2 and Experimental vertical excitation energies for Cytosine Singlet states $(\pi \rightarrow \pi^*)$

6.4. CONCLUSIONS 159

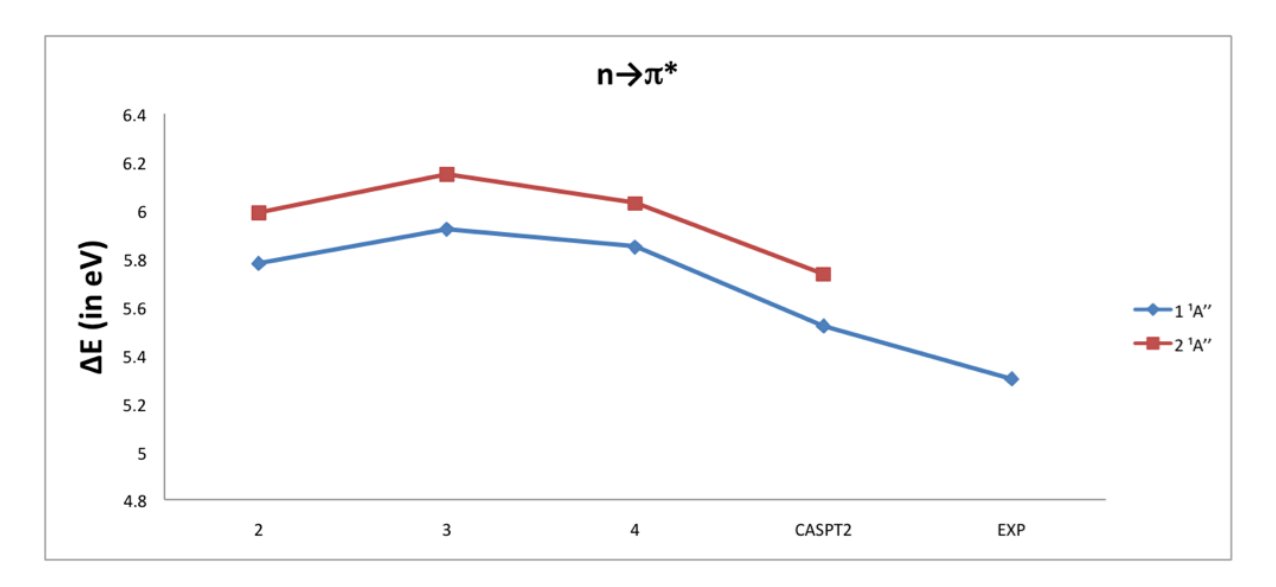


Figure 6.29: RASPT2 (max=2,3,4), CASPT2 and Experimental vertical excitation energies for Cytosine Singlet states ($n\rightarrow\pi^*$)

6.4 Conclusions

For the first time we have tested the MS-RASPT2 method here while computing the excited states of a number of paradigmatic set of 11 medium-sized organic molecules (aromatic hydrocarbons and nucleobases). We have studied a total of 71 singlet and 32 triplet electronic states, in particular the valence excited states at a uniform level. From the results obtained we can say that with quadruple excitations allowed within the RASPT2 protocol one achieves similar excitation energies to that of CASPT2 to within 0.2 eV when multi-state calculations are performed.

We also have shown that the ratio of number of CSFs of the excited state to the ground state becomes important while using MS-RASPT2. We notice that when the ratio of number of CSFs of the excited state to the ground state is closer to that of the CASPT2, the obtained excitation energy is also closer to the CASPT2 value. When the ratio is higher/lower than that seen in CASPT2, then the estimated energy difference seems to be higher/lower

Table 6.16: Vertical excitation energies E (eV) of the singlet and triplet states of Cytosine(Cs) with RAS2

		RASPT2			
Exc.State	$\max = 2$	$\max = 3$	$\max = 4$	CASPT2	Expt
Ground State $(1^1A')$					
Singlet states					
$2^{1}A'(\pi - \pi^{*})$	4.924	4.954	4.668	4.721	$4.6^{a,b,c}$
$1 {}^{1}A''(n-\pi^{*})$	5.711	5.896	5.326	5.519	$5.0^b, 5.3^c$
$3 {}^{1}A'(\pi - \pi^{*})$	6.354	6.183	5.922	5.952	$5.4^a, 5.6^b, 5.8^c$
$4^{1}A'(\pi - \pi^{*})$	7.223	6.963	6.882	6.852	$6.1^a, 6.2^c, 6.4^b$
$2 {}^{1}A''(n-\pi^{*})$	5.797	6.049	5.569	5.735	-
$5^{1}A'(\pi - \pi^*)$	7.243	7.128	6.992	7.000	$6.7^a, 7.1^c$
$6^{1}A'(\pi - \pi^{*})$	8.55	8.617	8.234	8.221	-
of [40]bD of [40]cD of [4 9]				

 a Ref. [48] b Ref. [49] c Ref. [43]

than the value obtained at CASPT2 level. This shows that both electronic states need to be described in a balanced manner.

Apart from that we have made a systematic evaluation is done on the effects of different active space choices and the outer RAS space excitations. In general we notice that when the main contributing molecular orbitals are included in RAS2, the electronic excitation energies improve slightly, more for the RASPT2 results with only double excitations. More studies need to be done to analyze the behaviour of the RAS approaches on the electronic states of larger systems.

6.4. CONCLUSIONS 161

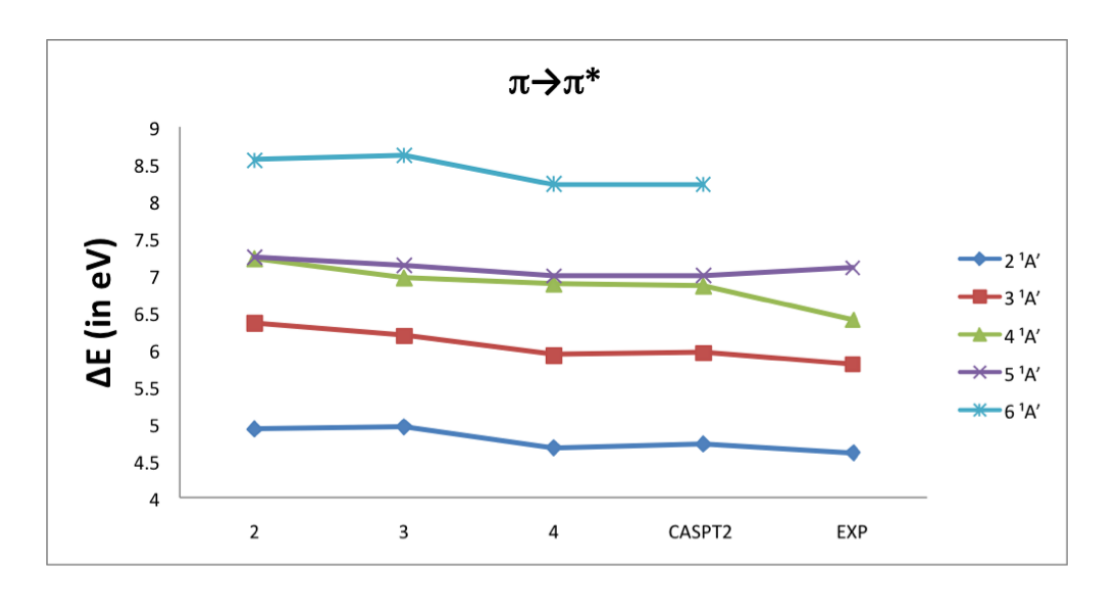


Figure 6.30: RASPT2 (max=2,3,4), CASPT2 and Experimental vertical excitation energies for Cytosine Singlet states $(\pi \rightarrow \pi^*)$ with RAS2

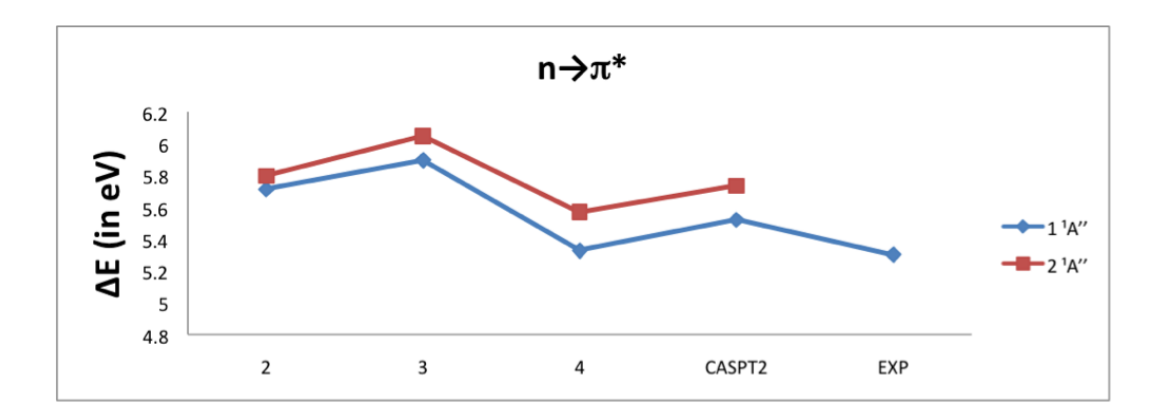


Figure 6.31: RASPT2 (max=2,3,4), CASPT2 and Experimental vertical excitation energies for Cytosine Singlet states ($n\rightarrow\pi^*$) with RAS2

Bibliography

- [1] K. Andersson, P.-Å. Malmqvist, B. O. Roos, A. J. Sadlej and K. Wolinski. J. Phys. Chem. 94, 1990: 5483.
- [2] K. Andersson, P. A. Malmqvist, B. O. Roos. J. Chem. Phys 96, 1992: 1218.
- [3] B. O. Roos, K. Andersson, M. P. Fulscher, P. A. Malmqvist, L. Serrano-Andres, K. Pierloot, M. Merchan. "Multiconfigurational Perturbation Theory: Applications in Electronic Spectroscopy." Advances in Chemical Physics: New Methods in Computational Quantum Mechanics, 1996: 219-331.
- [4] P. A. Malmqvist, K. Pierloot, A. R. Moughal Shahi, C. J. Cramer, L. Gagliardi. J. Chem. Phys.128, 2008: 204109.
- [5] S. M. Huber, A. R. Moughal Shahi, F. Aquilante, C. J. Cramer and L. Gagliardi. J. Chem. Theory Comput, 2009.
- [6] A. R. Moughal Shahi, C. J. Cramer and L. Gagliardi. Phys. Chem. Chem. Phys, 2009.
- [7] M. Schreiber, M. R. Silva-Junior, S. P. A. Sauer, W. Thiel. J. Chem. Phys. 128, 2008: 134110.
- [8] M. R. Silva-Junior, M. Schreiber, S. P. A. Sauer, W. Thiel. J. Chem. Phys. 129, 2008: 104103.
- [9] S. P. A. sauer, M. Schreiber, M. R. Silva-Junior, W. Thiel. J. Chem. Theory Comput. 5, 2009: 555-564.

164 BIBLIOGRAPHY

- [10] A. D. Becke. J. Chem. Phys. 98, 1993: 5648-5652.
- [11] A. Schäfer, C. Huber and R. Ahlrichs. J. Chem. Phys. 100, 1994: 5829.
- [12] R. Ahlrichs, M. Bar, M. Haser, H. Horn and C. Kolmel. Chem. Phys. Lett. 162, 1989: 165-169.
- [13] G. Karlström, R. Lindh, P.-Å. Malmqvist, B. O. Roos, U. Ryde, V. Veryazov, P.-O. Widmark, M. Cossi, B. Schimmelpfennig, P. Neogrady and L. Seijo. Comput. Mat. Sci. 287, 2003: 222-239.
- [14] G. Ghigo, B. O. Roos, and P.-Å. Malmqvist. Chem. Phys. Lett. 396, 2004: 142.
- [15] F. Aquilante, P.-A. Malmqvist, T. B. Pedersen, A. Ghosh and B. O. Roos. J. Chem. Theory Comput. 4, 2008: 694-702.
- [16] F. Aquilante, T. B. Pedersen and R. Lindh. J. Chem. Phys. 126, 2007: 194106-194111.
- [17] F. Aquilante, T. B. Pedersen, A. S. de Meras and H. Koch. J. Chem. Phys. 125, 2006: 174101-174107.
- [18] A. Hiraya and K. Shobatake. J. Chem. Phys. 94, 1991: 7700.
- [19] P. G. Wilkinson, Can. J. Phys. 34, 1956: 596.
- [20] N. Nakashima, M. Sumitani, I. Ohmine, and K. Yoshihara. J. Chem. Phys. 72, 1980: 2226.
- [21] J. P. Doering. J. Chem. Phys. 51, 1969: 2866.
- [22] J. Lorentzon, M. P. Fülscher, and B. O. Roos. J. Am. Chem. Soc. 117, 1995: 9265.
- [23] W. M. Flicker, O. A. Mosher, and A. Kuppermann. J. Chem. Phys. 64, 1976: 1315.
- [24] L. Serrano-Andrés, M. Merchán, I. Nebot-Gil, B. O. Roos, and M. P. Fülscher. J. Am. Chem. Soc. 115, 1993: 6184.
- [25] G. A. Morris, George and G. C. J. Mol. Spectrosc. 26, 1968: 67.

BIBLIOGRAPHY 165

[26] R. H. Huebner, S. R. Meilczarek, and C. E. Kuyatt. Chem. Phys. Letters 16, 1972: 464.

- [27] M. Ito, N. Mikami. Chem. Phys. Letters 31, 1975: 472.
- [28] M. Allan, L. Neuhaus, and E. Haselbach. Helv. Chim. Acta 7, 1984: 1776.
- [29] J. R. Platt, H. B. Klevens. J. Chem. Phys 17, 1949: 470.
- [30] E. E. Koch, A. Otto, and K. Radler. Chem. Phys. Letters 16, 1972: 131.
- [31] H. E. Hunziker. Chem. Phys. Letters 3, 1969: 504.
- [32] H. E. Hunziker. J. Chem. Phys 56, 1972: 300.
- [33] Y. H. Meyer, R. Astier, and J. M. Leclercq. J. Chem. Phys 56, 1972: 801.
- [34] M. Bavia, F. Bertinelli, C. Taliani, and C. Zauli, Mol. Phys. 31, 1976: 479.
- [35] E. H. Van Veen. Chem. Phys. Lett. 41, 1976: 535.
- [36] A. Bolovinos, P. Tsekeris, J. Philis, E. Pantos, and G. Andritsopoulos. J. Mol. Spectrosc. 103, 1984: 240.
- [37] K. K. Innes, I. G. Ross, and W. R. Moomaw. J. Mol. Spectrosc. 132, 1988: 492.
- [38] B. O. Roos, M. P. Fülscher. Theor. Chim. Acta 87, 1994: 403.
- [39] M. P. Fülscher, K. Andersson, and B. O. Roos. J. Phys. Chem. 96, 1992: 9204.
- [40] W. Voelter, R. Records, E. Bunnenberg, and C. Djerassi. J. Am. Chem. Soc. 90, 1968: 6163.
- [41] L. B. Clark, G. G. Peschel, and I. Tinoco. J. Phys. Chem. 69, 1965: 3615.
- [42] M. F. Maestre, W. C. Brunner. Biopolymers 14, 1975: 555.
- [43] C. A. Sprecher and W. C. Johnson, Jr. Biopolymers 16, 1977: 2243.
- [44] K. Griffin, J. C. Sutherland. Biopolymers 23, 1984: 2715.

166 BIBLIOGRAPHY

- [45] L. B. Clark, J. S. Novros. J. Phys. Chem. 90, 1986: 5666.
- [46] R. Abouaf, J. Pommier, and H. Dunet. Chem. Phys. Lett. 381, 2003: 486.
- [47] M. Fujii, T. Tamura, N. Mikami, and M. Ito. Chem. Phys. Lett. 126, 1986: 583.
- [48] K. Raksányi, I. Földváry, J. Fidy, and L. Kittler. Biopolymers 17, 1978: 887.
- [49] W. M. D., M. J. Robins, R. K. Robins, M. W. Winkley, and H. Eyring. J. Am. Chem. Soc. 91, 1969: 824.

Chapter 7

Concluding Remarks

Quantum chemical methods available today offer a great help in solving some key scientific questions. There has been an impressive development of new and efficient methods and the efforts are still ongoing both in method development and in applications. The synergy between these two is pushing the frontiers of computational chemistry. There are still limitations though and improvements can be made aiming at accurate computation by taking care of electron correlation.

In this thesis, we have described an extension of the CASSCF/CASPT2 method, namely, the Restricted Active Space (RAS)SCF/RASPT2 method. The focus of this work has been on the methodology involved in the development of RASPT2 method and on the detailed testing of this approach while studying various chemical problems. The basic difference between the CASSCF and RASSCF models relies on the manner the orbital active space is divided and the procedure to restrict the CI excitation level in certain subspaces in the latter. Whereas CASSCF may include at most 15-16 electrons and 15-16 orbitals in the active space when generating the multireference for the perturbative treatments, RASSCF allows to correlate up to 30 electrons in 30 active orbitals when generating CI spaces of similar sizes. Thus, the potential of this new method is notable, so RASPT2 extends the applicability of multiconfigurational procedures to new classes of problems that could not be treated so far.

Then this work is focused on the detailed testing of this quantum-chemical approach, the

RASPT2 method in various applications.

Firstly, we have examined the performance of the RASPT2 model for two challenging problems associated with the activation of O₂ by copper. Because of favorable combinations of covalency and oxidation/reduction potentials, the activation of molecular oxygen by its coordination to one or two supported (i.e., ligated) Cu(I) ions is common to a number of biological and inorganic catalytic processes In the case of monocopper species LCuO₂, where L is a general ligand or ligands, one possible oxidation state that may be assigned to the complex is $LCu(II)O_2(-)$; thus, the copper atom has been oxidized by one electron and the O_2 fragment is formally a superoxide radical anion. Similarly, in the case of dicopper species $(LCu)_2O_2$, one possible oxidation state of the complex is formally $[LCu(II)]_2[(O_2)(2-)]$; in this instance each copper atom has been oxidized by one electron and the O₂ fragment is formally a peroxide dianion. In both of these cases, the resulting compounds with a variety of ligands can have singlet ground states that exhibit substantial biradical character because of the spin separation associated either with two d⁹ Cu(II) ions or one such ion and a superoxide radical anion. Wave function theories restricted to a single determinant are poorly suited to the description of such species since singlet biradicals are intrinsically two-determinantal. Moreover, even when oxidation states more likely to be characterized as closed-shell in nature are considered, e.g., $[LCu(III)]_2[O(2-)]_2$, computational studies have found that large contributions from dynamical correlation effects influence relative isomer energetics. This applications show that in the mononuclear case, RASPT2 and CASPT2 provide very similar results. In the binuclear cases, however, RASPT2 proves quantitatively useful owing to the very large size of the necessary active space.

Then we have compared the CASPT2 and RASPT2 models for the determination of the singlet-triplet state-energy splittings of five intermediates associated with the formation and reaction of copper-oxo species derived from oxygenation of Cu(I)-α-ketocarboxylate complexes. Based on consideration of several active spaces, we determined that the CASPT2 model was well converged with a (12,12) active space. Including up to double excitations in the outer RAS spaces generated two orders of magnitude fewer configuration state functions than the full CASPT2(12,12) calculations but provided essentially equivalent accuracy.

Adding additional excitations in the outer RAS spaces led to small but systematic improvements in accuracy.

We have also applied RASSCF/RASPT2 method to compute one-electron ionization potentials and vertical electronic energy differences of oligomers of length n formed from ethylene (n=1-10), acetylene (n=1-5), and phenylene (n=1-3) subunits. The RASSCF/RASPT2 approach offers an accuracy similar to CASSCF/CASPT2 at significantly reduced computational expense (both methods show good agreement with experimental data where available). It is shown that RASPT2 extends the range of CASPT2-like approaches by permitting the use of larger active spaces.

In all instances, predictions at the RASPT2 level agree with those at the CASPT2 level (and with experiment) to within about 0.1 eV and this agreement is achieved using from one to three orders of magnitude fewer configuration state functions. The RASSCF/RASPT2 approach thus offers an accuracy similar to CASSCF/CASPT2, but with substantially reduced computational overhead, permitting application of the RASSCF/RASPT2 model to systems where electron/active space combinations exceed the practical limits of the CASSCF/CASPT2 model. This showed that the RASSCF/RASPT2 model shows considerable promise for future studies of highly correlated large systems.

Nevertheless, the RASSCF method is not as solid as CASSCF. Its convergence is not as well-behaved as in CASSCF and it is maybe even more dependent to the quality of the starting orbitals used in the calculation. Therefore, besides making a good choice of the active space, it is also important to obtain proper starting orbitals before running the suitable calculation, something that is applied also to its methodological predecessor. Up to recently, as dynamical correlation was not available on top of the RAS wave function, the utility of the RASSCF approach was limited to perform geometry optimizations or educated selections of the active space based on the occupancy of the natural orbitals for more restricted CASSCF calculations. The addition of the second- order perturbation treatment to the RASSCF formulation originating the RASPT2 method extend the applicability of the approach to quantitative chemical problems.

A final problem has to be mentioned in the RASPT2 formulation. By RAS constraints, only RAS1 and RAS3 subspaces should handle dynamical correlation whereas RAS2 should take into account all nondynamical correlation effects. Unfortunately, this subdivision is not well defined. Therefore, to address all dynamical correlation effects in the RASPT2, a perturbative treatment of the fully internal excitations must be included. This implies in the present formulation of H₀ building fourth-order density matrices and this is unpractical with larger active spaces. New approximations on H₀ are needed to solve this question, which, in any case its importance has to be evaluated. As it occurs with single-state CASPT2 calculations, in RASPT2 the states computed individually from a previous CASSCF reference are not orthogonal to the other states of the same spatial and spin symmetry. As a consequence the obtained solutions have ignored the coupling between the states. The multi-state CASPT2 (MS-CASPT2) procedure represents an extension of the CASPT2 method for the perturbation treatment of chemical situations that require two or more reference states. For instance, situations such as avoided crossings and near-degeneracy of valence and Rydberg states, and their proper description cannot be fully accounted for by just using a single-state perturbation treatment.

We have chosen a benchmark set of 11 medium sized organic molecules (aromatic hydrocarbons and nucleobases) to study the MS-RASPT2. Vertical excitation energies are computed for the valence excited states using both MS-CASPT2 and MS-RASPT2 at identical geometries obtained (DFT/B3LYP) and with the same basis set (TZVP). A systematic evaluation is done on the effects of different active space choices and the outer RAS space excitations. The RASPT2 results compare well to within (0.2 eV) with those obtained by CASPT2 method. The general applicability of the RASPT2 protocol to compute the excited states is discussed .

The main conclusions from these set of studies are:

1. The same accuracy as obtained in CASSCF/CASPT2 treatment is reached with RASSCF/RASPT2 (with quadruple excitations allowed) to within about 0.1 eV in most cases.

2. The RASSCF method is not as solid as CASSCF. Its convergence is not well-behaved as in CASSCF and is found to be more dependent on the quality of the starting orbitals. In cases of poor convergence of the RASSCF wave function, especially at //3 and //4 levels, it is found that using a optimized molecular orbitals from a previous //2 calculation, provides accurate excitation energies.

Nevertheless, we are still far away to emulate on theoretical grounds the behavior characteristics of living systems. Many challenges still exist and the interplay between theory and experiments will help in further progress of theoretical methods. Therefore the future of quantum chemistry seems to be splendid with plenty of problems to be addressed.

List of Published articles during my Ph.D studies at the Department of Physical Chemistry of the University of Geneva and not included in this thesis

1. I. Infante, A. Kovacs, G. La Macchia, A. R. Moughal Shahi, J. K. Gibson and L. Gagliardi

'Ionization energies along the actinide oxides series, from Th to Cm: theory versus experiment'

Submitted

2. D. Schultz, F. Biaso, A. R. Moughal Shahi, M. Geoffroy, K. Rissanen, L. Gagliardi, C.J. Cramer and J.R. Nitschke

'Helicate Extension as a Route to Molecular Wires'

Chemistry - A European Journal, 14 (24), 2008, p7180-7185

3. C.J. Cramer, J.R. Gour, A. Kinal, M. Wloch, P. Piecuch, A. R. Moughal Shahi and L. Gagliardi

'Stereoelectronic Effects on Molecular Geometries and State-Energy Splittings of Ligated Monocopper Dioxygen Complexes'

Journal of Physical Chemistry A, 112 (16), 2008, p3754-3767

4. G. Balazs, F. Geoffrey, N. Cloke, L. Gagliardi, J.C. Green, A. Harrison, P.B. Hitchcock, A. R. Moughal Shahi and O. T. Summerscales

'A Dichromium(II) Bis (η8-pentalene) Double-Sandwich Complex with a Spin Equilibrium: Synthetic, Structural, Magnetic and Theoretical Studies' Organometallics, 27 (9) , 2008 , p2013 -2020

5. M. Hutin, C.J. Cramer, L. Gagliardi, A. R. Moughal Shahi, G. Bernardinelli, R. Cerny and J.R. Nitschke

'Self-sorting Subcomponent Rearrangement During Crystallization' Journal of the American Chemical Society, 129 (28), 2007, p8774-8780

6. G. Ghigo, A. R. Moughal Shahi, L. Gagliardi, L.M. Solstad and C.J. Cramer 'Quantum Chemical Characterization of Low-energy States of Calicene in the Gas Phase and Solution'

Journal of Organic Chemistry, 72 (8), 2007, p2823-2831

- 7. A. R. Moughal Shahi, L. Gagliardi and P. Pyykkö 'Pocket and Antipocket conformations for the CH4@C84 endohedral fullerene' International Journal of Quantum Chemistry, 107 (5), 2007, p1162-1169
- 8. A. Pigliucci, P. Nikolov, A. R. Moughal Shahi, L. Gagliardi, C.J. Cramer and E. Vauthey 'Early Excited State Dynamics of 6-Styryl-Substituted Pyrylium Salts Exhibiting Dual Fluorescence'

Journal of Physical Chemistry A, 110 (33), 2006, p9988-9994